ROBUST PATH FOLLOWING CONTROL FOR INDEPENDENTLY ACTUATED AUTONOMOUS GROUND VEHICLES WITH TRANSIENT PERFORMANCE IMPROVEMENT

ROBUST PATH FOLLOWING CONTROL FOR INDEPENDENTLY ACTUATED AUTONOMOUS GROUND VEHICLES WITH TRANSIENT PERFORMANCE IMPROVEMENT

BY

CHUAN HU, B. ENG., M. ENG.

A THESIS

SUBMITTED TO THE DEPARTMENT OF MECHANICAL ENGINEERING

AND THE SCHOOL OF GRADUATE STUDIES

OF MCMASTER UNIVERSITY

IN PARTIAL FULFILMENT OF THE REQUIREMENTS

FOR THE DEGREE OF

PH.D. OF MECHANICAL ENGINEERING

Ph.D. of Mechanical Engineering (2017) McMaster University

(Mechanical Engineering) Hamilton, Ontario, Canada

TITLE:	ROBUST PATH FOLLOWING CONTROL FOR INDEPENDENTLY ACTUATED AUTONOMOUS GROUND VEHICLES WITH TRANSIENT PERFORMANCE IMPROVEMENT
AUTHOR:	Chuan Hu M. Eng., (Vehicle Operation Engineering) China Academy of Railway Sciences, Beijing, China B. Eng., (Automotive Engineering) Tsinghua University, Beijing, China
SUPERVISOR:	Prof. Fengjun Yan
NUMBER OF PAGES:	xxxv, 202

To my parents, for their unconditional love and support.

Lay Abstract

This thesis focuses on the constraint control in the path following of autonomous ground vehicles with transient performance improvement, where the system uncertainties, external disturbances and input saturations have been considered. The constraint control is used to constrain the path following errors in the safety regions, and the transient control is used to improve the transient performance. The ultimate control objective is to increase the path following accuracy and convergence speed, and thus to improve the vehicle stability, safety and ride comfort. This thesis proposed a novel desired-heading amendment to modify the traditional path following model to reduce the system overshoot, a novel output constraint strategy to constrain the lateral offset in reasonable bound, and two novel nonlinear control strategies to improve the transient performance. Also, experiments were conducted to verify the effectiveness of the differential drive assisted steering.

Abstract

This thesis addresses the path following control of independently actuated (IA) autonomous ground vehicles (AGVs), and focuses on the constraint control and transient performance improvement. The control aim is to inhibit overshoots and eliminate steady-state errors in path following manoeuvres, and thus to reduce the possibilities of AGVs to surpass safe driving bounds. Centering on this focus, this thesis proposes a novel path-following modeling method, a novel output constraint control approach, and two novel nonlinear control strategies for transient performance improvement. The contributions of this study lie on the following five aspects: 1) A novel definition for the desired heading is proposed using the sideslip-angle compensation, to reduce the steady-state errors in path following caused by the non-zero sideslip-angle and the large/changing path curvature; 2) A novel output constraint control approach using hyperbolic projection technique is proposed to compactly restrain the lateral offset, and thus to prevent the vehicle from surpassing safe lanes; 3) A novel integral sliding mode (ISM)-based composite nonlinear feedback (CNF) technique is proposed to improve the transient performance of path following, considering the system uncertainties, disturbances and actuator saturations; 4) A novel disturbance observer-based CNF technique is proposed to improve the transient performance for path following with differential drive assisted steering (DDAS) when the active steering system is in complete failure. Corresponding comparative simulations based on CarSim-Simulink were

conducted to verify the proposed modeling and control strategies in 1)-4); 5) Experiments have been conducted to verify the existence and effectiveness of the DDAS mechanism.

Acknowledgements

Firstly, I would like to express my great gratitude to my supervisor, Prof. Fengjun Yan, for his sustainable guidance and training throughout my Ph.D. program. With the speciality on control theory and vehicle engineering, he brought me into the research world of vehicle dynamics and control, where I found the research pleasure and achievability. Under his sagacious enlightenment and effective supervision, I have gradually acquired how to do research, make my own contributions, and write academic papers. His support is just like a lamp guiding me in darkness and encouraging me to overcome obstacles and pursue an academic career .

Secondly, I am very grateful to Prof. Rongrong Wang from Southeast University, China, for his wise comments and valuable counselling for my research work. He began to guide and collaborate with me from the summer of 2014. Since then, I had learned a great deal of knowledge from his academic wisdom and experience on vehicle dynamics and control, CarSim simulation, and paper writing. I had obtained several inspirations from the discussions with him, which enabled me to publish several papers on top journals in my research field. Also, I would like to thank Prof. Jinxiang Wang and Mr. Yunke Shi, who are in Prof. Wang's research group at Southeast University. I really appreciate their time and effort of helping me in the experiments of the differential steering.

Thirdly, I would like to thank my parents and my elder sister, for their love and support throughout my Ph.D. study.

Abbreviations

ABS	Antilock braking systems.
AFS	Active front-wheel steering.
AGV	Autonomous ground vehicle.
BMI	Bilinear matrix inequality.
CG	Center of gravity.
CNF	Composite nonlinear feedback.
DDAS	Differential drive assisted steering.
DoF	Degrees of freedom.
DYC	Direct yaw-moment control.
FDB	Feedback dominance backstepping.
FWIA	Four-wheel independently actuated.
HFDB	Hyperbolic projection-based feedback dominance backstepping.
IA	Independently actuated.
IAE	Integral of absolute-value of error.
ISM	Integral sliding mode.
ISV	Integral of the square value.
ITAE	Integral of time-multiplied absolute-value of error.
LDA	lane-departure avoidance.

LMI	Linear matrix inequalities.
LQR	Linear quadratic regulator.
MIMO	Multi-input multi-output.
MPC	Model predictive control.
PI	Proportion integration.
PID	Proportion integration differentiation.
SbW	Steer-by-wire.
SMC	Sliding mode control.
STA	Super-twisting algorithm.

Symbols

e	Lateral offset.
e_p	Lookahead (or preview) error.
e_{pa}	Amended lookahead error.
ψ	Heading error.
ψ_h	Actual heading angle of the vehicle.
ψ_d	Tangential angle of the desired path.
ψ_{da}	New desired-heading.
ψ_{Ame}	Amended definition of the heading error .
T	Closest point on the desired path from the center of gravity.
L	Lookahead (or preview) distance.
σ	Curvilinear coordinate of point T.
ρ	Curvature of the desired path.
m	Mass of the vehicle.
I_z	Yaw inertia of the vehicle.
$c_f,\ c_r$	Front and rear generalized cornering stiffnesses, respectively.
$c_{f0},\ c_{r0}$	Front and rear generalized nominal cornering stiffnesses, respectively.
$\Delta c_f,\ \Delta c_r$	Additional uncertain terms of c_{f0} and c_{r0}, respectively.

$\alpha_f,\ \alpha_r$	Front and rear wheel slip angles, respectively.
$F_{xi},\ F_{yi}$	Longitudinal and Lateral tire forces of the ith wheel, respectively.
$F_{yf},\ F_{yr}$	Generalized front and rear lateral tire forces, respectively.
$v_x,\ v_y$	Vehicle longitudinal and lateral velocities at the center of gravity, respectively.
a_y	Vehicle lateral acceleration at the center of gravity.
r	Vehicle yaw rate at the center of gravity.
β	Vehicle sideslip angle at the center of gravity.
β_d	Desired value of sideslip angle
r_d	Desired value of yaw rate.
γ	Reference vector for the controlled output z.
δ_f	Front wheel steering angle.
$l_f,\ l_r$	Distances from front and rear axles to the center of gravity, respectively.
l_s	Half of track width.
l	Half of the tire contact length.
r_σ	Scrub radius.
b_{eff}	Effective steering damping.
J_{eff}	Effective moment of inertia of the steering system.
ΔM_z	External yaw moment.
$\Delta M_{z\,\max}$	Saturation limit of the external yaw moment.
$\Delta T_{fl},\ \Delta T_{fr}$	Left and right wheel torque generated by the in-wheel motor, respectively.
τ_f	Friction torque of the steering system.
τ_a	Tire self-aligning moment of the steering system.
$\tau_{ds1},\ \tau_{ds2}$	Torque generated by the right and left longitudinal tire forces, respectively.

$\Delta M_1{}'$	Steering assisted torque.
F_s	Coulomb friction constant.
$x,\ y,\ z$	System state, measured output, controlled output, respectively.
ΔM_1	Front external yaw moment.
x_e	Reference value for the system state x.
$\tilde{x}$	Error between x and x_e.
ε	Tracking error for the controlled output.
u	Control input.
d	External disturbance.
$d_m,\ \dot{d}_m$	Bounds of the external disturbance d and its time-derivative, respectively.
$u_0,\ u_s$	Nominal controller and additional sliding mode controller, respectively.
$(u_s)_{eq}$	Equivalent controller for u_s.
$u_l,\ u_n$	Linear and nonlinear parts in the CNF controller, respectively.
s	Sliding surface.
Δ	Constrained nominal controller.
$s^\dagger$	Laplace variable.
$\kappa\,(\gamma,\ z)$	A smooth and non-positive function.
$\phi,\ \alpha$	Tunable positive scalars in function $\kappa\,(\gamma,\ z)$.
μ	Tire-road friction coefficient.
s_i	Tire longitudinal slip ratio the ith wheel.
sat, $\overline{\text{sat}}$	Saturation and partial saturation functions, respectively.

Declaration of Academic Achievement

This thesis has proposed a novel nonlinear control technique to constrain the lateral offset in the reasonable scope, and a novel path following modeling approach and two novel nonlinear control techniques to reduce the overshoots and steady-state errors in the path following control of autonomous ground vehicles (AGVs), respectively. The ultimate control objective is to increase the path following accuracy and speed, and reduce the AGV's possibility of surpassing the safety lanes, thus to improve the vehicle handling and stability as well as the vehicle ride comfort. In general, this research work focuses on constraining the path following errors and improving the transient performance for independently actuated (IA) AGVs, either by modeling amendment or controller design. The academic achievements are listed in the following five aspects:

I. Desired heading amendment for path following

The desired vehicle heading in path following is commonly defined as the tangent direction on the desired path. However, we find this traditional definition may deteriorate the path-following performance. Thus we provide an amendment to the definition of the desired heading, and redefine the heading error by adding up the traditionally defined heading error and the sideslip angle. The amendment can realize a more accurate path-following maneuver, and enables the path

following errors to be converged to zero simultaneously.

II. Output constraint control for lateral offset in path following

To restrict the lateral offset in path following for four-wheel independently actuated (FWIA) AGVs, we propose a novel output constraint controller to strictly bound the lateral offset to prevent the vehicle from transgressing the safety bound in path following. The control strategy is designed by using hyperbolic projection technique based on feedback dominance backstepping, which aims to overcome the explosive complexity in backstepping. The proposed nonlinear controller can make the vehicle lateral offset in path following strictly bounded.

III. Robust Composite Nonlinear Feedback Control for Path Following of FWIA AGVs

To compositively consider the system uncertainties, tire fore saturations and variation of the desired-path curvature in the path-following controller design, we propose an accurate, fast and robust path-following control approach for FWIA AGVs via integrated control of the AFS and DYC. A novel integral sliding mode (ISM)-based composite nonlinear feedback (CNF) control technique considering the multi-input multi-output and the time-varying tracking reference is designed. The proposed controller has combined the advantages of CNF control in improving the transient performance and ISM control in guaranteeing good robustness.

IV. Transient performance improvement for path following control of IA AGVs with Differential Steering

The front DDAS can be used to achieve the path following control for IA AGVs in the case of the complete failure of the active front-wheel steering system. To improve the transient performance of the fault-tolerant control with the DDAS, we propose a novel multiple-disturbances observer-based CNF approach to realize the path following control considering the tire force saturations. The disturbance

observer is designed to estimate the external multiple disturbances with unknown bounds.

V. Experiment Study of DDAS

Experiments have been conducted to verify the existence and effectiveness of the DDAS mechanism in the steering fault conditions. Through the model verification, it is found the differential torque between the left and right wheels can generate a differential steering angle when the steering motor completely fails. Lane change control was tested by using DDAS, which showed that the real yaw rate could track the desired value well.

Publications

Book Chapters

B1 **Chuan Hu**, "*Analysis Approach of Curve Passing for Rolling Stock*," as a chapter in the book *Dynamics of Rolling Stock* (in Chinese), by Jianwei Yao and Lixia Sun, Science Press, Beijing, 2014.

Journal Papers

J11 Jinxiang Wang, Junmin Wang, Rongrong Wang, and **Chuan Hu**, "A Framework of Vehicle Trajectory Replanning in Lane Exchanging with Considerations of Driver Characteristics," ***IEEE Transactions on Vehicular Technology***, vol. 66, no. 5, pp. 3583-3596, May 2017.

J10 **Chuan Hu**, Rongrong Wang, Fengjun Yan, and Nan Chen, "Robust Composite Nonlinear Feedback Path Following Control for Underactuated Surface Vessels with Desired-Heading Amendment," ***IEEE Transactions on Industrial Electronics***, vol. 63, no. 10, pp. 6386-6394, Oct. 2016.

J9 **Chuan Hu**, Rongrong Wang, Fengjun Yan, and Hamid Reza Karimi, "Robust Composite Nonlinear Feedback Path-Following Control for Independently Actuated Autonomous Vehicles with Differential Steering," ***IEEE Transactions on Transportation Electrification***, vol. 2, no. 3, pp. 312-321, Sep. 2016.

J8 **Chuan Hu**, Rongrong Wang, and Fengjun Yan, "Integral Sliding Mode-based Composite Nonlinear Feedback Control for Path Following of Four-Wheel Independently Actuated Autonomous Vehicles," ***IEEE Transactions on Transportation Electrification***, vol. 2, no. 2, pp. 221-230, Jun. 2016.

J7 Rongrong Wang, Hui Jing, **Chuan Hu**, Fengjun Yan, and Nan Chen, "Robust H_∞ Path Following Control for Autonomous Ground Vehicles with Delay and Data Dropout," ***IEEE Transactions on Intelligent Transportation Systems***, vol. 17, no. 7, pp. 2042-2050, Jul. 2016.

J6 Rongrong Wang, **Chuan Hu**, Fengjun Yan, and Mohammed Chadli, "Composite Nonlinear Feedback Control for Path Following of Four-Wheel Independently Actuated Autonomous Ground Vehicles," ***IEEE Transactions on Intelligent Transportation Systems***, vol. 17, no. 7, pp. 2063-2074, Jul. 2016.

J5 **Chuan Hu**, Hui Jing, Rongrong Wang, Fengjun Yan, and Mohammed Chadli, "Robust H_∞ Output-Feedback Control for Path Following of Autonomous Grou-nd Vehicles," ***Mechanical Systems and Signal Processing***, vol. 70-71, pp. 414-427, Mar. 2016.

J4 Rongrong Wang, Hui Jing, **Chuan Hu**, Mohammed Chadli, and Fengjun

Yan, "Robust H_∞ Output-Feedback Yaw Control for In-Wheel-Motor Driven Electric Ground Vehicles with Differential Steering," ***Neurocomputing***, vol. 173, no. 3, pp. 676-684, Jun. 2016.

J3 **Chuan Hu**, Rongrong Wang, Fengjun Yan, and Nan Chen, "Output Constraint Control on Path Following of Four-Wheel Independently Actuated Autonomous Ground Vehicles," ***IEEE Transactions on Vehicular Technology***, vol. 65, no. 6, pp. 4033-4043, Jun. 2016.

J2 **Chuan Hu**, Rongrong Wang, Fengjun Yan, and Nan Chen, "Should the Desired Heading in Path Following of Autonomous Vehicles be the Tangent Direction of the Desired Path?" ***IEEE Transactions on Intelligent Transportation Systems***, vol. 16, no. 6, pp. 3084-3094, Dec. 2015.

J1 Rongrong Wang, **Chuan Hu**, Zejiang Wang, Fengjun Yan, and Nan Chen, "Integrated Optimal Dynamics Control of 4WD4WS Electric Ground Vehicle with Tire-Road Frictional Coefficient Estimation," ***Mechanical Systems and Signal Processing***, vol. 60-61, pp. 727-741, Aug. 2015.

Submitted Journal Papers

- **Chuan Hu**, Rongrong Wang, and Fengjun Yan, "Integral Terminal Sliding Mode-based Composite Nonlinear Feedback Control for Path Following of A Fully Actuated Marine Surface Vessel," ***Transactions of the Institute of Measurement and Control***, under review, 2016.

- **Chuan Hu**, Rongrong Wang, and Fengjun Yan, "Differential Steering based Yaw Integral Sliding Mode Control for In-Wheel-Motor Driven Electric Ground

Vehicles with Mismatched Disturbances," ***IEEE Transactions on Intelligent Transportation Systems***, under review, 2016.

Conference Papers

C12 **Chuan Hu**, Rongrong Wang, and Fengjun Yan, "Integral Sliding Mode Yaw Control for In-Wheel-Motor Driven and Differentially Steered Electric Vehicles with Mismatched Disturbances," accepted, *the 2017 American Control Conference*, May 24-26, Seattle, WA, USA.

C11 **Chuan Hu**, Rongrong Wang, and Fengjun Yan, "Robust Composite Nonlinear Feedback Control for Path Following of Underactuated Surface Vessels with Desired-Heading Amendment", in *Proceedings of the ASME 2016 Dynamic Systems and Control Conference, October 12-14, 2016, Minneapolis, Minnesota, USA*, accepted, 2016.

C10 Hui Jing, Rongrong Wang, **Chuan Hu**, Jinxiang Wang, Fengjun Yan, and Nan Chen, "Vehicle Lateral Motion Control Considering Network-Induced Delay and Tire Force Saturation," In *American Control Conference (ACC)*, 2016, pp. 6881-6886. IEEE, 2016.

C9 **Chuan Hu**, Rongrong Wang, Fengjun Yan, Mohammed Chadli, and Hamid Reza Karimi, "Composite Nonlinear Feedback Control for Path Following of Four-Wheel Independently Actuated Autonomous Ground Vehicles," in *Decision and Control (CDC), 2015 IEEE 54th Annual Conference on*, pp. 203-208. IEEE, 2015.

C8 Hui Jing, **Chuan Hu**, Fengjun Yan, Mohammed Chadli, Rongrong Wang, and Nan Chen, "Robust H_∞ Output-Feedback Control for Path Following of

Autonomous Ground Vehicles," in *2015 54th IEEE Conference on Decision and Control (CDC)*, pp. 1515-1520. IEEE, 2015.

C7 Tian Mi, Cong Li, **Chuan Hu**, Jinxiang Wang, Nan Chen, and Rongrong Wang, "Robust H_∞ Output-Feedback Yaw Control for In-Wheel-Motor Driven Electric Vehicles with Differential Steering," in *2015 54th IEEE Conference on Decision and Control (CDC)*, pp. 1521-1526. IEEE, 2015.

C6 **Chuan Hu**, Hui Jing, Rongrong Wang, Fengjun Yan, Cong Li, and Nan Chen, "Fault-Tolerant Control of FWIA Electric Ground Vehicles with Differential Drive Assisted Steering," *IFAC-PapersOnLine*, vol. 48, no. 21, pp. 1180-1185, 2015.

C5 Hui Jing, Rongrong Wang, Mohammed Chadli, **Chuan Hu**, Fengjun Yan, and Cong Li, "Fault-Tolerant Control of Four-Wheel Independently Actuated Electric Vehicles with Active Steering Systems," *IFAC-PapersOnLine*, vol. 48, no. 21, pp. 1165-1172, 2015.

C4 Hui Jing, Rongrong Wang, Hamid Reza Karimi, Mohammed Chadli, **Chuan Hu**, and Fengjun Yan, "Robust Output-Feedback Based Fault-Tolerant Control of Active Suspension with Finite-Frequency Constraint," *IFAC-PapersOnLine*, vol. 48, no. 21, pp. 1173-1179, 2015.

C3 **Chuan Hu**, Rongrong Wang, Fengjun Yan, Mohammed Chadli, and Nan Chen, "Output Constraint Control on Path Following of Four-wheel Independently Actuated Autonomous Vehicles," in *American Control Conference (ACC)*, 2015, pp. 483-488. IEEE, 2015.

C2 **Chuan Hu**, Rongrong Wang, Zejiang Wang, Mohammed Chadli, and Fengjun Yan, "Integrated Optimal Dynamics Control of 4WS4WD Electric Ground

Vehicles with Tire-Road Frictional Coefficient Estimation," in *American Control Conference (ACC)*, 2015, pp. 5426-5431. IEEE, 2015.

C1 Rongrong Wang, **Chuan Hu**, Fengjun Yan, Mohammed Chadli, and Nan Chen, "Should the Desired Vehicle Heading in Path Following of Autonomous Vehicles be the Tangent Direction of the Desired Path?" In *American Control Conference (ACC)*, 2015, pp. 489-494. IEEE, 2015.

Statement of Co-Authorship

The statement of co-authorship is used to explain the respective contributions of the thesis author and the co-authors, as this Ph.D. thesis was completed according to the regulations of the "sandwich" Ph.D. thesis at McMaster University. This thesis consists of seven chapters, successively including the first chapter "introduction", the second to fifth chapters which present the theoretical work, the sixth chapter which presents the experiment study of DDAS, and the seventh chapter which presents the conclusions and future work. Each chapter from the second to the fifth chapter consists of a published IEEE Transactions journal paper with me as the first author. The experiment study work in the sixth chapter was conducted after the publications of these papers, and had not yet had time to be published at the time when this thesis was completed. The detailed inclusion relations and co-authorship descriptions are as follows:

Chapter 2 contains: [J2] Chuan Hu, Rongrong Wang, Fengjun Yan, and Nan Chen, "Should the Desired Heading in Path Following of Autonomous Vehicles be the Tangent Direction of the Desired Path?" *IEEE Transactions on Intelligent Transportation Systems*, vol. 16, no. 6, pp. 3084-3094, Dec. 2015. The main idea was jointly developed by me and Prof. Wang. I had primitively found that the desired heading should not be defined as the tangent direction of the desired path in the path following control, and then, inspired by Prof. Wang, I proposed the novel desired-heading amendment to modify the traditional path following

model. Prof. Wang gave me some suggestions about the paper structure and paper writing, and helped me in the CarSim simulation. He also helped me in the revisions of the manuscript and the replies to the review comments. Prof. Yan had discussed with me several times about the feasibility of the proposed approach, the stability of the closed-loop system, and the whole contribution of this paper. Prof. Chen also discussed with me about the proposed amendment, and gave me some helpful comments about the control strategy in this paper. Finally I completed the major work of the paper writing, simulation implementation and revisions.

Chapter 3 contains: [J3] Chuan Hu, Rongrong Wang, Fengjun Yan, and Nan Chen, "Output Constraint Control on Path Following of Four-Wheel Independently Actuated Autonomous Ground Vehicles," *IEEE Transactions on Vehicular Technology*, vol. 65, no. 6, pp. 4033-4043, Jun. 2016. The backstepping-based hyperbolic projection algorithm was primitively developed by Prof. Yan, which is a theoretical output constraint control algorithm. To apply this approach in the vehicle motion control, I had modified this algorithm, and combined it with the feedback dominance backstepping to overcome the "explosive complexity" in the standard backstepping in the higher-level controller. In the lower-level controller, I proposed the robust and adaptive LQR approach to reject the external disturbances and guarantee the vehicle lateral stability. The design of the adaptive gain in the lower-level controller was proposed by Prof. Wang. I had discussed the whole control strategy with Prof. Yan for several times, and discussed the vehicle modeling and application scenario of this paper with Prof. Wang. Also, Prof. Wang helped me solve several problems in the CarSim simulations. Prof. Wang and Prof. Chen discussed with me the paper writing, revisions and replies according to the review comments. I completed the major work of the paper writing, controller design, simulation and revisions.

Chapter 4 contains: [J8] Chuan Hu, Rongrong Wang, and Fengjun Yan, "Integral Sliding Mode-based Composite Nonlinear Feedback Control for Path Following of Four-Wheel Independently Actuated Autonomous Vehicles," *IEEE Transactions on Transportation Electrification*, vol. 2, no. 2, pp. 221-230, Jun. 2016. The idea of the modified composite nonlinear feedback (CNF) control based on sliding mode control was primitively proposed by me. I had discussed the correctness and feasibility of the control strategy with Prof. Yan, and discussed the stability and robustness of the control system with Prof. Wang. After their affirmations, I had implemented the controller design, and applied the proposed controller in the path following control of the autonomous vehicles. Prof. Wang gave me some comments on the tire force saturation issue, and checked the equations in this paper carefully. Then I conducted the CarSim simulations, and completed the major work of the paper writing. Prof. Yan and Prof. Wang gave me several suggestions in the revisions and replies according to the review comments.

Chapter 5 contains: [J9] Chuan Hu, Rongrong Wang, Fengjun Yan, and Hamid Reza Karimi, "Robust Composite Nonlinear Feedback Path-Following Control for Independently Actuated Autonomous Vehicles with Differential Steering," *IEEE Transactions on Transportation Electrification*, vol. 2, no. 3, pp. 312-321, Sep. 2016. The control issue of the vehicle motion control using differential steering was proposed by Prof. Wang. In this control scenario, I proposed the ideas of using CNF to improve the transient performance in the path following control with DDAS, and making the traditional CNF robust to the external disturbances with unknown bounds. Prof. Wang suggested me adopt a nonlinear disturbance observer, which then was proved to be effective to estimate multiple disturbances, and suitable to be integrated in the CNF framework. I completed the controller design and stability analysis, and Prof. Wang checked the overall proof of the

stability and robustness of the control system. Before the simulations, I had discussed with Prof. Yan about the contributions of this paper. I also discussed with Prof. Karimi, and got some useful suggestions about the integrated control strategy from him by Email. Then I completed the major work of the paper writing, revisions and replies according to the review comments.

Chapter 6 contains the experiment results of the path following control of an FWIA AGV using DDAS. The used vehicle and test platform were constructed by Prof. Wang and his research group in Southeast University, China. I had conducted the open-loop model verification experiments and the closed-loop lane change control experiments with the help of Prof. Wang's master student, Mr. Yunke Shi. The experiment schemes were jointly developed by Prof. Wang and me. The control strategy in the experiments, data processing and analysis were completed by me. The experiment study of DDAS in the sixth chapter was written by me.

To sum up, the Ph.D. thesis author had completed the major work in this thesis, and is the main contributor to these included co-authored articles and experiment study part. The literature reviews in these journal papers had been extracted and integrated into the Chapter 1 "Introduction". The different chapters contribute to the general theme of the thesis, that is, to improve the transient performance of the path following control of autonomous ground vehicles. The repetition of material (such as the system modeling, references, symbol descriptions, etc.) that appears in these journal papers had been merged in this thesis.

Contents

List of Tables

List of Figures

Chapter 1

Introduction

1.1 Overview

1.1.1 Path-Following Control for AGVs

Over the years, increasing demand and advanced technology for safety, efficiency, and mobility motivate the development of intelligent transportation means. Since traffic accident becomes more and more serious all over the world, autonomous ground vehicle (AGV), with the improved security, better road utilization, and greatly reduced mobility costs, offers the possibility of fundamentally changing the conventional transportation system, and thus becomes an emerging research focus (Anderson et al., 2014; Litman, 2014). The goal of an AGV is to enable vehicle to be autonomously driven either partly or entirely for the purposes of safety, intelligence, comfort, and energy saving. Undoubtedly, the most important mission for the AGVs is to relieve traffic accidents. Therefore, the security enhancement needs to be elevated to a top priority in the motion control design for AGVs (Bizon et al., 2014).

One of the most rudimentary issues for motion control of AGVs is path following (Snider, 2009; Girbés et al., 2014), whose control objective is to make the vehicle track a predefined or desired path according to the driver's intention, based on automatic vehicle steering. Path following control is expected to converge the path following errors (i.e., the lateral offset and the heading error) to zero, while maintaining good ride comfort and vehicle stability. The contents of path following for AGVs mainly includes lane keeping (i.e., line and curve followings) and lane changing, which are two most basic and common driving manoeuvres in practice (Khodayari et al., 2010). Vehicle lateral control is generally the main implementation approach for path following control, keeping the vehicle running in the center of the lane (lane-keeping maneuver), or steering the vehicle into an adjacent lane (lane-change maneuver). Maintaining good passenger comfort and avoiding collision with other vehicles or obstacles are also crucial for path following control. It is worth pointing out that, since the principal mission of AGVs is to reduce the traffic accidents (Bishop, 2000), security containment should be taken into consideration in the path-following control design for AGVs. In this sense, guaranteeing the path following errors (especially the lateral offset) in reasonable and safe regions, and improving the transient performance of path following error responses, either in mitigative or extreme driving condition, is of great significance for path following control design.

Path following control for autonomous vehicles is expected to deal with the general issues for transportation vehicles, such as underactuation, system uncertainties and disturbances, input saturations, unmeasurable states, etc. The nonlinearity of the tire forces and the presence of the tire sliding effects in ground vehicles have considerably increased the difficulties in path following control for AGVs. Several control strategies were proposed to handle those problem, which

are summarized in the later analysis. Since there are some differences between path following and lane keeping, their respective processing methods are different accordingly. Path following describes a more general problem, that is to make the vehicle track a random desired path from a random initial position. However, lane keeping usually refers to making the vehicle follow the lane centerline when the vehicle is already driven in the right lane, such that the initial values of the path following errors are usually sufficiently small. Actually, path following is composed of lane keeping and lane changing, and lane keeping is a special case of path following. This difference is critical and cannot be ignored, which then leads to the control strategy differences between path following and lane keeping.

For general path following manoeuvres, many different approaches were proposed and proved effective. For proportion integration (PI), Zhao et al. (2011) adopted a PI controller for an AGV navigated without GPS in unknown environments. In Marino et al. (2011) a nested PI steering controller was proposed for vision based AGVs in the case of roads with an uncertain curvature. For sliding mode control (SMC), in Fang et al. (2011) a robust anti-sliding controller was designed based on linear SMC for AGVs in presence of lateral disturbances. In Matveev et al. (2013) a nonlinear SMC controller was proposed for an unmanned agricultural tractor in the presence of sliding and control saturation. For model predictive control (MPC), Lenain et al. (2006) applied MPC method in order to preserve accurate guidance for agricultural vehicles in the presence of the sliding and pseudosliding effects. Raffo et al. (2009) presented two kinematic linear predictive control strategies for path tracking of terrestrial AGVs. For fuzzy logic control, in Tsui et al. (2008) two intelligent controllers were designed based on fuzzy logic and artificial neural network for an intelligent wall/lane-following vehicle. Silva et al. (2012) proposed a fuzzy path-following controller for the ISRobotCar equipped

with localization and perception systems for autonomous navigation. For chained systems theory, Nunes and Bento (2007) and Arogeti and Berman (2012) used analogous chained system approach to linearize the path following kinematics equations before adopting other linear control strategies. For optimal control, in Goodarzi et al. (2008) the linear quadratic regulator (LQR) method was adopted for automatic path controller design based on integrated steering and external yaw-moment control. In Yang et al. (2012) a quasi-linear optimal brake-based path controller was proposed for a passenger vehicle to reduce secondary collision risk.

As for lane keeping, the more commonly used approaches are linear control algorithms. That is because the path following errors are usually assumed sufficiently small in lane keeping control, and the system model can then be considerably simplified, usually to linear form. H_∞ control based on linear matrix inequalities (LMIs) is mostly used to deal with lane keeping manoeuvre, as there exist unavoidable system uncertainties and disturbances. Enache et al. (2009) proposed a concept linking Lyapunov theory with LMIs optimization to ensure the vehicle to remain within the lane borders while converging towards the centerline, and the torque control input is limited to safe values to guarantee the passengers' comfort. Wu et al. (2010) proposed an integrated robust model matching chassis controller to improve vehicle handling performance and lane keep ability based on H_∞ controller and LMIs, which integrates active rear wheel steering control, longitudinal force compensation and active yaw moment control. In Enache et al. (2010), a switching strategy was built to govern the driver-assistance interaction, and the resulting hybrid system was formalized as an input/output (I/O) hybrid automaton. Composite Lyapunov functions, polyhedral-like invariant sets, and LMI methods constitute the heart of the approach used to design the lane-departure avoidance

(LDA) system. Enache et al. (2011) presented the design and experimental test of an active steering assistance system that offers two functions: lane departure avoidance by temporary activation and maintaining vehicle heading by permanent activation. Specific constraints related to each of the two functions are taken into account in the control design of the steering assistance by using LMI and BMI (bilinear matrix inequality) optimization methods.

1.1.2 Lateral Control of Independently Actuated Vehicles

Autonomous driving is usually designed in electric vehicles (Pérez et al., 2011), since electric AGVs can retain considerable superiorities from vehicle electrification. There are many advantages for AGVs designed with electric drives. Electric AGVs will likely reduce energy consumption, environment pollution, and increase energy security (Hu et al., 2015; Zou et al., 2012). Autonomous driving requires that the AGVs have dependable security, efficiency and flexibility (Li et al., 2015). Under this circumstance, the emerging independently actuated (IA) electric vehicle (Wang et al., 2011) is a promising architecture to provide potentials for improving active security, maneuverability and flexibility of autonomous vehicles. The in-wheel motors (or hubs), mounted in IA vehicles to provide independent actuation, can bring flexible actuation, fast and precise torque responses (Wang and Wang, 2011), thus can yield better control performance and security. The IA AGV, incorporating the merits of independent actuation and AGV vehicle, is a promising solution for achieving greater road security. Numerous studies have revealed that IA AGV is a promising vehicle architecture for its capability in considerably enhancing the vehicle maneuverability, stability and safety in adverse or even defective driving conditions (Wang et al., 2015).

The control problems of vehicle lateral stability and handling have always been

crucial and attracting wide research interests (Naranjo et al., 2008). A series of lateral dynamics control strategies have been presented so far. Such as, antilock braking systems (ABS) control (Shim et al., 2008), traction control (Hu et al., 2011), active front-wheel steering (AFS) control (Doumiati et al., 2013), direct yaw-moment control (DYC) (Wang, 2007), etc. Among them, DYC has long been regarded as a promising lateral control method, owing to its capability in effectively enhancing vehicle active safety and handling, especially in severe driving maneuvers. DYC generally exists in IA vehicles, resulting from the actuator redundancies. Integrated AFS and DYC control has also been extensively utilized to further enhance vehicle handling and stability. A stabilizing observer-based control algorithm integrating AFS and DYC for an in-wheel-motored vehicle was proposed in (Geng et al., 2009). A multi-layer integrated controller of active front-wheel steering and direct yaw-moment was developed in (Mashadi and Majidi, 2011) for a hybrid electric vehicle with engine-driven front wheels and in-wheel traction motors at rear wheels. Nam et al. (2012) presented a method for using lateral tire force sensors to estimate vehicle sideslip angle and to improve vehicle stability of in-wheel-motor-driven electric vehicles based on active steering control and an independent in-wheel motor control scheme. A combined AFS and DYC controller with good robustness against in-vehicle network-induced time-varying delays for the lateral motion and stability control of four-wheel-independent-drive electric vehicles was proposed in (Shuai et al., 2014). As for autonomous driving, DYC's application can offer flexible actuation and rapid torque response and is likely to lend a strong support to solve related control issues of AGVs.

The actuator redundancies in IA AGVs greatly contribute to the vehicle motion control through the direct yaw moment, which is generated by the differential

driving forces. Besides that, another advantage of the IA electric vehicles compared with traditional electric vehicles is that the front direct yaw moment can produce a differential drive assisted steering angle, which can be utilized to steer the vehicle when the regular steering system fails. Differential drive assisted steering (DDAS) is a novel steering mechanism for IA AGVs, which is generated by the differential torque between the left and right wheels (Hu et al., 2016). When the regular steering system is in failure, DDAS mechanism in IA electric vehicles can be activated to steer the front wheels, and thus to guarantee the implementation of normal steering commands. The differential steering angle is generated by the differential torque between the front left and front right wheels, which are independently actuated by the in-wheel (or wheel) motors.

Several previous research achievements were made on the vehicle motion control with the DDAS system. Li et al. (1998) proposed a measure of assist steering based on integrated steering and traction/braking system. Its idea is derived from skid-steering of tracked vehicle, and applied to four non-steerable wheel-drive electric vehicle with independent wheel torque control. Its simulation results shows that this type of vehicle steered with this method can have similar moving trajectory to conventional vehicle with steerable front wheels. But when moving on large curvature path, due to priority of stability compensator, the vehicle's cornering radius is much bigger than conventional vehicle. Hoogterp et al. (1999) named skid-steering of wheeled combat vehicles as differential torque steer, this application is a tradeoff between the running speed and cross-country mobility. But the key point is that the combat vehicle does not have steerable wheel for space-saving, so it is still skid-steering. Besselink (2003) proposed an integration of steering system and traction system, which is also about how to utilize differential drive torque of rear axle to assist steering and improve vehicle's steering

performance. Some other literatures such as Jang et al. (2004); Nozaki (2005), also proposed the measure of utilizing differential braking torque to correct steering maneuver. Shuang et al. (2007) discussed skid steering applied to four wheel drive electric vehicles. In such vehicles, steering is achieved by differentially varying the speeds of the lines of wheels on different sides of the vehicle.

None of them mentioned above utilized the differential drive torque between the wheels on both sides to supply assist force to steer the vehicle when conventional steer linkages remains. They discussed the assisted steering measure using differential traction/braking torque, but did not consider a power steering measure to reduce the steering effort at all. Wu et al. (2008) has proposed similar idea to supply steering assist force by differential driving of two front wheels of electric vehicle, which has electrical steering system according steering geometry. However, it did not bring forward this power steering method formally and explicitly, and what was the effect of differential drive torque of rear axle on this power assisted steering system. Thacher et al. (2009) proposed a patent on an assisted steering system operated by controlling the speed of inner rear wheel to improve front axle steering maneuverability, when the rear axle of the utility off-road vehicle has large load distribution. Wang et al. (2011) proposed an indirect power steering measure named as differential drive torque assisted steering, and validated its feasibility of assisting steering, capability of road feel keeping and the effect of the torque distribution control system.

1.1.3 Problem Statement

From the above overview, it is concluded that the independent actuation is likely to achieve better control performance and obtain greater security for AGVs, and the DDAS angle generated by the front direct yaw moment can be utilized to

steer the vehicle when the regular steering system fails. In this context, this thesis investigates the robust path-following control issue for IA AGVs, and concentrates on transient performance improvement from a safety perspective. Based on the literature review, the following four problems are proposed as the motivations for the research of this thesis :

1. In the above literatures, the desired vehicle heading in path following is usually defined as the tangent direction on the desired path. Their strategies work well and the path following objectives are fulfilled effectively, in moderate driving conditions, i.e., in low-speed driving or around low-curvature road. However, few experiments or high-fidelity simulations were conducted to verify the reasonability of that practice. The extreme conditions, i.e., high-speed driving or large curvature, were always neglected. In fact, the control effects of the path following in extreme conditions may no longer be as satisfactory as that in gentle conditions shown in previous literatures, and thus needs further investigation;

2. The control approaches in the above literatures were proposed to just stabilize the path following errors, little research addressed the lateral offset constraint issue from a driving safety perspective, i.e., how to guarantee a sufficiently small and safe bound for lateral in presence of sliding effects and model uncertainties. In actual operation of AGVs, the driving lanes/safe regions are usually restricted. In such a situation, research on lateral constraint control is essential and significant. In addition, the literatures which investigated the path following problem for AGVs based on the integrated AFS and DYC control are rather limited;

3. Transient performance improvement is seldom considered in path-following control of AGVs, which impacts on the driving security and riding comfort.

The transient performance can be evaluated based on the indexes of the rise time, convergence speed, transient overshoots, and the steady-state errors, etc. Actually, it is generally hard to converge the two path following errors (i.e., lateral offset and heading error) to zero simultaneously for the path with changing or large curvature, and this effect is more severe in the presence of the input saturations, system uncertainties and external disturbances;

4. The previous research mainly regarded the differential drive as an assisted power source for steering to alleviate the driving manoeuvre. Actually, D-DAS can also be utilized as the exclusive steering power source to provide emergency steering actuation in case of the active steering system failure. When the steering motor breaks down, the regular active steering system will be out of control, triggering great danger to vehicles. In this situation, DDAS generated by the differential drive torque of the front axle can be utilized to realize the normal steering function. This principle can be employed for automatic steering without the external steering power in faulted-steering condition for path following control of AGVs, but few related literatures investigated that mechanism.

1.2 Contributions

To guarantee the vehicle lateral stability, the path following control for ground vehicles needs to consider the inevitable tire sliding effects, system uncertainties and disturbances and tire force saturations. Among the existing lateral dynamics control strategies, DYC can effectively enhance vehicle active safety and handling, especially in severe driving conditions. Integrated control with AFS and DYC can be utilized to further enhance vehicle handling and stability. Therefore, the

research of this thesis is to robustly improve the transient performance of path following for AGVs simultaneously considering more practical interference factors including the parametric uncertainties, input saturations for AFS and tire force, and states constraints, etc. Some critical vehicle states/road parameters may be continuously changing for path following in complex environment, such as tire cornering stiffness, vehicle longitudinal speed, tire-road friction coefficient and path curvature. Effective control actuation is a premise to guarantee the realization of the control objective, but due to the physical limit of the in-wheel motor and vehicle mechanism, control actuators have saturation problem, which may considerably affect the control effects or even system stability.

To this end, this thesis has proposed a novel nonlinear control technique to constrain the lateral offset in the reasonable scope, and a novel path following modeling approach and two novel nonlinear control techniques to reduce the overshoots and steady-state errors in the path following control of AGVs, respectively. The ultimate control objective is to increase the path following accuracy and speed, and reduce the AGV's possibility of surpassing the safety lanes, thus to improve the vehicle handling and stability as well as the vehicle ride comfort. In general, this research work focuses on constraining the path following errors and improving the transient performance for IA AGVs, either by modeling amendment or controller design. The contributions of the thesis are listed in the following five aspects:

A. Desired Heading Amendment for Path Following

The desired vehicle heading in path following is commonly defined as the tangent direction on the desired path. However, we find this traditional definition may deteriorate the path-following performance. Thus we provide an amendment to the definition of the desired heading, and redefine the heading error by adding

up the traditionally defined heading error and the sideslip angle. The amendment can realize a more accurate path-following maneuver, and enables the path following errors to be converged to zero simultaneously.

B. Output Constraint Control for Lateral Offset in Path Following

To restrict the lateral offset in path following for four-wheel independently actuated (FWIA) AGVs, we propose a novel output constraint controller to strictly bound the lateral offset to prevent the vehicle from transgressing the safety bound in path following. The control strategy is designed by using hyperbolic projection technique based on feedback dominance backstepping, which aims to overcome the explosive complexity in backstepping. The proposed nonlinear controller can make the vehicle lateral offset in path following strictly bounded.

C. Robust Composite Nonlinear Feedback Control for Path Following of FWIA AGVs

To compositively consider the system uncertainties, tire fore saturations and variation of the desired-path curvature in the path-following controller design, we propose an accurate, fast and robust path-following control approach for FWIA AGVs via integrated control of the AFS and DYC. A novel integral sliding mode (ISM)-based composite nonlinear feedback (CNF) control technique considering the multi-input multi-output and the time-varying tracking reference is designed. The proposed controller has combined the advantages of CNF control in improving the transient performance and ISM control in guaranteeing good robustness.

D. Transient Performance Improvement for Path Following Control of IA AGVs with Differential Steering

The front DDAS can be used to achieve the path following control for IA AGVs in the case of the complete failure of the active front-wheel steering system. To improve the transient performance of the fault-tolerant control with the DDAS,

we propose a novel multiple-disturbances observer-based CNF approach to realize the path following control considering the tire force saturations. The disturbance observer is designed to estimate the external multiple disturbances with unknown bounds.

E. Experiment Study of DDAS: Model Verification and Lane Change Control

Experiments have been conducted to verify the existence and effectiveness of the DDAS mechanism. Firstly, a open-loop model verification test was conducted to prove that the differential torque between the left and right wheels can generate a differential steering angle when the steering motor completely fails. Secondly, the closed-loop lane change control experiment was conducted, which shows that the generated DDAS angle can be used to guarantee normal steering function.

1.3 Organization

The rest of this thesis are organized as follows:

In Chapter 2, the path following for AGVs is investigated. This chapter points out that the traditional desired heading may deteriorate the path following performance, and provides an amendment to the definition of the desired heading, which realizes a more accurate path following manoeuvre with better performance.

In Chapter 3, the path following problem for FWIA AGVs is investigated. A novel output constraint controller is proposed to compactly bound the lateral offset in path following and maintain the vehicle lateral stability in the presence of tire sliding effects.

In Chapter 4, a novel ISM-based CNF control technique is proposed to improve the transient performance in the path following of FWIA AGVs considering the system uncertainties, input saturations and variation of the path curvature. Chattering is avoided by using a multivariable super-twisting algorithm (STA).

In Chapter 5, to improve the transient performance of the fault-tolerant control with the DDAS in the case of the complete failure of the active steering system, a novel multiple-disturbances observer-based CNF approach is proposed to realize the path following control for IA AGVs considering the tire force saturations.

In Chapter 6, the experiment results are presented to verify the existence and effectiveness of the DDAS mechanism. The open-loop test is used to prove that the differential torque can generate a differential angle. The closed-loop experiment is used to prove that DDAS can maintain the normal steering performance.

In Chapter 7, this dissertation is summarized and several further research directions are discussed.

Chapter 2

Desired Heading Amendment in Path Following of AGVs

This chapter includes the following **published IEEE Transactions journal paper**:

Chuan Hu, Rongrong Wang, Fengjun Yan, and Nan Chen, "Should the Desired Heading in Path Following of Autonomous Vehicles be the Tangent Direction of the Desired Path?" ***IEEE Transactions on Intelligent Transportation Systems***, vol. 16, no. 6, pp. 3084-3094, Dec. 2015.

C. Hu is with the Department of Mechanical Engineering, McMaster University, Hamilton, ON L8S 4L8, Canada, and also with the School of Mechanical Engineering, Southeast University, Nanjing 211189, China.

R. Wang and N. Chen are with the School of Mechanical Engineering, Southeast University, Nanjing 211189, China.

F. Yan is with the Department of Mechanical Engineering, McMaster University, Hamilton, ON L8S 4L8, Canada.

Co-authorship Declaration: The main idea was jointly developed by me and Prof. Wang. I had primitively found that the desired heading should not be defined as the tangent direction of the desired path in the path following control, and then, inspired by Prof. Wang, I proposed the novel desired-heading amendment to modify the traditional path following model. Prof. Wang gave me some suggestions about the paper structure and paper writing, and helped me in the CarSim simulation. He also helped me in the revisions of the manuscript and the replies to the review comments. Prof. Yan had discussed with me several times about the feasibility of the proposed approach, the stability of the closed-loop system, and the whole contribution of this paper. Prof. Chen also discussed with me about the proposed amendment, and gave me some helpful comments about the control strategy in this paper. Finally I completed the major work of the paper writing, simulation implementation and revisions.

Abstract

The path-following problem for autonomous vehicles is investigated in this paper. The desired vehicle heading is commonly chosen as the tangent direction on the desired path. This paper points out that the traditional definition of the desired heading may deteriorate the path-following performance, particularly when the vehicle is tracking a path with large curvature. That is because the sideslip angle

control and the yaw rate control are conflicting in the presence of sliding effects, and the sideslip angle does not equal to zero when the vehicle is tracking a curve path. This paper further provides an amendment to the definition of the desired heading, which realizes a more accurate path-following maneuver. In the controller design phase, backstepping is used to generate the required yaw rate, and an LQR controller is adopted to obtain the optimal active front steering input. The CarSim-Simulink joint simulation verifies the reasonability of the amendment to the desired heading.

Index Terms

Autonomous vehicles, path following, preview control, desired-heading amendment

2.1 Introduction

This Chapter implements a full-car model-based high-fidelity simulation based on CarSim-Simulink platform, and points out that, the desired heading in path following of AGVs should not be the tangent direction of the desired path, especially when the vehicle is tracking a path with large or changing curvature. Actually, in that condition, if the traditionally defined heading error is converged to zero, the lateral offset will hardly stay at zero. Similarly, if the vehicle accurately tracks a curve path without any lateral offset, the traditionally defined heading error cannot be zero. This dilemma is due to the following reasons: there exists unavoidable tire sliding effects, and the yaw rate is difficult to converge to the desired value as maintaining a reasonable sideslip angle is necessary for a smooth steering. In practice, it is not surprising that there exits drifting effects when vehicles are making fast turns. Since converging the lateral offset to zero is the primary task

for the path following, the heading control may need to be reconsidered.

Ultimately, the source of the above problem lies on that the traditional definition of the desired heading, which assumes that the desired vehicle heading is along the tangent direction on the desired path. Actually the direction of the vehicle's real velocity of the center of gravity (CG) does not coincide with the vehicle heading in curve path following, and the angle between them is exactly the sideslip angle. This can explain why the traditional definition of the desired heading, which neglects the sideslip angle, is unreasonable. If we follow the traditional definition of the desired heading to assume that the vehicle runs along the tangent direction of the desired path, it can be deduced that the real vehicle CG motion direction and the desired tangent direction differ by a sideslip angle. Since the sideslip angle increases in sharp turns, the control error would be aggrandized considerably in that situation, and the vehicle would be easily off course when tracking the curve path, especially in fast running or around sharp corners. Consequently, the lateral offset is difficult to converge to zero. To solve the above problem, this chapter proposes a novel definition for the desired heading in path following for AGVs in the presence of the sliding effects. By making an amendment to the desired heading, the lateral offset and the redefined heading error are feasible to be stabilized and converged to zero simultaneously, even in large-curvature path following, and the resultant path following effect is more accurate.

This chapter is organized as following. The modeling of path following and vehicle lateral dynamics are described in Section 2.2. The path following controller design based on the tradition definition of the desired heading is presented in Section 2.3. In this section the path following error kinematics is utilized to generate the required yaw rate based on backstepping, then an LQR controller is designed to give out the AFS input. Then a targeted case study is conducted,

via CarSim-Simulink simulation. The modification to the desired heading and the corresponding controller design are presented in Section 2.4, since the sideslip angle is usually hard to measure, an estimation method is employed to reconstruct it, followed by another verification case study. The conclusions complete this chapter in Section 2.5.

2.2 Modeling of Path following and Vehicle Lateral Dynamics

2.2.1 Path Following Model

The path following model is shown in Fig. 2.1. e is the lateral offset, which represents the distance from the CG of the vehicle to the closest point T on the desired path, i.e., the orthogonal projection point of CG on the desired path. ψ is the heading error, which is defined as the error between actual heading angle of the vehicle ψ_h, and tangential direction of the desired path ψ_d, i.e., $\psi = \psi_h - \psi_d$, while we know $\dot{\psi}_h = r$, where r is the yaw rate . L is the lookahead (or preview) distance, while e_p is the lookahead (or preview) error. v_x and v_y represent the vehicle longitudinal and lateral speed, respectively. σ represents the curvilinear coordinate (arc-length) of point T along the path from an initial position predetermined, and $\dot{\sigma} = d\sigma/dt$, while we can know $\sigma \geq 0$. ρ stands for the curvature of the desired path at the point T, and is related with σ.

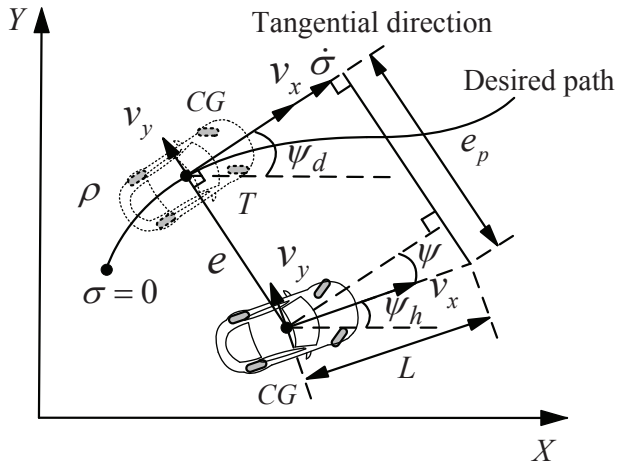

Figure 2.1: Path following model.

The curvilinear coordinate of point T along the path σ can be given as

$$\dot{\sigma} = \frac{1}{1 - e\rho(\sigma)} \left(v_x \cos\psi - v_y \sin\psi \right). \tag{2.1}$$

The path following error kinematics based on the Serret-Frenet equation is introduced in Skjetne and Fossen (2001), given by

$$\begin{cases} \dot{e} = v_x \sin\psi + v_y \cos\psi, \\ \dot{\psi} = \dot{\psi}_h - \dot{\psi}_d = r - \rho(\sigma)\, v_x, \end{cases} \tag{2.2}$$

where $\rho(\sigma)$ represents the curvature of the desired path. Generally, the control objective for path following problem in (2.2) is to globally asymptotically stabilize e and ψ, and converge them to zero.

Remark 2.2.1: The heading error in most of literatures is designed as the error between the vehicle's real heading and the tangent direction at the orthogonal projection point of CG on the desired path. However, this definition does not take into consideration the sideslip angle, which would not converge to zero if the vehicle tracks curve paths. The real CG velocity direction does not coincide with

the heading, they differ by a sideslip angle. If the traditional definition of the desired heading is adopted, when the heading error is rendered zero, the existence of the sideslip angle will make the CG move in a diverging direction (the direction of the real CG velocity). Additionally, since the sideslip angle is rather large in fast steering manoeuvre, the path following control effect would be deteriorated greatly. In the following discussion we will show the irrationality of this definition both in theory and simulation, and give a new definition of the desired heading.

Remark 2.2.2: In path following control design, preview control is a popularly used practice (Kritayakirana and Gerdes, 2012; Le and Stiharu, 2013; Janbakhsh et al., 2013; Mashadi et al., 2014). The preview error can be expressed as

$$e_p = e + L\sin\psi, \tag{2.3}$$

where a small angle approximation for ψ is commonly used, so the above equation is simplified into

$$e_p = e + L\psi. \tag{2.4}$$

Through converging e_p and ψ to zero, the lateral offset e can be converged to zero eventually, and then the path following objective can be achieved. As for how these literatures used the preview error to design control laws, Kritayakirana and Gerdes (2012) directly used e_p to design a proportion integration differentiation (PID) controller for the steering angle input without any stability proof; Le and Stiharu (2013), Janbakhsh et al. (2013), and Mashadi et al. (2014) designed controllers using e_p based on stabilization oriented strategies. Although good control results were obtained in these literatures, the controllers were rather complex and hard to tune. In the following passage we will show how the Lyapunov-based control law proposed in this chapter, which is more concise but with the stability vindicability,

is related with the preview control method.

2.2.2 Vehicle Lateral Dynamics Model

In this study, a 2 degrees of freedom (DoF) lateral dynamics model of vehicles is presented for controller design as shown in Fig. 2.2. The vehicle has mass m, the moment of inertia I_z through the CG about the yaw axis. The front and rear wheel axles are located at distances l_f and l_r from CG, respectively. β and r stand for the sideslip angle and the yaw rate of the vehicle, respectively. F_{yi} means the lateral tire force of the ith tire, where $i = fl, rl, fr, rr$. The front and rear lateral tire forces F_{yf} and F_{yr} are related with the front and rear wheels slip angles α_f and α_r, respectively. δ_f is the steering angle and is the only control input in this chapter. We assume that v_x is a constant, and the steering angles, tire slip angles of the left and right tires are the same, respectively.

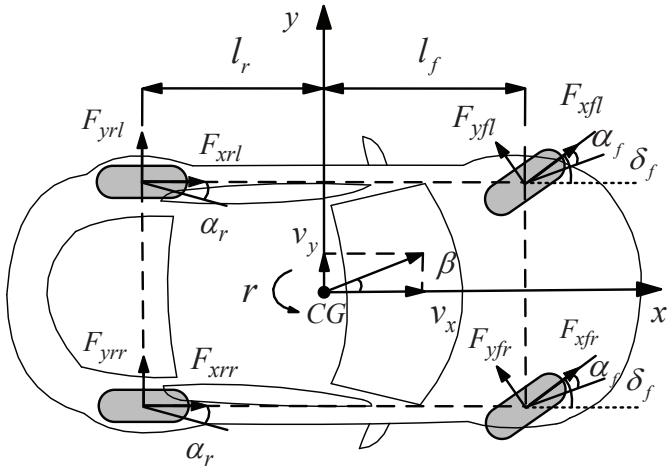

Figure 2.2: 2-DoF model of vehicle in the presence of sliding effects.

The handling dynamics equations for the 2-DoF model of vehicle in the yaw

plane can be given as follows (Abe, 2015)

$$\begin{cases} \dot{\beta} = a_{11}\beta + a_{12}r + b_1\delta_f, \\ \dot{r} = a_{21}\beta + a_{22}r + b_2\delta_f, \end{cases} \tag{2.5}$$

the model parameters in (2.5) are given as

$$\begin{aligned} a_{11} &= -\frac{2\left(c_f + c_r\right)}{mv_x}, \quad a_{12} = -1 - \frac{2\left(l_f c_f - l_r c_r\right)}{mv_x^2}, \\ a_{21} &= \frac{2\left(l_r c_r - l_f c_f\right)}{I_z}, \quad a_{22} = -\frac{2\left({l_f}^2 c_f + {l_r}^2 c_r\right)}{v_x I_z}, \\ b_1 &= \frac{2c_f}{mv_x}, \quad b_2 = \frac{2l_f c_f}{I_z}, \end{aligned} \tag{2.6}$$

where c_f and c_r stand for the cornering stiffnesses of the front and rear tires, respectively, in the condition that the tires operate in the linear region. (2.5) can be transformed into linear state expression as

$$\dot{x}(t) = Ax(t) + Bu(t), \tag{2.7}$$

where, $x(t) = [\beta,\ r]^T$, and

$$A = \begin{bmatrix} a_{11} & a_{12} \\ a_{21} & a_{22} \end{bmatrix}, \quad B = \begin{bmatrix} b_1 \\ b_2 \end{bmatrix}, \quad u = \delta_f. \tag{2.8}$$

Generally, the control objective for vehicle lateral motion control is to make the sideslip angle and yaw rate track their respective required value. And, usually the desired sideslip angle is set as zero to improve the vehicle lateral stability (Ahmadi et al., 2009; Du et al., 2011; Tchamna and Youn, 2013). The required yaw rate is generated according to the path following desire. Our control objective towards systems (2.5) and (2.2) is to globally asymptotically stabilize the two path

following error variables e and ψ with the control input δ_f .

2.3 Path Following Control based on Traditional Definition of the Desired Heading

In this section, we focus on the path following controller design with basic and commonly-used control method using the traditional definition of the desired heading, which is the tangent direction at the orthogonal projection point of vehicle CG on the desired path. The required yaw rate is generated using backstepping method, and has a form of P controller; the steering angle input is obtained via the optimal control towards the vehicle handling and stability. Then a verifying case study is conducted based on a CarSim-Simulink simulation.

2.3.1 Controller Design

1) *Required Yaw Rate Generation*

In this section, we will give a required yaw rate based on (2.2), which can satisfy the path following objective. It is designed by backstepping method (Li et al., 2009). The controller is supposed to globally asymptotically stabilize e and ψ.

Step 1: Design the first Lyapunov function $V_1(t) = \frac{1}{2}e^2$, its derivative is given by

$$\dot{V}_1 = e\dot{e} = e\left[v_x \frac{\sin\psi}{\psi}(\psi - \alpha_1 + \alpha_1) + v_x\beta\cos\psi\right]. \tag{2.9}$$

Select $\alpha_1 = -k_1 e$, $z_2 = \psi - \alpha_1$, where k_1 is a positive constant. Then we have

$$\dot{V}_1 = -k_1 v_x e^2 \frac{\sin\psi}{\psi} + v_x e \frac{\sin\psi}{\psi} z_2 + v_x \beta e \cos\psi, \tag{2.10}$$

which indicates, if $z_2 = 0$, $|e(\infty)| \leq \bar{e}(t) = \frac{|\beta|}{k_1}\left|\frac{\psi}{\tan\psi}\right|$, and if k_1 is chosen sufficiently large, we have $e \to 0$, as $\beta \to 0$.

Step 2: Design the second Lyapunov function $V_2(t) = V_1(t) + \frac{p_1}{2}z_2^2$, where p_1 is a positive constant, whose role will be apparent in the subsequent analysis. $\dot{V}_2$ is given by

$$\begin{aligned}\dot{V}_2 &= -k_1 v_x e^2 \frac{\sin\psi}{\psi} + v_x \beta e \cos\psi + v_x e \frac{\sin\psi}{\psi} z_2 + p_1 z_2 \dot{z}_2 \\ &= -k_1 v_x e^2 \frac{\sin\psi}{\psi} + v_x \beta e \cos\psi + \\ &\quad p_1 z_2 \left[r - \rho v_x + k_1 v_x \frac{\sin\psi}{\psi} z_2 + \left(\frac{1}{p_1} - k_1^2\right) e v_x \frac{\sin\psi}{\psi} + k_1 v_x \beta \cos\psi \right].\end{aligned} \tag{2.11}$$

If we select $p_1 = 1/k_1^2$, (2.11) becomes

$$\begin{aligned}\dot{V}_2 = &-k_1 v_x e^2 \frac{\sin\psi}{\psi} + v_x \beta e \cos\psi + \\ &\frac{1}{k_1^2} z_2 \left[r - \rho v_x + k_1 v_x \frac{\sin\psi}{\psi} z_2 + k_1 v_x \beta \cos\psi \right].\end{aligned} \tag{2.12}$$

Selecting $\alpha_2 = -k_2 z_2$, $z_3 = r - \rho v_x - \alpha_2$, and choose a positive constant k_2, to satisfy $k_2 > k_1 v_x$, we have

$$\begin{aligned}\dot{V}_2 = &-k_1 v_x e^2 \frac{\sin\psi}{\psi} + v_x \beta e \cos\psi - \frac{k_2}{k_1^2} z_2^2 \left[1 - \frac{k_1 v_x}{k_2} \frac{\sin\psi}{\psi} \right] \\ &+ \frac{1}{k_1^2} z_2 \left[z_3 + k_1 v_x \beta \cos\psi \right],\end{aligned} \tag{2.13}$$

which implies, if $z_3 \to 0$ or z_3 is bounded, $|z_2(\infty)| \leq \bar{z}_2(t) = \frac{[k_1 v_x \beta \cos\psi]}{k_2\left[1 - \frac{k_1 v_x}{k_2}\frac{\sin\psi}{\psi}\right]}$, and $z_2 \to 0$ as $\beta \to 0$ and k_2 is chosen sufficiently large. By making $z_3 = 0$, we can get

the required yaw rate (the desired yaw rate r_d) for path following objective,

$$\begin{aligned} r_\alpha(r_d) &= \rho(\sigma) v_x + \alpha_2 \\ &= \rho(\sigma) v_x - k_2(\psi + k_1 e), \end{aligned} \tag{2.14}$$

where k_1 and k_2 are positive constants, and satisfy $k_2 > k_1 v_x$. If $e \to 0$ and $z_2 \to 0$, since $\alpha_2 = -k_2 z_2$, $z_2 = \psi - \alpha_1$, $\alpha_1 = -k_1 e$, we can conclude that $\psi \to 0$, i.e., the path following objective is achieved if the real yaw rate r tracks the required value r_α.

Remark 2.3.1: Notice that the required yaw rate generation and vehicle motion control are not completely independent, i.e., the required yaw rate generation actually uses the current vehicle state and the path following errors, and is not entirely based on the path information, so there will be no error accumulation problem for the path following control.

Remark 2.3.2: Actually, the control law for the required yaw rate for path following objective can be expressed as $r_\alpha = r_{\alpha,\,\mathrm{ff}} + r_{\alpha,\,\mathrm{fb}}$, where $r_{\alpha,\,\mathrm{ff}}$ and $r_{\alpha,\,\mathrm{fb}}$ are the feedforward and feedback parts (Kritayakirana and Gerdes, 2012) of the required yaw rate, respectively. $r_{\alpha,\,\mathrm{ff}} = \rho v_x$, and $r_{\alpha,\,\mathrm{fb}}$ is actually designed as a P controller related with the two path following errors, and is expressed as $r_{\alpha,\,\mathrm{fb}} = -k_2(\psi + k_1 e)$.

Remark 2.3.3: (2.14) can be rewritten as

$$r_\alpha = \rho v_x - k_2(k_1 e + \psi) = \rho v_x - k_2 k_1 \left(e + \frac{1}{k_1}\psi \right). \tag{2.15}$$

Comparing (2.4) and (2.15), it is reasonable to deem that $\frac{1}{k_1} = L$, thus the required

yaw rate can be finally expressed as

$$r_\alpha = \rho v_x - \frac{k_2}{L} e_p, \tag{2.16}$$

where k_2 should be chosen to satisfy that $k_2 > \frac{v_x}{L}$. While in high speed path following, the preview distance L can be set about 20 m (Kritayakirana and Gerdes, 2012). No more work is needed except finding the appropriate k_2, whose lower bound is fixed, making the tuning work further simplified.

2) *AFS Control Law Design*

In this section, we focus on giving out the required AFS (Doumiati et al., 2013; Mashadi et al., 2013) input. The control input is designed to make the sideslip angle and the yaw rate track their respectively required values. The desired values of vehicle lateral dynamics states are selected as: the desired sideslip angle $\beta_d = 0$, the required yaw rate $r_\alpha = \rho v_x + \alpha_2$ as obtained in (2.14).

Here we deploy an LQR controller to minimize the errors of the sideslip angle β, yaw rate r with their respectively required values, and simultaneously, restrict the control input effort. Denote $x_d = [\beta_d \quad r_d]^T$, $\varepsilon = x - x_d = [\beta - \beta_d, \quad r - r_d]^T$, where $\beta_d = 0$, $r_d = r_\alpha$, the integrated performance index of the optimal control is defined as:

$$J_1 = \frac{1}{2} \int_0^\infty \left[\varepsilon^T Q \varepsilon + u^T R u \right] dt, \tag{2.17}$$

where $Q = \mathrm{diag}\,(Q_y, \ Q_z)$, $R = R_y$.

For the control input vector u can be designed as:

$$u = -R^{-1} B^T P \left(x - x_d \right), \tag{2.18}$$

in which the symmetric positive definite P is the solution of the Algebraic Riccati

Equation

$$PA + A^T P + Q - PBR^{-1}B^T P = 0. \tag{2.19}$$

Remark 2.3.4: This chapter focuses on the desired-heading amendment in path following of autonomous vehicles, and the investigated problem is a fundamental but critical issue for autonomous vehicles control design. Notice this chapter only uses the classic and commonly-used control method to design the path following controller, that is because we would like to avoid the misunderstanding that the investigated problem and the improved effect on path following in this chapter are just the results of the application of certain particular control algorithms. Therefore, we focus on highlighting the problem that whether the desired heading in path following of autonomous vehicles should be the tangent direction of the desired path, and the effectiveness of the desired-heading amendment, which are the two main innovations of this chapter, rather than the control algorithms.

2.3.2 Case Study 1

In this section, we present an S-turn simulation case implemented on CarSim-Simulink platform. In the simulation, the vehicle runs at a high speed (v_x =30 m/s) on a road with a high road friction ($\mu = 0.8$), and is supposed to track a clothoid curve, which is designed to approximate an S-turn path, with the curvature ρ_0 shown in Fig. 2.3. In Case Study 1, we perform three sub-simulation cases, by multiplying the original curvature ρ_0 by 1, 2, 3, respectively. The different sub-cases are represented by ρ_0, $2\rho_0$, $3\rho_0$ in the later figures, respectively. The S-turn path designed here consists of two path primitives: clothoids and arcs, with the curvatures of each path segment defined as the different functions of the distance σ along the path (Funke and Gerdes, 2013).

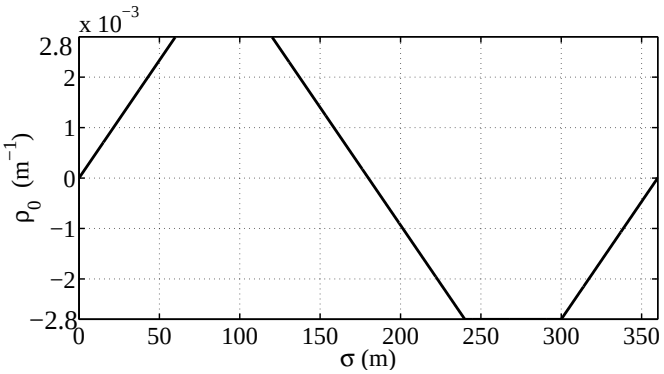

Figure 2.3: The curvature of the clothoid curve in the S-turn simulation.

The lateral offset result based on the traditional desired-heading is shown in Fig. 2.4. One can see when the vehicle tracks the curvature-varying path, the lateral offset e is difficult be to stabilized and converged to zero, and e increases with the increasing curvature. Notice that the case for the curvature $3\rho_0$ is an extreme case, the deviation of the lateral offset reaches about 0.6 m, causing great danger to the vehicle, since the vehicle's driving lane is usually limited. The heading error result is shown in Fig. 2.5. Similarly, when the curvature is varying, the heading error cannot be stabilized nor converged, and it grows as the path curvature is enlarged. That is because, the vehicle has to maintain a nonzero heading error with the reference path to resist the tire sliding effects, so as to better make the lateral offset converge to zero. Also, since the sideslip angle is not zero when the vehicle tracks a curve path, the heading error remains nonzero in order to render the velocity of CG along the tangent direction of the desired path. It can also be explained from the control process perspective, since our control objective is to converge $e_p = e + L\psi$ to zero, even if e_p is zero, the sliding effects and the nonzero sideslip angle will make ψ difficult to converge to zero, thus e cannot converge to zero, either.

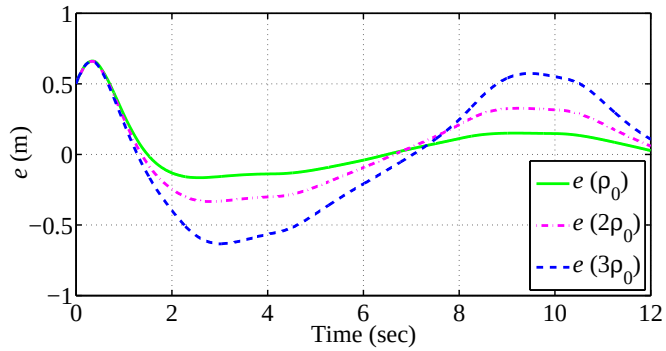

Figure 2.4: The lateral offset result based on the traditional desired-heading.

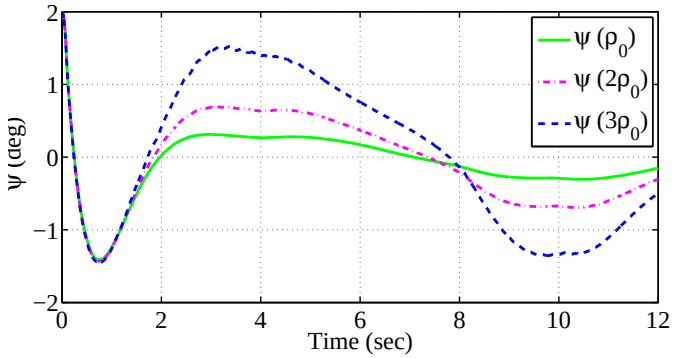

Figure 2.5: The heading error result based on the traditional desired-heading.

The sideslip angle is shown in Fig. 2.6. We can see that it cannot be stabilized nor converged, but it increases with the increase in path curvature. Owing to the LQR controller, the β remains in the safe region, which means the vehicle is stable through the path following process. Note that the appearance of the shake of the sideslip angle before 2 seconds is because we choose large initial path following errors to show the validity of the desired-heading amendment. Also, we can see the when the curvature increases, there are some chattering in the sideslip angle, that can be explained that when the vehicle states are large and close to the unstable region, the tires works near the nonlinear region, the measurement values of the vehicle states are with chattering thus the measurement cumulation errors are considerable. The lateral acceleration is shown in Fig. 2.7, we can

see that it increases with the increasing curvature, and when the curvature is $3\rho_0$, the lateral acceleration approaches the maximum acceleration μg. At that extreme condition, the tires begin to work in the nonlinear region, and the vehicle is easy to lose stability and control, which will cause fluctuations in the lateral acceleration and other vehicle states.

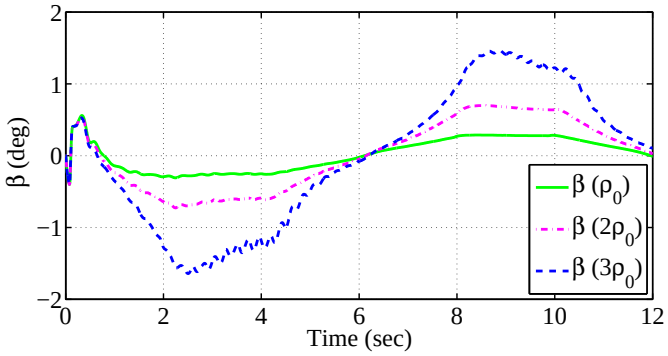

Figure 2.6: The sideslip angle result based on the traditional desired-heading.

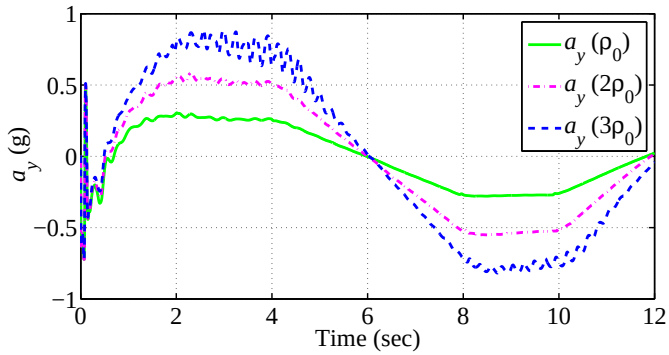

Figure 2.7: The lateral acceleration result based on the traditional desired-heading.

From Fig. 2.4- Fig. 2.6, we can conclude that the path following errors grow if the sideslip angle grows. When the sliding effect becomes more serious, that phenomenon will be more distinct, which reveals that the sideslip angle is a critical vehicle state impacting the lateral offset. According to the expression of the preview error $e_p = e + L\psi$, making amendment to the definition of the desired heading is a preferred way to make the new heading error and the lateral offset

zero simultaneously. In more practical terms, since the sideslip angle is not zero in steering manoeuvre, which means the lateral velocity is not zero, even if the longitudinal velocity is along the tangent direction of the desired path, the lateral offset cannot be zero. Therefore, making the longitudinal velocity deviated from the tangent direction at an certain angle is a possible solution to make the lateral offset zero, and this angle rightly should be the sideslip angle. Actually, comparing Fig. 2.5 and Fig. 2.6, we find that the heading error and the sideslip angle have almost the same contours but reversal-sign steady-state values, so it is a reasonable alternative to use sideslip angle to amend the heading error. That explains why we add up the traditionally defined heading error and the sideslip angle to define the new heading error in the following discussion.

The path following results are shown in Fig. 2.8, we can see the path following result based on the traditional definition of the desired heading is poor and needs to be improved. The path following effect is deteriorated if the path curvature becomes large, leading vehicles vulnerable in extreme conditions.

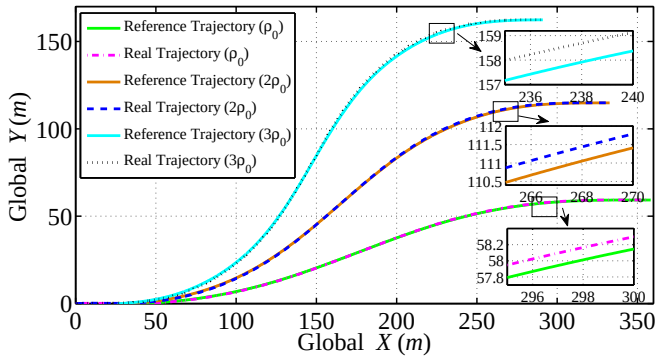

Figure 2.8: The path following result result based on the traditional desired-heading.

2.4 Path Following Control based on the Amended Definition of the Desired Heading

In this section we propose a novel definition to the desired heading to improve the path following effect, and the corresponding controller is designed based on the same control method shown in Section 2.2. Since the sideslip angle is usually hard to directly measure with low-cost sensors, we present an estimation using other measurable vehicle states. Then simulation results based on a high-fidelity and full-car model on CarSim-Simulink platform are presented to verify the effectiveness of the definition of the amended desired heading.

2.4.1 Amendment of the Desired Heading

As stated above, to converge e and ψ, our realization way includes two aspects: the first aspect is to converge the sideslip angle to zero; the second one is to keep the real yaw rate to track the required value. However, these two targets are conflicting (Gao et al., 2013), and it is generally difficult to achieve both these two targets simultaneously, especially for curve paths following. Actually, the existence of the sideslip angle is conducive to steering. Undoubtedly, necessary compromise should be made. Essentially, the main aspect of path following is to make the lateral offset converge to zero. From the practical application perspective, it is reasonable to converge only the lateral offset to zero, and tolerate a certain degree of deviation in the heading error. In this sense, the definition of the desired heading needs to be remade. The amendment of the definition for the desired heading will likely eliminate the deviation of the lateral offset, which is caused by the control conflict of the vehicle lateral dynamics, and thus make path following process more accurate.

The amended path following error kinematics model is shown in Fig. 2.9, where the subscript "a" represents the corresponding item after the desired heading is amended. The purpose of the amendment is to make the real CG velocity along the tangent direction on the desired path, since the sideslip angle is not zero when vehicle follows the curve path. Inevitably, the intersection angle between the new desired-heading and the tangent direction on the desired path equals exactly to the sideslip angle.

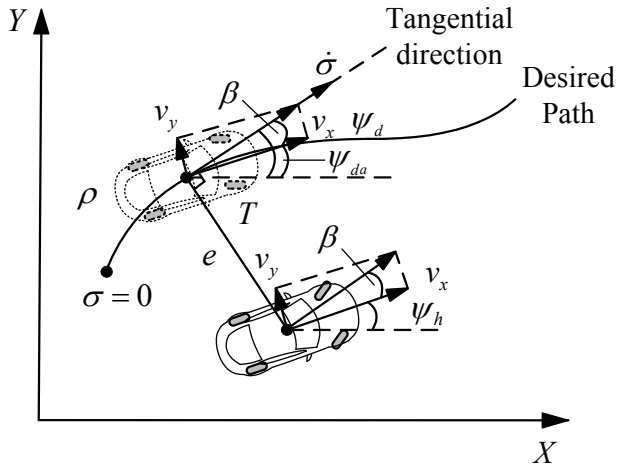

Figure 2.9: Amended path following error kinematics model

Based on Fig. 2.9, we define the new desired-heading ψ_{da} as

$$\psi_{da} = \psi_d - \beta. \tag{2.20}$$

Thereby, the amended definition of the heading error ψ_{Ame} is proposed in this chapter as

$$\psi_{Ame} = \psi_h - \psi_{da} = \psi_h - \psi_d + \beta = \psi + \beta. \tag{2.21}$$

Then the path following error kinematics in (2.2) can be modified as

$$\begin{cases} \dot{e} = v_x \sin \psi_{Ame} + v_y \cos \psi_{Ame}, \\ \dot{\psi}_{Ame} = r - \rho(\sigma) v_x + \dot{\beta}, \end{cases} \tag{2.22}$$

while the preview error is modified as

$$e_{pa} = e + L\psi_{Ame}, \tag{2.23}$$

and then (2.14) should be amended as

$$r_{\alpha a} = \rho v_x + \alpha_{2a} - \dot{\beta}, \tag{2.24}$$

where $\alpha_{2a} = -k_2(\psi_{Ame} + k_1 e) = -k_2 e_{pa}/L$.

The AFS control design for vehicle actuation is just similar as what is shown in Section 2.2. With the amendment, the new control objective is to make the lateral offset and the amended heading error to zero. Since the amendment is made as a sacrifice to bear the influence of the vehicle lateral control conflict, the lateral offset is likely to be stabilized and converged to zero more smoothly.

2.4.2 Sideslip Angle Estimation

The sideslip angle is usually difficult to be directly measured with low cost sensors (Zhao et al., 2011; Yoon and Peng, 2014). Here a classic sideslip angle reconstruction method (Fang et al., 2011) based on the linear 2-DoF vehicle model is adopted to obtain the vehicle slip angle. According to the lateral kinematic relationship, we have

$$\dot{v}_y = a_y - v_x r, \tag{2.25}$$

where a_y is the lateral acceleration, and is measurable, while r can be measured by a yaw gyroscope. a_y can be rewritten as

$$a_y = [v_x \;\; 0 \;\; v_x] \begin{bmatrix} \dot{\beta} \\ \dot{r} \\ \dot{\psi}_h \end{bmatrix} = H\dot{\xi}, \tag{2.26}$$

where ξ and H are defined as $\xi = [\beta \;\; r \;\; \psi_h]^T$, and $H = [v_x \;\; 0 \;\; v_x]$. Based on (2.5), the dynamics of ξ can be given by

$$\dot{\xi} = A_\xi \xi + B_\xi u, \tag{2.27}$$

where

$$A_\xi = \begin{bmatrix} a_{11} & a_{12} & 0 \\ a_{21} & a_{22} & 0 \\ 0 & 1 & 0 \end{bmatrix}, \quad B_\xi = \begin{bmatrix} b_1 \\ b_2 \\ 0 \end{bmatrix}. \tag{2.28}$$

Substitute (2.27) into (2.26), we have

$$a_y = HA_\xi \xi + HB_\xi u. \tag{2.29}$$

By solving the above equation, the sideslip angle can be reconstructed as

$$\beta = -\frac{m}{2\left(c_f + c_r\right)} a_y - \frac{\left(l_f c_f - l_r c_r\right)}{\left(c_f + c_r\right) v_x} r + \frac{c_f}{\left(c_f + c_r\right)} \delta_f. \tag{2.30}$$

Note that CarSim can provide the accurate measurement value of the sideslip angle, so a verification about the effectiveness of the slip angle estimation based control is achievable.

Remark 2.4.1: It should be noted that, the sideslip angle estimation is not

the focal point in this chapter, what we focus on is the desired-heading amendment and path following improvement. Hence a basic sideslip angle estimator is adopted to rule out the doubt that the advantage of proposed desired-heading amendment is only the result of the used advanced sideslip estimator. The linear estimator for the sideslip angle has already shown good estimation performance. Since the linear tire model is used in the sideslip angle estimation here, the estimator only works effectively in the linear region. Though the estimated sideslip angle may have relatively larger estimation error in the extreme driving condition, it will not impact the final conclusion made in this chapter, as the path following effect can still be substantially improved with the proposed method. Note that there are already many more accurate online sideslip angle estimation strategies, using nonlinear and more precise tire dynamics model (Zhao et al., 2011; Yoon and Peng, 2014; Li et al., 2014; Zhang et al., 2014), these sideslip angle estimation methods can be adopted here to improve the control effects. In general, in this work we are not dedicated on the control algorithm or the estimation strategy, instead, we concentrate on a fundamental and critical issue in path following.

2.4.3 Case Study 2

In this case study, we re-implement the CarSim-Simulink simulation based on the desired-heading amendment, with the sideslip angle estimated by the above proposed estimator. Similarly, we present an S-turn simulation case on a road with a high tire-road friction ($\mu = 0.8$). The vehicle runs at a high speed (v_x =30 m/s), and is supposed to track the same clothoid curve. We conduct simulations for three sub-cases to demonstrate our amendment strategy:

1. The sideslip angle comes from the estimation; the path curvatures are ρ_0, $2\rho_0$ and $3\rho_0$, respectively, where ρ_0 is shown in Fig. 2.3; the desired heading

follows the traditional definition; the abbreviation "Est, ρ ($2\rho_0$, $3\rho_0$), Tra" is used to stand for the first case;

2. The sideslip angle comes from the estimation; the path curvatures are ρ_0, $2\rho_0$ and $3\rho_0$, respectively; the desired heading follows the amended definition; the abbreviation "Est, ρ ($2\rho_0$, $3\rho_0$), Ame" is used to stand for the second case;

3. The sideslip angle comes from the measurement of CarSim; the path curvatures are ρ_0, $2\rho_0$ and $3\rho_0$, respectively; the desired heading follows the amended definition; the abbreviation "Car, ρ ($2\rho_0$, $3\rho_0$), Ame" is used to stand for the third case.

Note that the case that the sideslip angle comes from CarSim, the path curvature are ρ_0, $2\rho_0$ and $3\rho_0$, respectively, and the desired heading follows the traditional definition is simulated in Section 2.2, here the abbreviation "Car, ρ ($2\rho_0$, $3\rho_0$), Tra" is used to stand for that case. And the simulation results for the lateral acceleration are omitted in Case Study 2, one can refer to Fig. 2.7 for the elaboration of a_y.

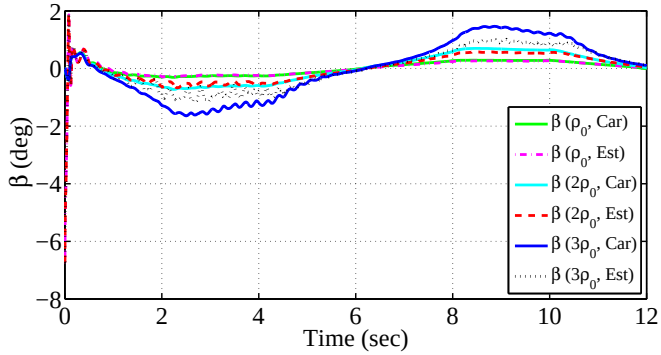

Figure 2.10: The sideslip angle estimation result result based on the traditional desired-heading.

The sideslip angle estimation based on the traditional desired-heading definition is shown in Fig. 2.10. We can see that the sideslip angle estimation is more

accurate when the path curvature is smaller. That can be explained that when the curvature increases, the tire slip angle and longitudinal slip ratio increase, and are likely to enter the nonlinear region. When that happens, the cornering stiffnesses of tires begin to decrease, and the decline is more severe if the sideslip angle becomes larger. However, our sideslip angle estimator is based on the 2-DoF linear model, and uses the constant cornering stiffnesses for calculation, so the consequent estimation error inevitably appears and is considerable. According to (2.30), the chosen cornering stiffnesses for estimation are larger than the real values, so the estimation value for the sideslip angle is relatively smaller than the real value, and if the curvature increases, the estimation error increases.

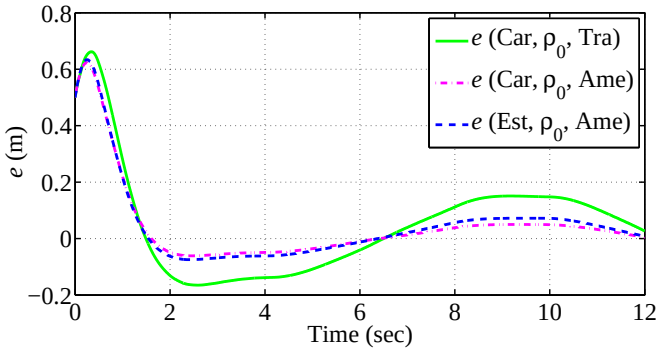

(a) ρ_o

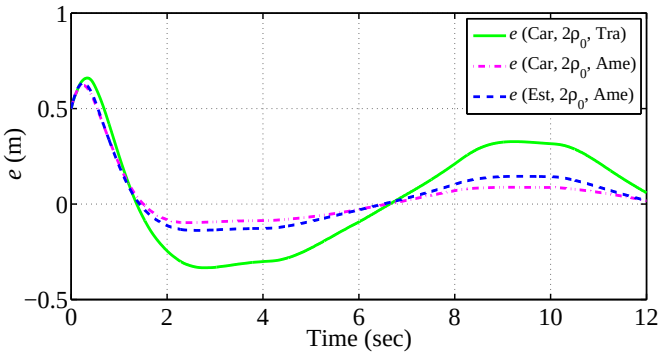

(b) $2\rho_o$

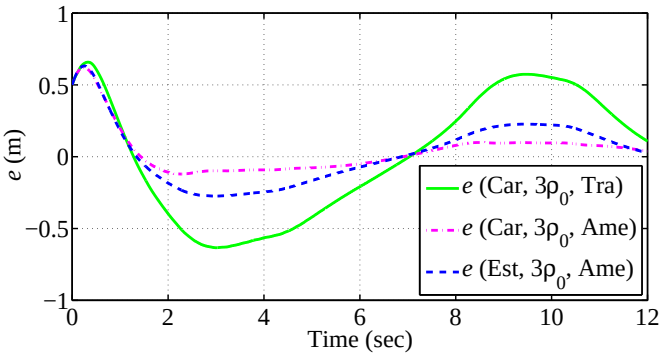

(c) $3\rho_o$

Figure 2.11: The lateral offsets result based on the traditional and the amended desired-headings, respectively.

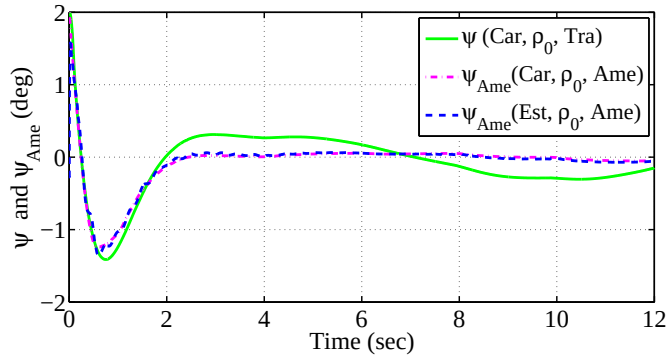

(a) ρ_o

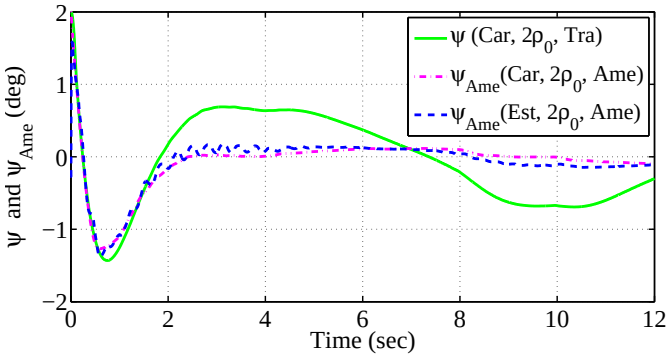

(b) $2\rho_o$

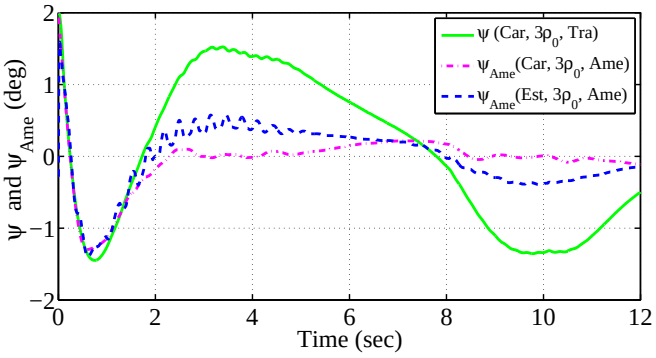

(c) $3\rho_o$

Figure 2.12: The heading errors result based on the traditional and the amended desired-headings, respectively.

The lateral offset result is shown in Fig. 2.11. One can see that by modifying the desired heading, the steady-state value of the lateral offset is effectively

reduced, even in extreme driving conditions. Though the linear sideslip angle estimator adopted in this chapter has large error when the curvature increases, the diminution in the lateral offset is still evident. Constraining the bound of the lateral offset in sharp corners contributes to better realization of the path following objective, and more importantly, reducing the possibility of the vehicle surpassing the safe driving zone. The increase in curvature will deteriorate the control effects for the lateral offset, this comes from the inaccurate estimation of the sideslip angle. It can be deduced that more accurate sideslip angle estimator will likely effectively improve the constraint control effect on the lateral offset. The heading error result is shown in Fig. 2.12. Similarly, when the curvature changes, the heading error is hard to be stabilized nor converged to zero. After the definition of the desired heading is amended, the new heading error ψ_{Ame} can be stabilized and converged to zero. Note that in extreme conditions, ψ_{Ame} has some chattering, which would be a normal phenomenon. The control effect on the new heading error is attenuated when the curvature increases, that is also due to the sideslip angle estimation error. However, by Fig. 2.12 the rationality of the amendment on the desired heading proposed in this chapter can be still convincingly proved.

The sideslip angle result is shown in Fig. 2.13. We can see that it cannot converge to zero in sharp corners, and it increases with the increase in the path curvature. The amendment to the desired heading does not impact much on the sideslip angle. It remains in the safe region, which means the vehicle is stable through the path following. Note that the large estimation error of the sideslip angle in extreme conditions is the cause of the control effects deterioration for other vehicle states.

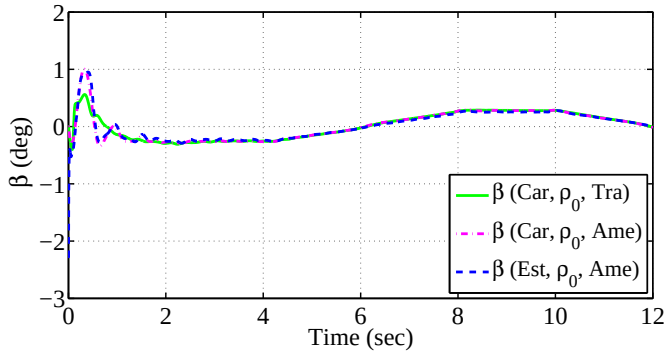

(a) ρ_o

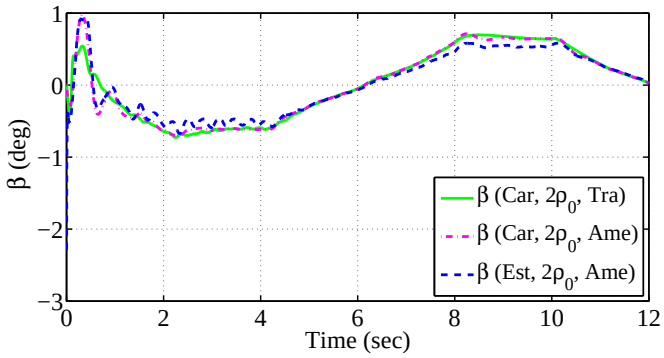

(b) $2\rho_o$

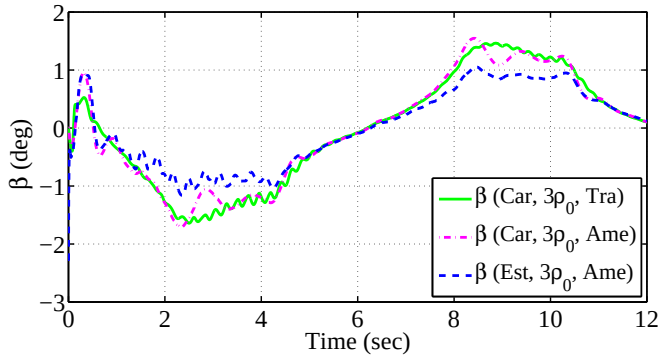

(c) $3\rho_o$

Figure 2.13: The sideslip angles result based on the traditional and the amended desired-headings, respectively.

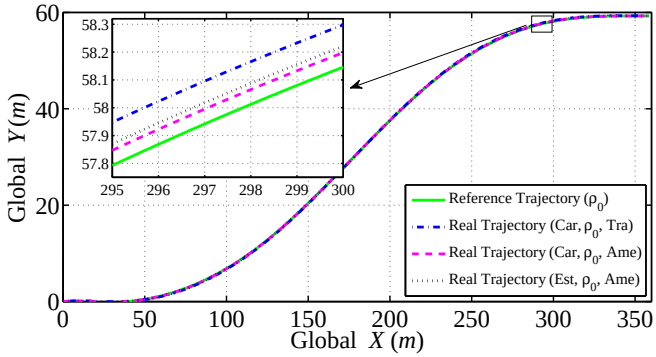

(a) ρ_o

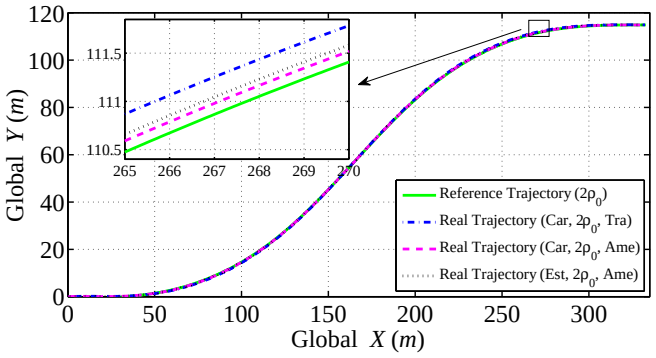

(b) $2\rho_o$

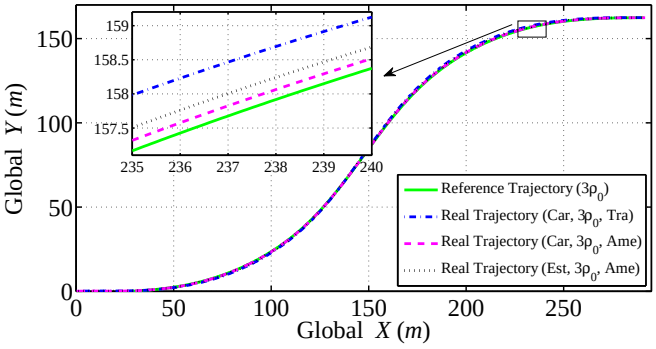

(c) $3\rho_o$

Figure 2.14: The path following results based on the traditional and the amended desired-headings, respectively.

The path following results are shown in Fig. 2.14, we can see the path following result based on the traditional definition of the desired heading is poor, and

after the desired heading is amended, the path tracking effect is improved considerably, which implies that vehicle can track the desired path more accurately. Even though the error in sideslip angle estimation deteriorates the improvement effects on the path following, it does not affect the conclusion that the desired-heading amendment can effectively improve path following effects, especially in sharp corners.

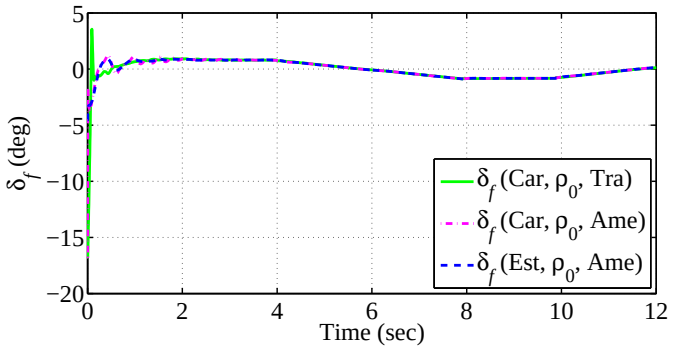

(a) ρ_o

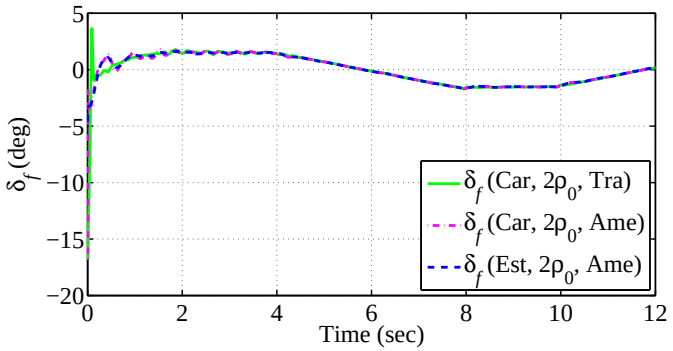

(b) $2\rho_o$

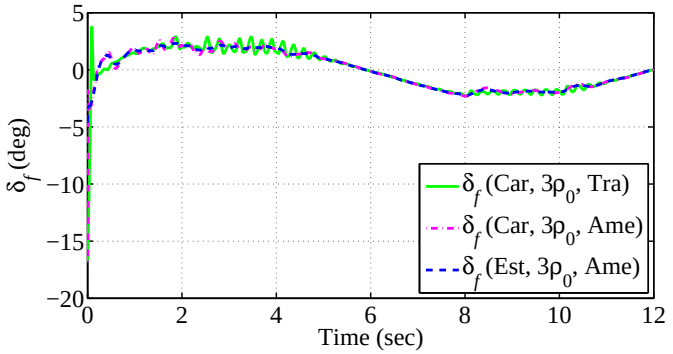

(c) $3\rho_o$

Figure 2.15: The steering angle results based on the traditional and the amended desired-headings, respectively.

Fig. 2.15 presents the steering angle input results in the S-turn simulation, and indicates that the steering angles are maintained in reasonable region with

the LQR controller. It is understandable that the magnitude of the steering angle increases with the increase in the path curvature. Also, we can find that the desired-heading amendment has relatively limited effect on the steering angle input. Similarly, the chattering in the response of the steering angle in the "$3\rho_0$" case is caused by the inaccuracy of the sideslip angle estimation.

2.5 Conclusion

This chapter deals with the path following control problem for autonomous vehicles, and proposes a new problem in path following errors convergence. The problem is whether the desired heading in path following of autonomous vehicles should be the tangent direction of the desired path, and the answer is "No". This chapter points out the reason for the negative answer is that there exists inevitable sliding effects, the sideslip angle control and the yaw rate control are conflicting, and the vehicle should maintain a reasonable sideslip angle for a smooth steering. Furthermore, this chapter makes an amendment to the definition of the desired heading. By making this amendment, the lateral offset and the new heading error can be smoothly stabilized and converged to zero simultaneously, even in large-curvature roads. The path following controller in this chapter is designed based on backstepping and LQR method, through active front steering. The results of two S-turn simulation cases based on a high-fidelity and full-car model via CarSim-Simulink have validated the desired-heading amendment can effectively improve the stabilization and convergence performances of the path following errors. It should also be noted that, the traditional definition for the desired heading can still work well in mitigatory driving conditions, however, it loses efficacy in extreme driving conditions. Our amendment can be applicable to wider range of driving conditions. It is worth pointing out that after adopting the

desired-heading amendment in the path following, the stable region of the vehicle may change. It is critical to maintain the equal vehicle stability when improving the path following effect, and we leave this issue for the future study.

References

Skjetne, Roger, and Thor I. Fossen. "Nonlinear maneuvering and control of ships." *OCEANS, 2001. MTS/IEEE Conference and Exhibition*. Vol. 3. IEEE, 2001.

Kritayakirana, Krisada, and J. Christian Gerdes. "Using the centre of percussion to design a steering controller for an autonomous race car." *Vehicle System Dynamics* 50.sup1 (2012): 33-51.

Le, Thanh Phuc, and Ion Stiharu. "An optimal preview driver model applied to a non-linear vehicle and an impaired driver." *Proceedings of the Institution of Mechanical Engineers, Part D: Journal of automobile engineering* 227.4 (2013): 536-548.

Janbakhsh, Amir Ali, Mohsen Bayani Khaknejad, and Reza Kazemi. "Simultaneous vehicle-handling and path-tracking improvement using adaptive dynamic surface control via a steer-by-wire system." *Proceedings of the Institution of Mechanical Engineers, Part D: Journal of automobile engineering* 227.3 (2013): 345-360.

Mashadi, Behrooz, Mehdi Mahmoudi-Kaleybar, Pouyan Ahmadizadeh, et al. "A path-following driver/vehicle model with optimized lateral dynamic controller." *Latin American journal of solids and structures* 11.4 (2014): 613-630.

Abe, Masato. *Vehicle handling dynamics: theory and application*. Butterworth-Heinemann, 2015.

Ahmadi, Javad, Ali Khaki Sedigh, and Mansour Kabganian. "Adaptive vehicle lateral-plane motion control using optimal tire friction forces with saturation limits consideration." *IEEE Transactions on vehicular technology* 58.8 (2009): 4098-4107.

Du, Haiping, Nong Zhang, and Fazel Naghdy. "Velocity-dependent robust control for improving vehicle lateral dynamics." Transportation research part C: emerging technologies 19.3 (2011): 454-468.

Tchamna, R., and I. Youn. "Yaw rate and side-slip control considering vehicle longitudinal dynamics." *International Journal of Automotive Technology* 14.1 (2013): 53-60.

Li, Zhen, Jing Sun, and Soryeok Oh. "Design, analysis and experimental validation of a robust nonlinear path following controller for marine surface vessels." *Automatica* 45.7 (2009): 1649-1658.

Kritayakirana, Krisada, and J. Christian Gerdes. "Autonomous vehicle control at the limits of handling." *International Journal of Vehicle Autonomous Systems* 10.4 (2012): 271-296.

Doumiati, Moustapha, Olivier Sename, Luc Dugard, et al. "Integrated vehicle dynamics control via coordination of active front steering and rear braking." *European Journal of Control* 19.2 (2013): 121-143.

Mashadi, Behrooz, Mehdi Mahmoodi-K, Amir H Kakaee, et al. "Vehicle path following control in the presence of driver inputs." *Proceedings of the Institution*

of Mechanical Engineers, Part K: Journal of Multi-body Dynamics 227.2 (2013): 115-132.

Funke, Joseph, and J. Christian Gerdes. "Simple clothoid paths for autonomous vehicle lane changes at the limits of handling." *ASME 2013 Dynamic Systems and Control Conference*. American Society of Mechanical Engineers, 2013.

Gao, Huijun, Weichao Sun, Shen Yin, et al. "Stability control for lateral vehicle motion with uncertain parameters and external nonlinearities." *Control Conference (CCC), 2013 32nd Chinese. IEEE*, 2013.

Zhao, Lin-Hui, Zhi-Yuan Liu, and Hong Chen. "Design of a nonlinear observer for vehicle velocity estimation and experiments." *IEEE Transactions on Control Systems Technology* 19.3 (2011): 664-672.

Yoon, Jong-Hwa, and Huei Peng. "Robust vehicle sideslip angle estimation through a disturbance rejection filter that integrates a magnetometer with GPS." *IEEE Transactions on Intelligent Transportation Systems* 15.1 (2014): 191-204.

Fang, Hao, Lihua Dou, Jie Chen, et al. "Robust anti-sliding control of autonomous vehicles in presence of lateral disturbances." *Control Engineering Practice* 19.5 (2011): 468-478.

Li, Liang, Gang Jia, Xu Ran, et al. "A variable structure extended Kalman filter for vehicle sideslip angle estimation on a low friction road." *Vehicle System Dynamics* 52.2 (2014): 280-308.

Zhang, Hui, Xiaoyu Huang, Junmin Wang, et al. "Robust energy-to-peak sideslip angle estimation with applications to ground vehicles." *Mechatronics* 30 (2015): 338-347.

Chapter 3

Output Constraint Control on Path Following of FWIA AGVs

This chapter includes the following **published IEEE Transactions journal paper**:

Chuan Hu, Rongrong Wang, Fengjun Yan, and Nan Chen, "Output Constraint Control on Path Following of Four-Wheel Independently Actuated Autonomous Ground Vehicles," ***IEEE Transactions on Vehicular Technology***, vol. 65, no. 6, pp. 4033-4043, Jun. 2016.

C. Hu is with the Department of Mechanical Engineering, McMaster University, Hamilton, ON L8S 4L8, Canada, and also with the School of Mechanical Engineering, Southeast University, Nanjing 211189, China.

R. Wang and N. Chen are with the School of Mechanical Engineering, Southeast University, Nanjing 211189, China.

F. Yan is with the Department of Mechanical Engineering, McMaster University, Hamilton, ON L8S 4L8, Canada.

Co-authorship Declaration: The backstepping-based hyperbolic projection algorithm was primitively developed by Prof. Yan, which is a theoretical output constraint control algorithm. To apply this approach in the vehicle motion control, I had modified this algorithm, and combined it with the feedback dominance backstepping to overcome the "explosive complexity" in the standard backstepping in the higher-level controller. In the lower-level controller, I proposed the robust and adaptive LQR approach to reject the external disturbances and guarantee the vehicle lateral stability. The design of the adaptive gain in the lower-level controller was proposed by Prof. Wang. I had discussed the whole control strategy with Prof. Yan for several times, and discussed the vehicle modeling and application scenario of this paper with Prof. Wang. Also, Prof. Wang helped me solve several problems in the CarSim simulations. Prof. Wang and Prof. Chen discussed with me the paper writing, revisions and replies according to the review comments. I completed the major work of the paper writing, controller design, simulation and revisions.

Abstract

The path-following problem for four-wheel independently actuated autonomous ground vehicles is investigated in this paper. A novel output constraint controller is proposed to deal with the lateral offset control in path following and maintain the

vehicle lateral stability in the presence of tire sliding effects. The innovations of this work lie in the following two aspects: 1) A novel output constraint control strategy, namely, the hyperbolic projection method, is proposed to strictly bound the lateral offset to prevent the vehicle from transgressing the safety bound in path following; 2) an adaptive and robust linear quadratic regulator controller is adopted to obtain the optimal active front-wheel steering and direct yaw-moment control inputs with vehicle lateral stability consideration and to eliminate the effect of parameter uncertainties. CarSim-Simulink joint simulation results indicate that the proposed controller can compactly bound the lateral offset to avoid transgressing the safe boundary during path following, particularly in extreme driving conditions, in the presence of tire sliding effects and system uncertainties.

Index Terms

Autonomous ground vehicles (AGVs), four-wheel independently actuated (FWIA), hyperbolic projection, output constraint control, path following

3.1 Introduction

This chapter investigates the output constraint control on the lateral offset in path following of an FWIA AGV to prevent the vehicle from surpassing the safe zone, and make two contributions: 1) A novel output constraint control strategy is proposed by using hyperbolic projection techniques, based on feedback dominance backstepping (FDB) (Li et al., 2009), which is aiming to overcome the "explosive complexity" in backstepping. The proposed nonlinear controller is to make the vehicle lateral offset in path following strictly bounded; 2) An adaptive and robust LQR controller is employed to obtain the optimal AFS and DYC control inputs

and to eliminate the parameter uncertainties (or the lumped disturbances) in the 2-DoF linear vehicle model, with considering the vehicle lateral stability.

For the wheel torque distribution for the longitudinal tire forces, there are some existing works. Yuan and Wang (2012) presented an optimized torque distribution strategy for maximizing the overall motor efficiency for a front and rear-wheel-driven electric vehicle over a new European driving cycle. In Pennycott et al. (2014) the optimal wheel torque distribution for minimal power losses from the electric motor drives was evaluated in an offline optimisation procedure and then approximated using a simple function for online control allocation. A novel offline optimization procedure was developed in De Novellis et al. (2014) to assess the performance of alternative objective functions for the optimal wheel torque distribution of a four-wheel-drive fully electric vehicle. In Shyrokau et al. (2015) a new approach for integrated vehicle motion control was presented coordinating multiple vehicle subsystems of a passenger car based on restriction weights into the cost function of optimization-based control allocation. The above literatures had made good achievements, representing the recent progress in wheel torque distribution research. Nevertheless, since this chapter focuses on the output constraint control for the path following problem for autonomous vehicles, so a sample optimal wheel torque distribution method is used, with considering the vehicle load transfer.

The rest of this chapter is organized as following. The vehicle model and path following error kinematics are described in Section 3.2. The path following controller design is presented using hyperbolic projection-based feedback dominance backstepping (HFDB) in Section 3.3. Simulation results are illustrated in Section 3.4, followed by the conclusion in Section 3.5.

3.2 Modeling Of Vehicle Dynamics and Path following

3.2.1 Vehicle Dynamics Model

In this study, a 2-DoF dynamics model of FWIA vehicles is presented for controller design as shown in Fig. 3.1. The vehicle has the total mass m, the moment of inertia I_z through the CG about the yaw axis. The front and rear wheel axles are located at distances l_f and l_r from CG, respectively. v_x and v_y represent the longitudinal and lateral velocities of the vehicle, respectively. β and r stand for the sideslip angle and the yaw rate of the vehicle, respectively. F_{yi} means the lateral tire force of the ith tire, where $i = 1,\ 2,\ 3,\ 4 = fl,\ fr,\ rl,\ rr$, and we denote F_{yf} and F_{yr} as the generalized lateral tire forces of the front and rear tires, respectively, i.e., $F_{yf} = F_{yfl} + F_{yfr},\ F_{yr} = F_{yrl} + F_{yrr}$. The steering angle δ_f changes the heading direction of the front wheel, ΔM_z denotes the external yaw moment generated by in-wheel motors, and δ_f and ΔM_z are two control inputs in this chapter. We assume that v_x is a constant, and the steering angles, tire slip angles of the left and right tires are the same, respectively.

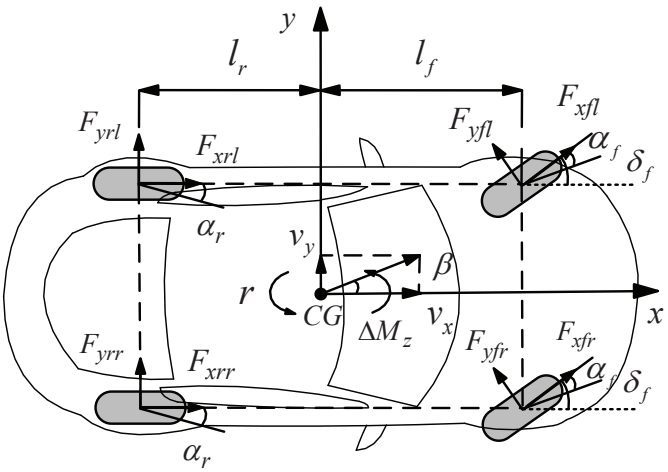

Figure 3.1: 2-DoF model of vehicle.

The handling dynamics equations for the 2-DoF model of vehicle in the yaw plane can be given as follows (Abe, 2015)

$$\begin{cases} mv_x\dot{\beta}\left(t\right) = F_{yf}\left(t\right) + F_{yr}\left(t\right) - mv_x r\left(t\right), \\ I_z\dot{r}\left(t\right) = l_f F_{yf}\left(t\right) - l_r F_{yr}\left(t\right) + \Delta M_z\left(t\right), \end{cases} \tag{3.1}$$

and $\Delta M_z\left(t\right)$ can be written as

$$\Delta M_z = \sum_{i=1}^{2} F_{xi}\left[(-1)^i l_s \cos\delta_f + l_f \sin\delta_f\right] + \sum_{i=3}^{4}(-1)^i l_s F_{xi}, \tag{3.2}$$

where l_s is the half of the wheel-base, F_{xi} means the longitudinal tire force of the ith tire, which needs to be obtained through control allocation. The front and rear lateral tire forces F_{yf} and F_{yr} are related with the front and rear wheels slip angles α_f and α_r, respectively, and can be expressed by

$$F_{yf} = c_f\alpha_f\left(t\right), \quad F_{yr} = c_r\alpha_r\left(t\right), \tag{3.3}$$

where c_f and c_r stand for the generalized cornering stiffnesses of the front and rear tires, respectively, and can be expressed as

$$c_f = c_{f0} + \Delta c_f, \quad c_r = c_{r0} + \Delta c_r, \tag{3.4}$$

where c_{f0} and c_{r0} stand for the generalized normal cornering stiffnesses of the front and rear tires, respectively, in the condition that the tires operate in the linear region. Δc_f, Δc_r represent the additional nonlinear terms, and are assumed

bounded. The front and rear slip angles can be given as

$$\begin{cases} \alpha_f(t) = \delta_f(t) - \dfrac{l_f r(t)}{v_x} - \beta(t), \\ \alpha_r(t) = \dfrac{l_r r(t)}{v_x} - \beta(t). \end{cases} \tag{3.5}$$

Substituting (3.3) and (3.5) into (3.1), the following equations can be derived

$$\begin{cases} \dot{\beta} = a_{11}\beta + a_{12}r + b_{11}\delta_f, \\ \dot{r} = a_{21}\beta + a_{22}r + b_{21}\delta_f + b_{22}\Delta M_z, \end{cases} \tag{3.6}$$

where the model parameters in (3.6) can be given as

$$\begin{aligned} &a_{11} = -\frac{c_f + c_r}{m v_x}, \quad a_{12} = -1 - \frac{l_f c_f - l_r c_r}{M v_x^2}, \\ &a_{21} = \frac{l_r c_r - l_f c_f}{I_z}, \quad a_{22} = -\frac{{l_f}^2 c_f + {l_r}^2 c_r}{v_x I_z}, \\ &b_{11} = \frac{c_f}{m v_x}, \quad b_{21} = \frac{l_f c_f}{I_z}, \quad b_{22} = \frac{1}{I_z}. \end{aligned} \tag{3.7}$$

System (3.6) can be transformed into linear state expression as

$$\dot{x} = \bar{A}x + \bar{B}u, \tag{3.8}$$

where, $x = [\beta,\ r]^T$, and

$$\bar{A} = \begin{bmatrix} a_{11} & a_{12} \\ a_{21} & a_{22} \end{bmatrix}, \quad \bar{B} = \begin{bmatrix} b_{11} & 0 \\ b_{21} & b_{22} \end{bmatrix}, \quad u = \begin{bmatrix} \delta_f \\ \Delta M_z \end{bmatrix}. \tag{3.9}$$

Equation (3.8) can be modified into

$$\dot{x} = (A + \Delta A)\, x + (B + \Delta B)\, u, \tag{3.10}$$

where A and B can be obtained by substituting $c_f = c_{f0}$ and $c_r = c_{r0}$ in (3.9), and ΔA and ΔB are the uncertainties due to the probable inaccuracy of the cornering stiffness c_f and c_r.

Generally, the control objective for system (3.6) is to design controller to make the sideslip angle and yaw rate track their respective required values. The desired sideslip angle is usually set as zero to improve the vehicle lateral stability (Ahmadi et al., 2009; Tchamna and Youn, 2013). In traditional manual driving vehicle, the required yaw rate is generally related with the driver's steering command, however, in AGVs, it is generated according to the path following desire.

3.2.2 Path Following Model

The path following error kinematics model is shown in Fig. 3.2. This figure shows the lane on which the AGV is supposed to drive. e represents the distance from CG to the closest point T on the desired path, i.e., the orthogonal projection point of CG on the desired path. e is named as "lateral offset" here. ψ is defined as the error between actual heading angle of the vehicle, ψ_a, and tangential direction of the desired path, ψ_d, i.e., $\psi = \psi_h - \psi_d$, while we know $\dot{\psi}_h = r$. ψ is named as "heading error". σ represents the curvilinear coordinate (arc-length) of point T along the path from an initial position predetermined, while we can know $\sigma \geq 0$, $\dot{\sigma} = d\sigma/dt$. ρ stands for the curvature of the desired path at the point T, and is related with σ. In actual driving situations for AGVs, the widths of their lanes are limited. In Fig. 3.2, a desired path is shown in the safe zone, i.e., the lane that the corresponding AGV is supposed to drive on; except the safe zone, there is the unsafe zone, e.g., the lane of other AGVs, road shoulder, or other dangerous regions.

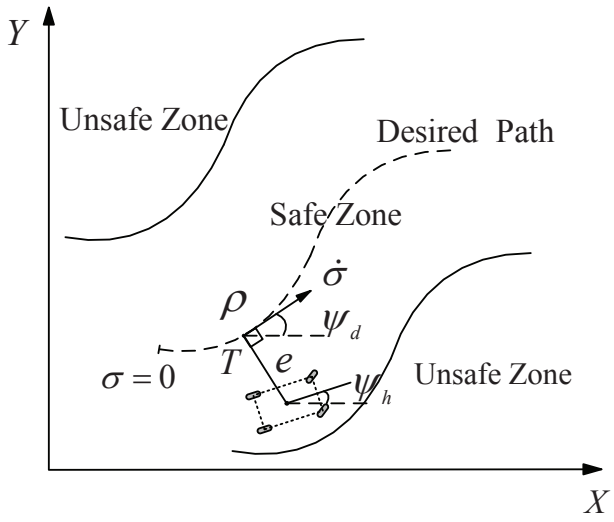

Figure 3.2: Path following error kinematics model.

The path following error kinematics can be given by

$$\begin{cases} \dot{e} = v_x \sin\psi + v_y \cos\psi, \\ \dot{\psi} = \dot{\psi}_a - \dot{\psi}_d = r - \rho(\sigma)\, v_x, \end{cases} \tag{3.11}$$

where $\rho(\sigma)$ represents the curvature of the desired path. Generally, the control objective for path following problem in (3.11) is to design controller to globally asymptotically stabilize e and ψ.

Our control objective towards (3.8) and (3.11) is to globally asymptotically stabilize the two path following error variables e and ψ with two control inputs δ_f and ΔM_z, with vehicle stability consideration. At the same time, we also consider reducing the magnitude of the bound of the lateral offset e, which has important impact on path following safety. It should be noted that vehicle stability consideration here means the vehicle lateral stability is guaranteed (the sideslip angle is constrained in a certain bound by a barrier function through an LQR controller later) when the path following objective is achieved, while path following safety here means the lateral offset is constrained to prevent the vehicle from surpassing

the safe zone.

3.3 Path Following Controller Design

In this section, we focus on the path following control design with vehicle stability and safety consideration. The output constraint control design on lateral offset, which simultaneously generates the required yaw rate, is presented in Section 3.2.1; the robust and adaptive optimal control on the vehicle handling and stability for path following objective and the optimal allocation for the yaw moment are presented in Section 3.2.2.

3.3.1 Output Constraint Control Design For Path Following

In this section, we will give a required yaw rate based on (3.11), which can satisfy the path following objective. At the same time, to make the lateral offset compactly bounded, we present an output constraint controller to system (3.11). It is designed by hyperbolic projection-based feedback dominance backstepping (HFDB) method. The advantage of feedback dominance backstepping (FDB) lies on overcoming the problem of explosion of complexity through feedback dominance, since the explosion of complexity is generally generated by standard feedback linearization and nonlinearity cancelation in conventional backstepping. The hyperbolic projection is proposed to reduce the overshoot of the lateral offset, and make the lateral offset compactly bounded. It can be inferred that if the vehicle starts running from a poor initial condition, i.e., the vehicle is driving away from the desired path at the beginning, the lateral offset e will encounter a considerable overshoot in its transient response. An oversize lateral offset is both a stability

threat and a security threat for the vehicle, in this situation, research on effectively reducing the bound of the lateral offset is very important. We use the subscript "h" to represent the HFDB method. The design procedure based on HFDB is shown in two steps as following:

Step 1: We project e to a new variable z_1 by hyperbolic sine function, $z_1 = \sinh\ \kappa e$, where κ is a positive regulating parameter. Design the first Lyapunov function $V_{1h} = \frac{1}{2}z_1^2$, its derivative is

$$\dot{V}_{1h} = \kappa z_1 \cosh \kappa e \cdot \left[v_x \frac{\sin\psi}{\psi} \left(\psi - \alpha_{1h} + \alpha_{1h}\right) + v_x \beta \cos\psi \right]. \tag{3.12}$$

By choosing a virtual variable of ψ, and denoting $\alpha_{1h} = -k_1 z_1$ and $z_{2h} = \psi - \alpha_{1h}$, (3.12) can be transformed into

$$\begin{aligned} \dot{V}_{1h} = & -\kappa k_1 z_1^2 \cosh \kappa e \cdot v_x \frac{\sin\psi}{\psi} + \\ & \kappa z_1 \cosh \kappa e \cdot v_x \frac{\sin\psi}{\psi} z_{2h} + \kappa z_1 \cosh \kappa e \cdot v_x \beta \cos\psi, \end{aligned} \tag{3.13}$$

which implies, if $z_{2h} = 0$, $|z_1(\infty)| \leq \bar{z}_1(t) = \frac{|\beta|}{k_1}\left|\frac{\psi}{\tan\psi}\right|$, and $z_1 \to 0$, $e \to 0$, as $\beta \to 0$.

Step 2: Design the second Lyapunov function, $V_{2h} = V_{1h} + \frac{p_1}{2}z_{2h}^2$, where p_1 is chosen to satisfy $p_1 = 1/k_1^2$. $\dot{V}_2$ is then given by

$$\begin{aligned} \dot{V}_{2h} = & -\kappa k_1 z_1^2 \cosh \kappa e \cdot v_x \frac{\sin\psi}{\psi} + \kappa z_1 \cosh \kappa e \cdot v_x \beta \cos\psi \\ & + \frac{\kappa}{k_1^2} z_{2h} \left[r - \rho v_x + k_1 \cosh \kappa e \cdot v_x \frac{\sin\psi}{\psi} z_{2h} + \right. \\ & \left. k_1 \cosh \kappa e \cdot v_x \beta \cos\psi \right]. \end{aligned} \tag{3.14}$$

To design the next virtual control for r dynamics, we use feedback dominance instead of feedback linearization to simplify the deduction,

$$\begin{aligned}\dot{V}_{2h} =& -\kappa k_1 z_1^2 \cosh\kappa e \cdot v_x \frac{\sin\psi}{\psi} + \kappa z_1 \cosh\kappa e \cdot v_x \beta \cos\psi \\ & - \frac{k_2}{k_1^2}\kappa \cosh\kappa e \cdot z_{2h}^2 \left[1 - \frac{k_1 v_x}{k_2}\frac{\sin\psi}{\psi}\right] \\ & + \frac{1}{k_1^2}\kappa z_{2h}\left[r - \rho v_x + k_1 \cosh\kappa e \cdot v_x \beta \cos\psi - \alpha_{2h}\right],\end{aligned} \tag{3.15}$$

where $\alpha_{2h} = -k_2 z_{2h} \cosh\kappa e$, we choose $z_{3h} = r - \rho v_x - \alpha_{2h}$, with k_2 a constant, $k_2 \geq k_1 v_x$. So if $z_{3h} = 0$, (3.15) can be simplified as

$$\begin{aligned}\dot{V}_{2h} =& -\kappa k_1 z_1^2 \cosh\kappa e \cdot v_x \frac{\sin\psi}{\psi} + \kappa z_1 \cosh\kappa e \cdot v_x \beta \cos\psi \\ & - \frac{k_2}{k_1^2}\kappa \cosh\kappa e \cdot z_{2h}^2 \left[1 - \frac{k_1 v_x}{k_2}\frac{\sin\psi}{\psi}\right] \\ & + \frac{1}{k_1}\kappa z_{2h} \cosh\kappa e \cdot v_x \beta \cos\psi,\end{aligned} \tag{3.16}$$

which implies

$$|z_{2h}(\infty)| \leq \bar{z}_{2h}(t) = \frac{k_1 v_x |\beta \cos\psi|}{k_2\left(1 - \frac{k_1 v_x}{k_2}\frac{\sin\psi}{\psi}\right)}, \tag{3.17}$$

and $z_{2h} \to 0$ as $\beta \to 0$. By making $z_{3h} = 0$, we can get the required yaw rate for path following objective,

$$r_{\alpha h} = \rho v_x + \alpha_{2h}. \tag{3.18}$$

where $\alpha_{2h} = -k_2 z_{2h} \cosh\kappa e$, $z_{2h} = \psi - \alpha_{1h}$, $\alpha_{1h} = -k_1 z_1$. If $z_1 \to 0$ and $z_{2h} \to 0$, since $z_1 = \sinh\kappa e$, we can conclude that, $e \to 0$ and $\psi \to 0$, i.e., the path following objective is achieved if the real yaw rate r tracks the required value $r_{\alpha h}$.

Remark 3.3.1: Notice that the required yaw rate generation and vehicle motion control is not completely independent, i.e., the required yaw rate generation actually uses the current vehicle states and the path following errors, and is not entirely based on the path information, so there will be no problem of error cumulation for path following control.

Remark 3.3.2: In classic path following control design, preview control is a popularly used practice (Le and Stiharu, 2013; Mashadi et al., 2014). The preview error can be expressed by adopting a small angle approximation for ψ as

$$e_p = e + L\psi. \tag{3.19}$$

Through converging e_p and ψ to zero, the lateral offset e can be converged to zero eventually, and then the path following objective can be achieved. The lateral offset e can be generally assumed small, so (3.18) can be rewritten as

$$r_{\alpha h} = \rho v_x - k_2 k_1 \kappa \left(e + \frac{1}{k_1 \kappa} \psi \right). \tag{3.20}$$

Comparing (3.19) and (3.20), it is reasonable to deem that $k_1\kappa = L^{-1}$, thus the required yaw rate can be finally expressed as

$$r_{\alpha h} = \rho v_x - \frac{k_2}{L} e_p, \tag{3.21}$$

where the preview distance L should be chosen in proportion to the vehicle longitudinal speed (Kritayakirana and Gerdes, 2012). The remaining work is to find the appropriate k_2, whose lower bound is fixed by $k_2 \geq k_1 v_x = \frac{v_x}{\kappa L}$, where κ is a regulating parameter chosen around 1, hence the tuning work is further simplified.

In what follows, the lateral offset bound of HFDB method is estimated. If at the initial moment $t = t_0$, $|z_1(t)| \leq \bar{z}_1(t)$, $|z_{2h}(t)| \leq \bar{z}_{2h}(t)$, then this result will always hold, $\forall t \geq t_0$, i.e. z_1, z_{2h} stay in a ball near the origin, when $t \to \infty$, $\beta \to 0$, thus $z_1 \to 0$, $z_{2h} \to 0$. If at the initial moment t_0,$|z_1(t_0)| > \bar{z}_1(t)$, $|z_{2h}(t_0)| > \bar{z}_{2h}(t)$, from (26), we know $\dot{V}_2 < 0$, thus the bound of z_1 is given by

the following inequality according to the definition of $V_{2h}(t)$

$$\begin{aligned} \tfrac{1}{2}z_1^2(t) \leq V_{2h}(t) &= \frac{1}{2}z_1^2(t) + \frac{p_1}{2}z_{2h}^2(t) \\ &\leq V_{2h}(t_0), \ \ \forall\, t \geq t_0. \end{aligned} \tag{3.22}$$

$$\Rightarrow z_1(t) \leq \sqrt{2V_{2h}(t_0)}, \quad \forall t \geq t_0. \tag{3.23}$$

From (3.23) we can obtain the bound of e as

$$|e(t)| \leq \operatorname{arcsinh}\sqrt{2V_{2h}(t_0)}, \quad \forall t \geq t_0, \tag{3.24}$$

with

$$V_{2h}(t_0) = \frac{1}{2}\sinh^2 \kappa e(t_0) + \frac{p_1}{2}(\psi(t_0) + k_1 \sinh\ \kappa e(t_0))^2, \tag{3.25}$$

and we assume $\bar{z}_1(t) < \sqrt{2V_{2h}(t_0)}$, $\bar{z}_{2h}(t) < \sqrt{2V_{2h}(t_0)}$ which can be guaranteed since we can appropriately choose k_1 and k_2.

For comparison, here the lateral offset bound estimation of FDB method is briefly given as

$$|e| \leq \sqrt{2V_2(t_0)}, \ \forall t \geq t_0, \tag{3.26}$$

where

$$V_2(t_0) = \frac{1}{2}e(t_0)^2 + \frac{p_1}{2}(\psi(t_0) + k_1 e(t_0))^2, \tag{3.27}$$

which gives an estimated bound for e, where k_1 and k_2 can be used for adjusting its bound. However, the magnitudes of e and z_2 ($z_2 = \psi - \alpha_1$, and $\alpha_1 = -k_1 e$) are generally equally weighted, resulting in a relative large and loose bound for e.

As shown in (3.26), conventional bound estimation method, which is based on quadratic Lyapunov function, may result in a relative large bound for the output we concern. This problem comes from that all the state variables in quadratic

Lyapunov forms are usually equally weighted. Given this problem, hyperbolic projection approach proposed in this chapter offers an effective solution for output constraint control problem. This approach is developed in combination with backstepping method, making use of the characteristics of hyperbolic functions. By projecting the concerned output variable to a new, significantly large variable via hyperbolic function, this technique generates a considerable small, compact bound for the concerned output.

To provide a vivid comparison of the output bounds in (3.26) and (3.24) , we employ two illustrative functions:

$$\begin{cases} B_c\left(y\right) = \sqrt{x^2 + \left(x+y\right)^2}, \\ B_h\left(y\right) = \operatorname{arcsinh}\left(\sqrt{\sinh^2 x + \left(\sinh x + y\right)^2}\right), \end{cases} \tag{3.28}$$

where x and y are assumed with the same sign, and y is assumed with a sufficient small bound. "B" represents the evaluation function for the "bound" of x; the subscript "c" and "h" represent the conventional backstepping and hyperbolic projection-based backstepping, respectively. We choose $x = 1$ for simplicity. The bounds comparison between the quadratic Lyapunov function and the hyperbolic projection method is shown in the Fig. 3.3. We assume the initial value of x is within the safe bound. Therefore, when y is small, the bound of x is small and close to its initial value. As shown in Fig. 3.3, when y becomes large, the bound of x of hyperbolic method is significantly smaller than that of conventional method. Similar result can be obtained when we choose other values of x, and the constraint effect is more explicit when y becomes larger.

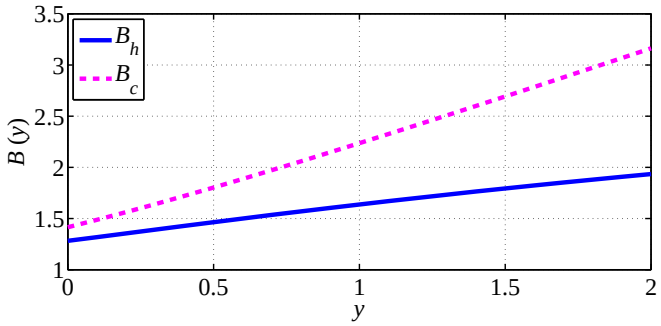

Figure 3.3: Comparison of $B_c(y)$ and $B_h(y)$

In this study, we address the more dangerous initial condition that, the initial values of e and ψ are with the same signs. i.e., the vehicle drives away from the centerline of the desired lane. In that case, the vehicle is more likely to transcend the safe driving zone. Due to the periodicity and the physical condition of the azimuth angle, it is reasonable to assume $|\psi| < \pi$. Utilizing the property of (arc-) hyperbolic functions, the comparison of the bounds (3.26) and (3.24) obtained via conventional method and hyperbolic projection method respectively is given by

$$\operatorname{arcsinh}\sqrt{2V_{2h}(t_0)} \leq \sqrt{2V_2(t_0)}. \tag{3.29}$$

Remark 3.3.3: Actually, the left item in (3.29) can be sufficiently smaller than the right item, if the variables except the constrained one become larger. It follows that the lateral offset can be confined in a sufficiently small region by HFDB controller.

3.3.2 Integrated AFS and DYC Design

In this section, we focus on giving the required control inputs including the steering angle δ_f and the external yaw moment ΔM_z, using an adaptive and robust LQR controller. The control inputs are designed to make the vehicle track its required

motion, i.e, to make the sideslip angle and the yaw rate track their respectively required values. Furthermore, we present the control allocation of ΔM_z to the four tires, to give the optimal longitudinal force of each tire. Commonly the desired value of vehicle lateral velocity is chosen as zero, which results in a zero sideslip angle of the vehicle. The required yaw rate is given in Section 3.2.1.

To handle the parametric uncertainties, here we make an assumption as a preliminary for the controller design:

Assumption 3.3.1: Assume that a lumped disturbance $D(x,t)$ can be defined to include the nonlinear terms caused by the parametric uncertainties $D(x,t) = \Delta Ax + \Delta Bu$, and assume that $D(x,t)$ for the system plant (3.10) satisfies the matching condition such that $D(x,t) = Bd(x,t)$.

Note that the *Assumption* 3.3.1 can be adopted because the magnitude of ΔBu is much smaller than ΔAx, which can be observed from (3.7)-(3.9), moreover, when we calculate the upper bound of the magnitude of $D(x,t)$, we use the saturation limit of the control input u. Therefore, $D(x,t)$ is bounded actually. Owing to the LQR controller, the magnitude of the control inputs can be maintained in reasonable regions. Thus the lumped disturbance $D(x,t)$ can include the input u. The assumption about the matching condition can be made because the matrix B is invertible. Therefore, here we can assume that the disturbance input $D(x,t)$ includes the control input and satisfies the matching condition. This assumption is made for facilitating the robust LQR controller design, to handle the multiple lumped disturbances. We further assume that the equivalent-input extended disturbance $d(x,t)$ is upper bounded by an unknown positive constant d_m, i.e., $\|d(x,t)\| < d_m$. Hence (3.10) can be rewritten as

$$\dot{x} = Ax + B(u + d). \tag{3.30}$$

The desired values of vehicle lateral dynamics are selected as: the desired sideslip angle $\beta_d = 0$, the required yaw rate $r_{\alpha h} = \rho v_x + \alpha_{2h}$ as obtained in (3.18).

Remark 3.3.4: Since we assume 30% uncertainties for the cornering stiffnesses, and the sideslip angle is constrained within a certain bound shown in the later analysis, the yaw rate is in the bound $\mu g/v_x$, the control inputs (the steering angle and the yaw moment) have their respective actuator saturation limits, thus the bound of $d(x,t)$ can be calculated.

Here we deploy an adaptive and robust LQR controller to minimize the errors of the sideslip angle β and the yaw rate r with their respectively required values, and simultaneously, restrict the control input efforts, the steering angle and the yaw moment, in reasonable regions. The innovation of the proposed LQR lies on two points: firstly, we can adjust the weights in the LQR tuning, to maintain vehicle stability through the path following process; secondly, we adopt an integrated control law to deal with the model uncertainties (or the lumped disturbances).

Denote $x_d = [\beta_d \quad r_d]^T$, $\varepsilon = x - x_d = [\beta - \beta_d, \quad r - r_d]^T$, where $\beta_d = 0$, $r_d = r_\alpha$, by assuming the control inputs in the steady states are zero, the (3.30) can be rewritten as $\dot{\varepsilon} = A\varepsilon + B(u + d)$. The integrated performance index of the optimal control is defined as:

$$J_1 = \frac{1}{2}\int_0^\infty \left[\varepsilon^T Q \varepsilon + u^T R u\right] dt, \tag{3.31}$$

where $Q = \mathrm{diag}(Q_y, \ Q_z)$, $R = \mathrm{diag}(R_y, \ R_z)$. Here we utilize a theorem to design the robust LQR controller:

Theorem 3.3.1: Given $d(x,t)$ is norm-bounded, the linear system (3.30) will possess global asymptotic stability, if the control input vector $u(t)$ is designed as:

$$u(t) = u_l(t) + u_n(t), \tag{3.32}$$

where the linear item $u_l(t)$ is

$$u_l = -R^{-1}B^T P(x - x_d), \tag{3.33}$$

in which the symmetric positive definite P is the solution of the algebraic Riccati equation

$$PA + A^T P + Q - PBR^{-1}B^T P = 0, \tag{3.34}$$

the nonlinear $u_n(t)$ item is designed as

$$u_n(t) = \begin{cases} -\Lambda \dfrac{B^T P\varepsilon}{\|B^T P\varepsilon\|_2}, & B^T P\varepsilon \neq 0, \\ 0 \quad , & B^T P\varepsilon = 0, \end{cases} \tag{3.35}$$

where the controller gain Λ should satisfy $\Lambda > d_m$.

The proof can be found in Liu et al. (2014).

In this work, there are only two system states in (3.30), so the Riccati equation can be algebraically solved (Wang et al., 2015).

To guarantee the vehicle lateral stability, the following adaptive tuning function about Q_y is introduced

$$Q_y = \frac{\lambda}{(1 - \beta_n)^\eta}, \tag{3.36}$$

where λ is a positive regulating constant, and η is a positive constant which is used to determine the shape of the weighting factor, and $\beta_n = \beta/\beta_p$ is the normalized sideslip angle, with β_p corresponding to the maximum permissible sideslip angle. By using this barrier function, we can maintain the sideslip angle in the stable region.

In what follows the required yaw moment is allocated to the four tires. The cost function for allocating the external yaw moment ΔM_z to the four tire forces

can be defined as

$$J = F_x^T W F_x + (GF_x - u_2)^T H\,(GF_x - u_2), \tag{3.37}$$

where in the right side of the equal sign in (3.37), the first item is used to maintain the driving stability and prevent tire sliding, where $W = \mathrm{diag}\,[w_1,\ w_2,\ w_3,\ w_4]$ is the control allocation weight matrix, which effects the magnitude of F_x; the second item is used to satisfy the control demand for the higher-level controller such that the vehicle dynamics performance can be maintained, where $H = h_1$ is the regulating matrix which affects the magnitude of $(GF_x - u_2)$. $F_x = [F_{x1}\ \ F_{x2}\ \ F_{x3}\ \ F_{x4}]^T$ is the longitudinal tire forces. $u_2 = \Delta M_z$ is the required external yaw moment obtained by the proposed LQR controller. G is the control effectiveness matrix and can be written according to (3.2)

$$G = [-\cos\delta_f \cdot l_s + \sin\delta_f \cdot l_f,\quad \cos\delta_f \cdot l_s + \sin\delta_f \cdot l_f,\ \ -l_s,\ \ l_s]\,. \tag{3.38}$$

Based on (3.37), we have

$$\begin{aligned} \frac{\partial J}{\partial F_x} &= WF_x + G^T H\,(GF_x - u_2)\,, \\ &= \left(W + G^T HG\right) F_x - G^T H u_2, \end{aligned} \tag{3.39}$$

and

$$N = \frac{\partial^2 J}{\partial^2 F_x} = W + G^T HG. \tag{3.40}$$

As $W > 0$ and $G^T HG \geq 0$, we always have $N > 0$, which indicates that the objective function J has a global minimum when F_x is chosen as

$$F_x = \left(W + G^T HG\right)^{-1} G^T H u_2. \tag{3.41}$$

Considering that the control allocation of longitudinal tire forces is much dependent on the vehicle load transfer, the W is designed as the function of the tire normal loads as $w_i = \bar{F}_z/F_{zi}$, where $\bar{F}_z = \frac{1}{4}mg$, F_{zi} represents the normal load of the ith tire. According to (3.41), W can be changed according to the variation of the F_{zi}, then the allocated F_{xi} can be adaptively adjusted, i.e., when F_{zi} increases, the corresponding F_{xi} increases. H can be chosen as $H = I$ in the following simulation. Since the dynamics response of the in-wheel motor is much faster that of the vehicle, the dynamics characteristic of the in-wheel motor is not considered in this work.

Remark 3.3.5: Note that the actuator saturation issue is not considered in this work, since our main contribution lies on the proposed output constraint control strategy, hyperbolic projection method. As for the saturation problem of the longitudinal tire forces, we can handle that in the yaw moment allocation part. As can be seen in from (3.37), there exists a control allocation weight matrix W. We can properly design a W as a barrier function of the slip ratio to ensure all the tires work in the stable region. The barrier function can be similar as the one proposed for constraining the sideslip angle in this work, which can be used to prevent the longitudinal tire forces from surpassing the saturation bound. One can refer to our previous work Wang et al. (2015) for the detail of the barrier function design, or other peoples works on handling the tire forces saturation (Shyrokau et al., 2015; Canale et al., 2009; Du et al., 2010).

3.4 Simulation Results

In this section, we present two simulation cases, implemented based on CarSim-Simulink platform. One is J-turn maneuver, another is lane change maneuver. The vehicle parameter used in the following simulation is presented in Table 3.1,

and the uncertainty for the cornering stiffness is set as 30% of the normal value. The controller gains for both of the two simulation cases are chosen in the following way: (1) Because the preview distance L should be chosen in proportion to the vehicle longitudinal speed (Kritayakirana and Gerdes, 2012), k_1 should be inversely proportional to v_x. Note that the vehicle is more likely to be uncontrollable or unstable in the higher-speed running, so in this work we only investigate the dangerous cases for the path following that the vehicle is running with a middle or high speed. At the same time v_x is assumed as a constant with a small change to facilitate the control law design. Therefore, in the simulation v_x will not be very small, and finally we choose $k_1 = 3/v_x$; (2) k_2 should satisfy that $k_2 \geq k_1 v_x$ according to (3.15), and thus we can choose $k_2 = 30k_1$; (3) κ is a regulating parameter around 1, which affects the output constraint performance and the control input magnitude, so after the comprehensive consideration of the trade-off, here we can choose $\kappa = 1.3$; (4) The maximum permissible sideslip angle β_p is always chosen around 5 deg to maintain the lateral vehicle stability, thus here we can choose $\beta_p = 3$ deg; (5) λ is a positive regulating constant and can be simply chosen as $\lambda = 1$; (6) η is a positive constant which is used to determine the shape of the weighting factor, which affects the control performance of the sideslip angle, and can cause fluctuations for the system response. Thus after the comprehensive consideration of the trade-off, we choose $\eta = 0.5$ in our simulation; (7) The gains of the LQR controller can be fixed based on Brysons rule (Bryson, 1975), with the comprehensive consideration of the vehicle longitudinal speed, tire-road friction coefficient, and the trade-off between the errors of vehicle states and the control inputs. Thus we finally choose $Q_z = 10^2,\ R_y = 10^2,\ R_z = 2 \times 10^7$.

Table 3.1: Vehicle parameter used in the simulation.

Symbol	Description	Values and Units
m	Vehicle total mass	1500 kg
l_s	Half of the wheel-base	0.75 m
l_f	Distance of front wheel axle from CG	1 m
l_r	Distance of rear wheel axle from CG	1.6 m
I_z	Vehicle moment of inertia about yaw axis	3240 kg·m^2
c_{f0}	Generalized normal cornering stiffness of the front tires	160000 N/rad
c_{r0}	Generalized normal cornering stiffness of the rear tires	160000 N/rad

3.4.1 J-Turn Simulation

In this case, the vehicle runs at a low speed 10 m/s on a slippery road with a low road friction ($\mu = 0.4$). The vehicle is supposed to make a J-turn along a circle, whose curvature is 0.003 m^{-1}. We aim at controlling the vehicle such that the actual vehicle can follow the reference path and can be stabilized.

The lateral offset and heading error result is shown in Fig. 3.4, where the subscript "h" represents the corresponding result using HFDB method, similarly hereinafter. One can see that the lateral offset can be converged to zero, and by using the hyperbolic method, we can reduce the overshoot of e considerably. The output constraint effect can be more remarkable, if the initial condition is more extreme, i.e., the initial values of the lateral offset or/and the heading error are chosen larger. The heading error can be stabilized and converged to zero, and after using the hyperbolic projection the overshoot of the heading error is increased a little, which can be explained that more control effort is focused on the lateral offset control. Note that since we want to simulate the dangerous situation, the initial value of the heading error is suppose to make the vehicle drive away from the

desired path at the beginning, which thus causes a relative large overshoot in the lateral offset. The initial values of the path following errors are chosen small due to the consideration of the real driving on roads. Although the enhancement of the hyperbolic method may not be vary significant, its effectiveness is still apparent, and may play an important role in some dangerous situation.

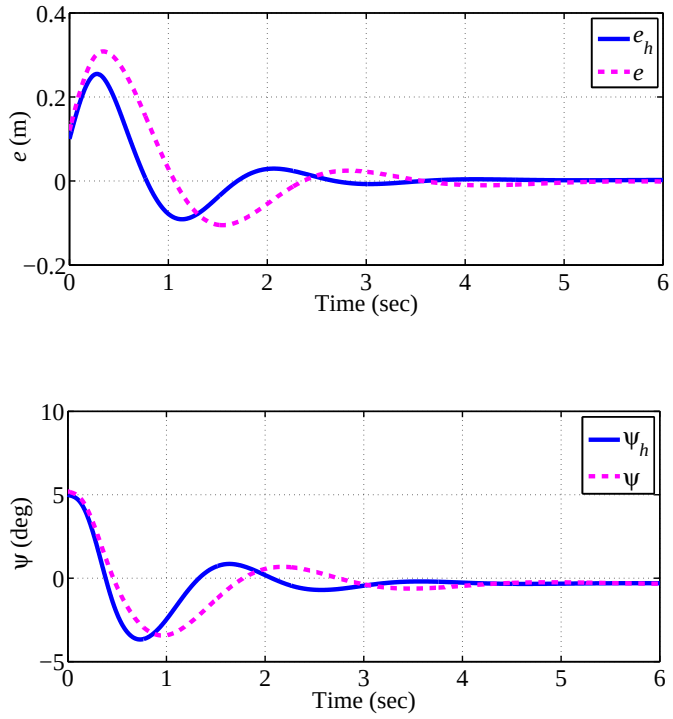

Figure 3.4: The path following errors results in the J-turn simulation.

The sideslip angle and yaw rate tracking results are shown in Fig. 3.5. It is shown that they can be stabilized and converged, which indicates that the vehicle is stable through the path following process. By using the adaptive LQR controller, the sideslip angle is constrained in safe region. Note that the hyperbolic method will increase the sideslip angle and the yaw rate, but they are still in reasonable regions. One can conclude that there exists a trade-off between the output constraint control and the system stability control. When the vehicle is

driving in limited safe zone and close to the safe boundary, the vehicle safety is a priority concern, so the lateral offset reduction is more significant and then the hyperbolic projection can be deployed to realize its function.

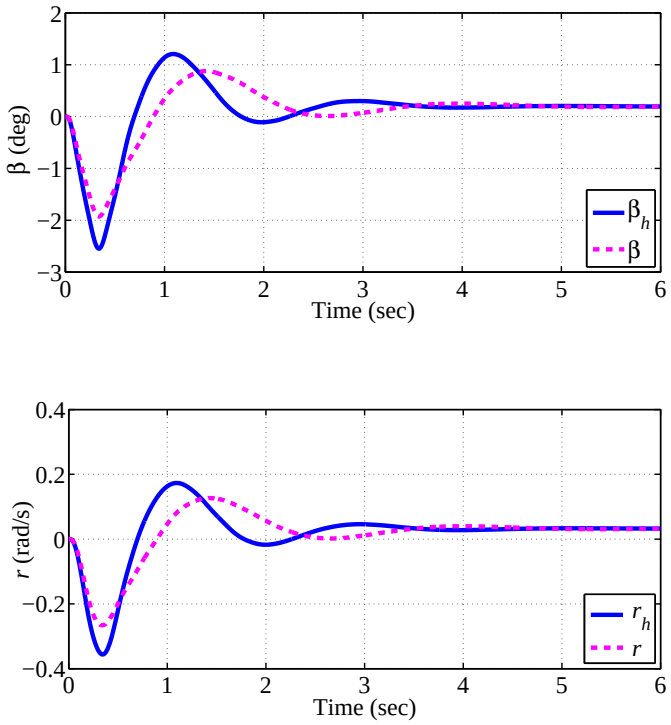

Figure 3.5: The sideslip angle and yaw rate results in the J-turn simulation.

The slip ratios and the lateral acceleration are shown in Fig. 3.6. The tire longitudinal slip ratio s_i is defined as the relative difference between the tire center speed and tire circumferential speed. It can be found that they are all stabilized in safe regions. The simulation result for the slip ratio is used to show the effect of the DYC on the vehicle longitudinal motion, we can see that the slip ratios are time-varying and very small. The hyperbolic method will increase the lateral acceleration a_y, this is because the yaw rate is enlarged. a_y is maintained in reasonable region, which is less than the extreme acceleration μg the road can provide, and stabilizes at about 3 m/s^2 when the system is stabilized.

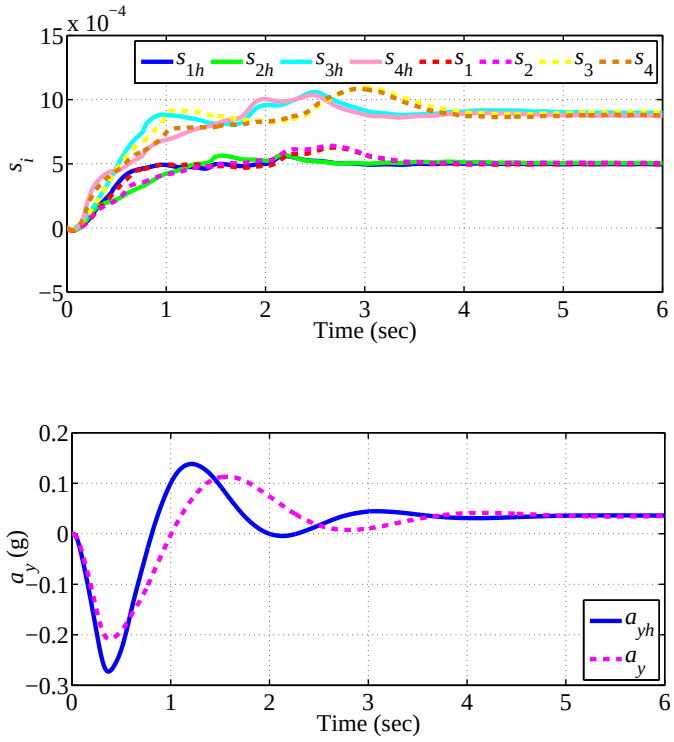

Figure 3.6: The slip ratios and lateral acceleration results in the J-turn simulation.

The steering angle of the front wheel, the external yaw moment and the longitudinal tire forces are shown in Fig. 3.7. We can see that they are maintained in reasonable regions, although they encounter some fluctuations at the beginning, and they are all increased in the transit phase by the hyperbolic projection. The path following results are shown in Fig. 3.8. We can see the circle tracking objective is completed, and the output constraint approach proposed in this chapter is effective to reduce the bound of the lateral offset, which can be of great benefit for driver's safety, especially in extreme driving conditions.

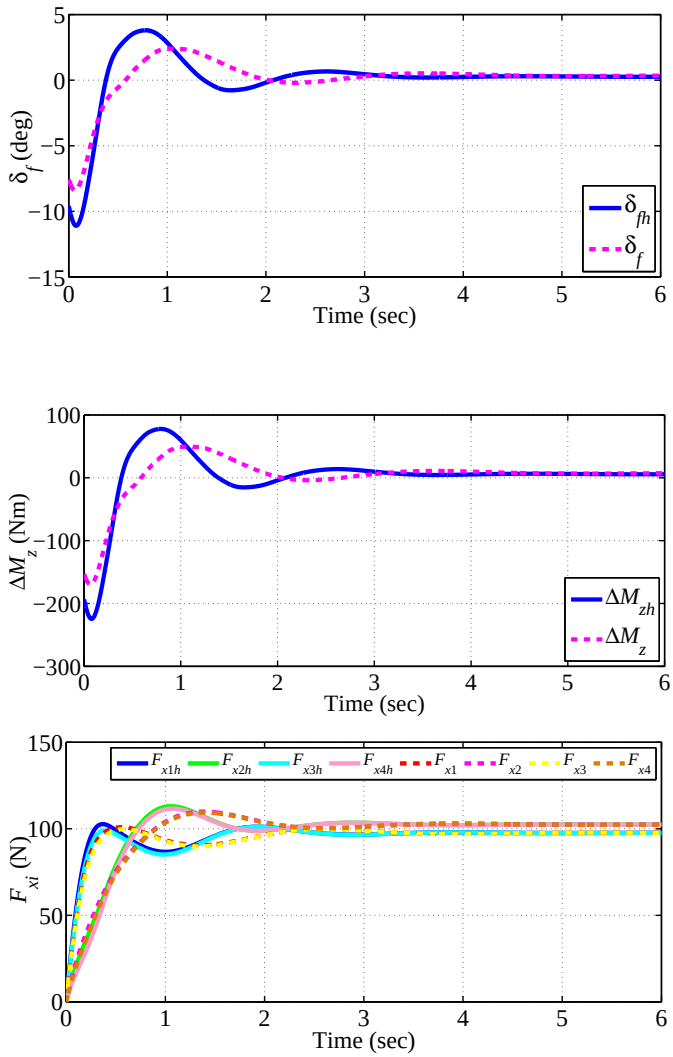

Figure 3.7: The control inputs results in the J-turn simulation.

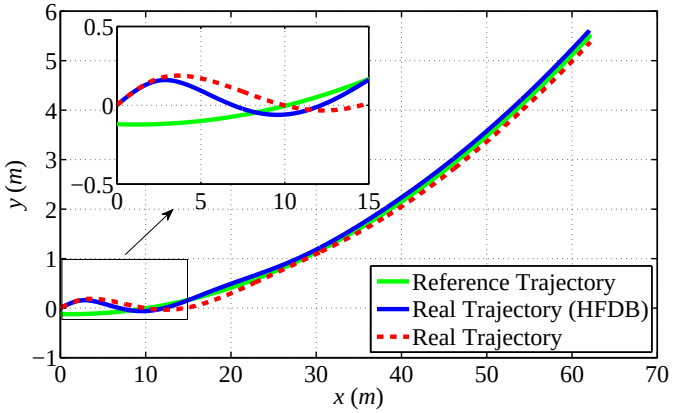

Figure 3.8: The path following result in the J-turn simulation.

3.4.2 Lane Change Simulation

In the second case, the vehicle runs at a high speed 30 m/s on a dry road with a high road friction ($\mu = 0.8$). We make the vehicle track a clothoid curve, which is designed to approximate a lane change path. The clothoid curve is designed here consisting of three path primitives: straights, clothoids and arcs. The curvature ρ of each path segment is defined as the different functions of the distance σ along the path (Funke and Gerdes, 2013), as shown in Fig. 3.9. From 4 second to 6 second, the vehicle makes a lane change maneuver.

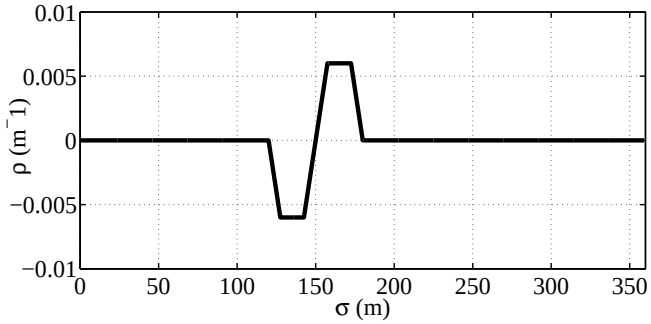

Figure 3.9: The curvature of the clothoid curve in the lane change simulation

The lateral offset and heading error result is shown in Fig. 3.10. One can see that the path following errors can be converged to zero when the vehicle tracks the line path, and since the vehicle begins to change the lane from 4 second, the lateral offset begins to shake, until the lane change manoeuvre is completed. Because the vehicle finishes the lane change in 2 second, the lateral offset does not have enough time to be converged. However, by using the hyperbolic method, we can reduce the overshoot of e distinctly and make e compactly bounded. After using the hyperbolic projection, the overshoot of the heading error is increased a little, that is because more control effort is used to exert constraint control on the lateral offset.

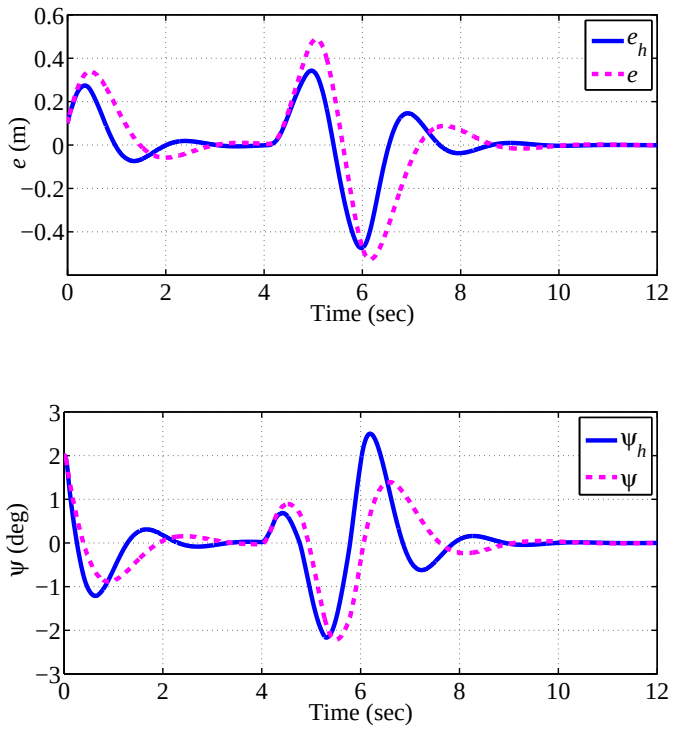

Figure 3.10: The path following errors results in the lane change simulation.

The sideslip angle and yaw rate tracking results are represented in Fig. 3.11. We can see that when making a lane change, the sideslip angle and yaw rate can be stabilized and converged, even they have some shock at the beginning. By using the adaptive LQR controller with sideslip angle barrier function, the sideslip angle is constrained within 5 degree, which maintains the vehicle stability through the path following process. The sideslip and the yaw rate are both enlarged a little, resulting from the larger control inputs by the hyperbolic projection.

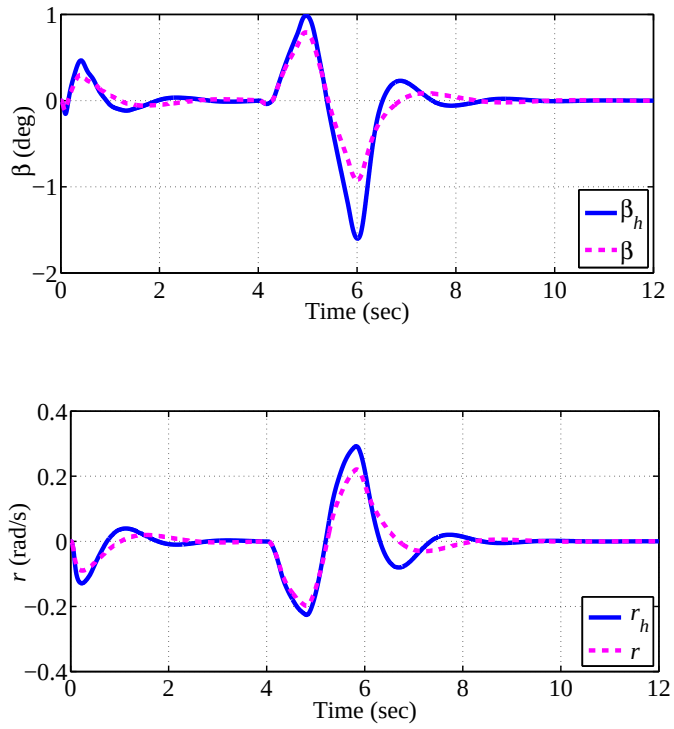

Figure 3.11: The sideslip angle and yaw rate results in the lane change simulation.

Fig. 3.12 present the results for the slip ratios and the lateral acceleration. They are all stabilized and converged in safe regions, even though, at the beginning they have some shocks. The slip ratios are maintained in small magnitudes, and the lateral acceleration increases a little which is caused by the hyperbolic projection, but still remains in safe region. Fig. 3.13 show the simulation results of the steering angle of the front wheel, the external yaw moment and the four longitudinal tire forces. We can see that by using LQR controller, they are maintained in reasonable region and can be converged eventually, although they encounter some shocks at the beginning. Since more control effort is used for the constraint control on the lateral offset, the control inputs are enlarged a little. The steering angle is maintained in a small magnitude, considering that the longitudinal speed is high. The path following results are shown in Fig. 3.14. We can see the lane

change objective is completed, and the output constraint approach proposed in this chapter is effective to reduce the bound of the lateral offset. The enhancement can be expected to be more significant in extreme driving conditions.

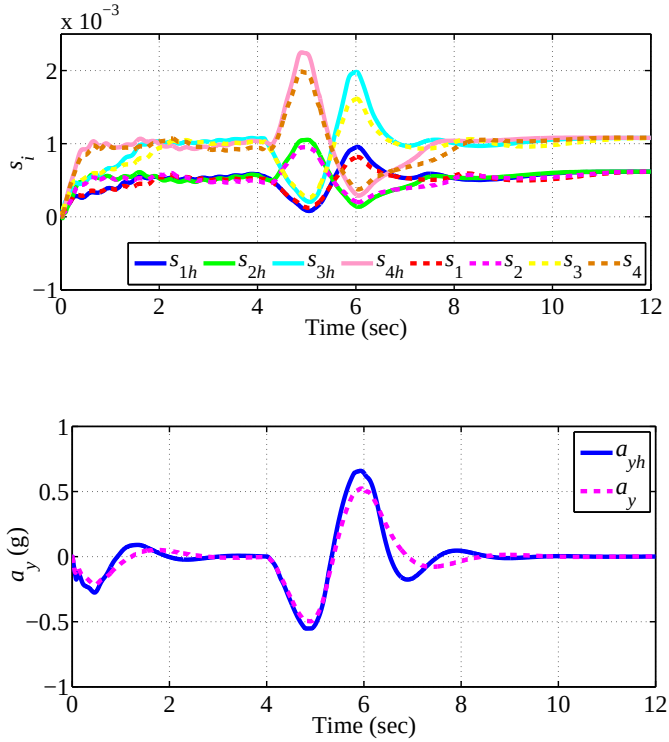

Figure 3.12: The slip ratios and lateral acceleration results in the lane change simulation.

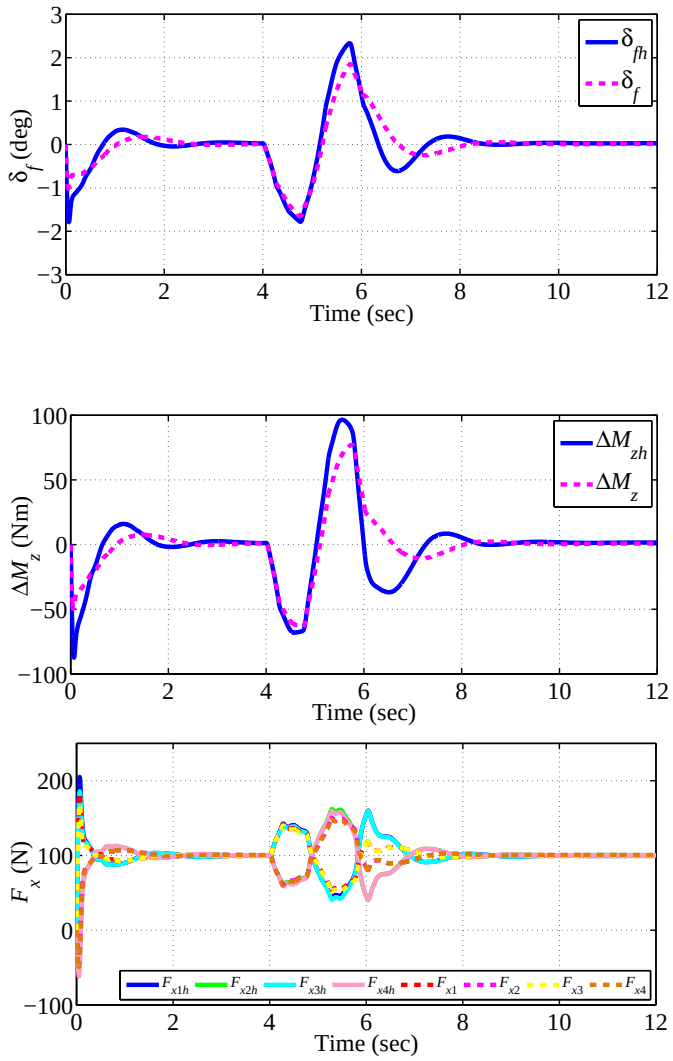

Figure 3.13: The control inputs results in the lane change simulation.

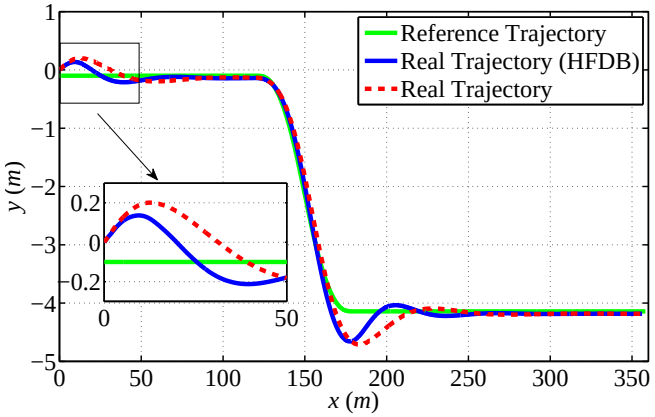

Figure 3.14: The path following result in the lane change simulation.

3.5 Conclusion

This chapter proposes a novel output constraint control technique, hyperbolic projection, to deal with the path following control problems for FWIA AGVs, via integrated AFS and DYC control. The path following controller is developed on hyperbolic projection-based feedback dominance backstepping, to overcome the "explosive complexity" of standard backstepping. The robust LQR controller with adaptive weight is designed to give out the steering angle and yaw moment, and guarantee the vehicle lateral stability. Then the yaw moment is allocated to the four tires through an optimal cost function with considering the vehicle load transfer. Using the proposed approach, the path following errors are globally and asymptotically stabilized, synchronously, the lateral offset is strictly boundedly confined. Simulation results based on a high-fidelity and full-ca model using CarSim have validated the effectiveness of the proposed approach. It should be noted that some points should be considered in actual application, e.g., the sideslip angle may not be measureable with low cost sensors, the saturation issue for the steering angle, etc. These points will be considered in our future experiment study.

References

Li, Zhen, Jing Sun, and Soryeok Oh. "Design, analysis and experimental validation of a robust nonlinear path following controller for marine surface vessels." *Automatica* 45.7 (2009): 1649-1658.

Yuan, Xibo, and Jiabin Wang. "Torque distribution strategy for a front-and rear-wheel-driven electric vehicle." *IEEE Transactions on Vehicular Technology* 61.8 (2012): 3365-3374.

Pennycott, Andrew, Leonardo De Novellis, Alessio Sabbatini, et al. "Reducing the motor power losses of a four-wheel drive, fully electric vehicle via wheel torque allocation." *Proceedings of the Institution of Mechanical Engineers, Part D: Journal of Automobile Engineering* (2014): 0954407013516106.

De Novellis, Leonardo, Aldo Sorniotti, and Patrick Gruber. "Wheel torque distribution criteria for electric vehicles with torque-vectoring differentials." *IEEE Transactions on Vehicular Technology* 63.4 (2014): 1593-1602.

Shyrokau, Barys, Danwei Wang, Dzmitry Savitski, et al. "Vehicle motion control with subsystem prioritization." *Mechatronics* 30 (2015): 297-315.

Abe, Masato. *Vehicle handling dynamics: theory and application*. Butterworth-Heinemann, 2015.

Ahmadi, Javad, Ali Khaki Sedigh, and Mansour Kabganian. "Adaptive vehicle lateral-plane motion control using optimal tire friction forces with saturation limits consideration." *IEEE Transactions on vehicular technology* 58.8 (2009): 4098-4107.

Tchamna, R., and I. Youn. "Yaw rate and side-slip control considering vehicle longitudinal dynamics." *International Journal of Automotive Technology* 14.1 (2013): 53-60.

Le, Thanh Phuc, and Ion Stiharu. "An optimal preview driver model applied to a non-linear vehicle and an impaired driver." *Proceedings of the Institution of Mechanical Engineers, Part D: Journal of automobile engineering* 227.4 (2013): 536-548.

Mashadi, Behrooz, Mehdi Mahmoudi-Kaleybar, Pouyan Ahmadizadeh, et al. "A path-following driver/vehicle model with optimized lateral dynamic controller." *Latin American journal of solids and structures* 11.4 (2014): 613-630.

Kritayakirana, Krisada, and J. Christian Gerdes. "Using the centre of percussion to design a steering controller for an autonomous race car." *Vehicle System Dynamics* 50.sup1 (2012): 33-51.

Liu, Xiaodong, Yunjie Wu, Yu Zhang, et al. "A control method to make LQR robust: A planes cluster approaching mode." *International Journal of Control, Automation and Systems* 12.2 (2014): 302-308.

Wang, Rongrong, Chuan Hu, Zejiang Wang, et al. "Integrated optimal dynamics control of 4WD4WS electric ground vehicle with tire-road frictional coefficient estimation." *Mechanical Systems and Signal Processing* 60 (2015): 727-741.

Shyrokau, Barys, Danwei Wang, Dzmitry Savitski, et al. "Vehicle motion control with subsystem prioritization." *Mechatronics* 30 (2015): 297-315.

Canale, Massimo, Lorenzo Fagiano ; Antonella Ferrara, et al. "Comparing internal model control and sliding-mode approaches for vehicle yaw control." *IEEE Transactions on Intelligent Transportation Systems* 10.1 (2009): 31-41.

Du, Haiping, Nong Zhang, Guangming Dong. "Stabilizing vehicle lateral dynamics with considerations of parameter uncertainties and control saturation through robust yaw control," *IEEE Transactions on Vehicular Technology* 59.5 (2010): 2593-2597.

Bryson, Arthur Earl. *Applied optimal control: optimization, estimation and control*. CRC Press, 1975.

Funke, Joseph, and J. Christian Gerdes. "Simple clothoid paths for autonomous vehicle lane changes at the limits of handling." *ASME 2013 Dynamic Systems and Control Conference*. American Society of Mechanical Engineers, 2013.

Chapter 4

ISM-based CNF Control for Path Following of FWIA AGVs

This chapter includes the following **published IEEE Transactions journal paper**:

Chuan Hu, Rongrong Wang, and Fengjun Yan, "Integral Sliding Mode-based Composite Nonlinear Feedback Control for Path Following of Four-Wheel Independently Actuated Autonomous Vehicles," ***IEEE Transactions on Transportation Electrification***, vol. 2, no. 2, pp. 221-230, Jun. 2016.

C. Hu is with the Department of Mechanical Engineering, McMaster University, Hamilton, ON L8S4L8, Canada, and also with the School of Mechanical Engineering, Southeast University, Nanjing 211189, China.

R. Wang is with the School of Mechanical Engineering, Southeast University, Nanjing 211189, China.

F. Yan is with the Department of Mechanical Engineering, McMaster University, Hamilton, ON L8S4L8, Canada.

Co-authorship Declaration: The idea of the modified composite nonlinear feedback (CNF) control based on sliding mode control was primitively proposed by me. I had discussed the correctness and feasibility of the control strategy with Prof. Yan, and discussed the stability and robustness of the control system with Prof. Wang. After their affirmations, I had implemented the controller design, and applied the proposed controller in the path following control of the autonomous vehicles. Prof. Wang gave me some comments on the tire force saturation issue, and checked the equations in this paper carefully. Then I conducted the CarSim simulations, and completed the major work of the paper writing. Prof. Yan and Prof. Wang gave me several suggestions in the revisions and replies according to the review comments.

Abstract

This paper presents an accurate, fast and robust path-following control approach for four-wheel independently actuated (FWIA) autonomous vehicles via integrated control of the active front-wheel steering (AFS) and direct yaw-moment control (DYC). The path following is realized through simultaneously converging the yaw rate and lateral velocity to their respective desired values which are generated according to the path following demand. A novel integral sliding mode (ISM)-based composite nonlinear feedback (CNF) control technique considering the multi-input

multi-output and the time-varying tracking reference is proposed, which has combined the advantages of CNF control in improving the transient performance and ISM control in guaranteeing good robustness. Chattering is avoided by using a continuous ISM controller instead of generally adopted discontinuous ones based on a multivariable super-twisting algorithm (STA). System uncertainties, tire fore saturations and variation of the desired-path curvature are compositively considered in the ISM-CNF controller design, with the stability of the overall system proved using Lyapunov method. CarSim-Simulink simulations have verified the effectiveness of the proposed controller in improving the transient path following performance, inhibiting the overshoots, eliminating the steady-state errors, and rejecting the lumped disturbance considering the tire forces saturations and the varying path curvature.

Index Terms

Autonomous vehicles, four-wheel independently actuated, path following, integral sliding mode control, composite nonlinear feedback.

4.1 Introduction

This chapter deals with the path following control issue for FWIA AGVs with considerations of the tire forces saturations, system uncertainties, and the variation of the desired-path curvature. The control aim is to improve the transient performance of the path following manoeuvre.

One of the control techniques specializing in transient performance improvement is composite nonlinear feedback (CNF) control proposed in Chen et al. (2003), which may provide an inspiration for vehicle motion control. CNF is

a composite nonlinear control algorithm used for linear system, consisting of a linear feedback portion and a nonlinear feedback portion without any switching terms. The linear part is designed to yield a fast response with a small damping ratio within the actuator saturation limit. The nonlinear part then is used to increase the damping ratio when the controlled outputs approach the target references, therefore the overshoots can be reduced and the steady-state errors can be eliminated. However, the traditional CNF controller is more applicable for the tracking control for the constant reference (Chen et al., 2003; Cheng and Peng, 2007). Several related literatures (Wang et al., 2014; Yang and Chen, 2014; Majd and Mobayen, 2015) were proposed to deal with time-varying target references using CNF, however, they usually have some strict assumptions on the reference and the controlled output, which are not appropriate for vehicle motion control. In order to achieve better tracking performance for systems with random references, traditional CNF needs to be modified to include the information of the time-derivatives of the target references.

System disturbances intensively interfere with the system stability and transient performance. Currently, CNF lacks the robustness to deal with systems with randomly-changing (or multiple) disturbance(s). The existing literatures usually require some assumptions for the disturbances to design CNF control law with disturbance compensation (Zhang and Lan, 2013; Wang et al., 2014). As a widely applicable control technique, SMC has been proposed to be combined with CNF in the form of the integrated sliding mode (ISM) controller to cope with disturbances. However, ISM-CNF technique has also inherited some disadvantages of SMC, such as, the input saturation is hard to handle, and the variation of the reference is hard to be included. In Majd and Mobayen (2015) and Mobayen (2014) the CNF-based ISM controller was proposed to investigate the tracking control for

uncertain multi-input multi-output (MIMO) linear systems with multiple external disturbances, however the actuator saturation is not considered, and the target reference is assumed to have special form. In addition, since in the ISM framework the discontinous controller is usually used to reject the disturbance, chattering phenomenon is difficult to avoid, thus the application value of ISM-CNF technique is quite limited for vehicle motion control. Although the newly-emerging super-twisting algorithm (STA) has demonstrated the effectiveness in attenuating the chattering effects, few ISM strategies adopting STA for MIMO systems were reported to deal with the input saturation and transient performance improvement, as the overall stability is hard to guarantee.

To this end, this chapter proposes a novel ISM-CNF technique for path following control of AGVs, with contributions made on the following two aspects: 1) The proposed controller has simultaneously considered the tire forces saturations, system uncertainties, and the varying path curvature based on a modified integrated sliding surface; 2) To avoid chattering effects, a continuous ISM controller is proposed to replace the widely-chosen discontinuous controller using multivariable STA. The path following is achieved by the tracking control of the yaw rare and lateral velocity towards their respective desired values, which are calculated according to the path following command. CNF is used to improve the transient tracking performance by reducing the overshoots and eliminating the steady-state errors, and deal with input saturation. STA-based ISM controller is used to reject the multiple disturbances with continuous control input such that chattering effect is attenuated. The overall stability of the scheme is proved based on the Lyapunov method.

The rest of this chapter is organized as following. The modellings for path following and vehicle lateral dynamics are described in Section 4.2. The nominal

controller design using CNF is presented in Section 4.3. The continuous ISM controller design using multivariable STA is presented in Section 4.4. Simulation results are illustrated in Section 4.5, followed by the conclusion in Section 4.6.

4.2 Modelings of Vehicle Lateral Dynamics

As the focus of this work lies on the path following control of AGVs on the yaw plane, the roll, pitch, and vertical motions are neglected in the vehicle dynamics modelling. In this study, a 2-DoF dynamics model of vehicles as shown in Fig. 3.1 is adopted for controller design.

The handling dynamics equations for the 2-DoF model of the vehicle in the yaw plane are given as (Abe, 2015)

$$\begin{cases} I_z\dot{r} = (l_f F_{yf} - l_r F_{yr}) + \Delta M_z, \\ m\dot{v_y} = (F_{yf} + F_{yr}) - m v_x r, \end{cases} \tag{4.1}$$

where ΔM_z is the external yaw moment given as

$$\Delta M_z = \sum_{i=1}^{2} F_{xi}\left[(-1)^i l_s \cos\delta_f + l_f \sin\delta_f\right] + \sum_{i=3}^{4} (-1)^i l_s F_{xi}. \tag{4.2}$$

The generalized front and rear lateral tire forces F_{yf} and F_{yr} are assumed to be linearly related with the front and rear wheels slip angles α_f and α_r, respectively, which can be modeled as

$$F_{yf} = c_f\alpha_f \ , \ F_{yr} = c_r\alpha_r, \tag{4.3}$$

where c_f and c_r represents the generalized cornering stiffness of the front and rear

tire, respectively, and can be expressed as (Hsu, 2009)

$$c_f = c_{f0} + \Delta c_f, \quad c_r = c_{r0} + \Delta c_r, \tag{4.4}$$

where c_{f0} and c_{r0} stand for the generalized nominal cornering stiffnesses of the front and rear tire, respectively, in the condition that the tires operate in the linear work region. Δc_f, Δc_r represent the additional uncertain terms, and can be assumed bounded.

The front and rear slip angles in (4.3) can be calculated from

$$\alpha_f = \delta_f - \frac{l_f r}{v_x} - \beta, \quad \alpha_r = \frac{l_r r}{v_x} - \beta. \tag{4.5}$$

By substituting (4.3) and (4.5) into (4.1), the final vehicle handling equations can be derived as

$$\begin{cases} \dot{r} = a_{11} r + a_{12} v_y + b_{11} \delta_f + b_{12} \Delta M_z, \\ \dot{v}_y = a_{21} r + a_{22} v_y + b_{21} \delta_f, \end{cases} \tag{4.6}$$

where the model parameters in (4.6) are given as

$$\begin{aligned} a_{11} &= -\frac{\left(l_f{}^2 c_f + l_r{}^2 c_r\right)}{v_x I_z}, \quad a_{12} = \frac{(l_r c_r - l_f c_f)}{I_z v_x}, \\ a_{21} &= -v_x - \frac{(l_f c_f - l_r c_r)}{m v_x}, \quad a_{22} = -\frac{(c_f + c_r)}{m v_x}, \\ b_{11} &= \frac{l_f c_f}{I_z}, \quad b_{12} = \frac{1}{I_z}, \quad b_{21} = \frac{c_f}{m}. \end{aligned} \tag{4.7}$$

System (4.6) can be transformed into state-space form as

$$\dot{x} = \bar{A} x + \bar{B} u, \tag{4.8}$$

where $x = [r \;\; v_y]^T$, $u = [\delta_f \;\; \Delta M_z]^T$, and the system matrices are given by

$$\bar{A} = \begin{bmatrix} a_{11} & a_{12} \\ a_{21} & a_{22} \end{bmatrix}, \quad \bar{B} = \begin{bmatrix} b_{11} & b_{12} \\ b_{21} & 0 \end{bmatrix}. \tag{4.9}$$

Considering the system uncertainties, (4.8) can be rewritten as

$$\dot{x} = (A + \Delta A)\, x + (B + \Delta B)\, u, \tag{4.10}$$

where A and B are the nominal system matrices obtained by substituting $c_f = c_{f0}$ and $c_r = c_{r0}$ in (4.9), and ΔA and ΔB are the uncertainties due to the changing of the tire cornering stiffnesses (Hu et al., 2016). Define the lumped disturbance $D(x,t)$ as

$$D(x,t) = \Delta A x + \Delta B u. \tag{4.11}$$

Since the matrix B is invertible in this work, we can assume that the lumped disturbance $D(x,t)$ satisfies the matching condition as

$$D(x,t) = B d(x,t), \tag{4.12}$$

where $d(x,t)$ is a lumped disturbance vector. Considering the physical limits of the vehicle states and parameters, we can further assume that the norms of the lumped disturbance $d(x,t)$ and its time-derivative $\dot{d}(x,t)$ are bounded by respective known positive constants d_{m} and $\dot{d}_m$

$$\|d(x,t)\| < d_{\mathrm{m}}, \;\; \|\dot{d}(x,t)\| < \dot{d}_m. \tag{4.13}$$

Hence (4.10) can be rewritten as

$$\dot{x} = Ax + B\left(u + d\right). \tag{4.14}$$

The variation proportion for tire cornering stiffness used in previous work is usually about 10%-50% (Canale et al., 2009; Zhang et al., 2014; Du et al., 2014). By considering the nonlinear tire model, it can be assumed that the variation for the cornering stiffness in this study is 30% of the nominal value, that is, the cornering stiffness can be varying within the range 112,000 N/rad-208,000 N/rad. Note that this chapter investigates the FWIA autonomous electric vehicles, where the AFS and DYC are simultaneously used to control the vehicle motion, and the tire force saturations are considered to prevent tires from entering the nonlinear region. These strategies will make the vehicle more stable in path following.

Note that the vehicle states and control inputs have the respective limit values, thus according to (4.7), (4.11) and (4.12), the bounds of $d\left(x,t\right)$ and $\dot{d}\left(x,t\right)$ can be calculated accordingly, where $d\left(x,t\right) = B^{-1}\left(\Delta Ax + \Delta Bu\right)$ and $\dot{d}\left(x,t\right) = B^{-1}\left(\Delta A\dot{x} + \Delta B\dot{u}\right)$.

Remark 4.2.1: Note that it is reasonable to assume that $\dot{d}\left(x,t\right)$ exists all the time and is bounded in this study. According to (4.11) and (4.12), we know $d\left(x,t\right) = B^{-1}\left(\Delta Ax + \Delta Bu\right)$ and $\dot{d}\left(x,t\right) = B^{-1}\left(\Delta A\dot{x} + \Delta B\dot{u}\right)$. As this work investigates the normal driving manoeuvres for vehicle path following in mild road and environment conditions, the vehicle states are maintained in reasonable regions with reasonable control inputs which are constrained within the saturation limits. Also, this chapter uses the ISM-CNF control, where the super-twisting algorithm is used to make the integrated controller continuous thus to avoid the chattering effects. Therefore, the vehicle states and control inputs change continuously without step-changes, and in general cases, there will not be step changes

in the lumped disturbance $d(x,t)$. The vehicle states and control inputs change continuously in reasonable regions, hence their time-derivatives exist. The vehicle states and their time-derivatives are bounded due to the physical limits and tire road adhesion condition. Simultaneously, the control inputs are constrained within the saturation limits by the proposed CNF controller, and thus their time-derivatives are also bounded. Therefore, we know $\dot{d}(x,t)$ exists all the time and is bounded.

In this work the path following problem is translated into the vehicle yaw and lateral motion control, i.e., making the vehicle yaw rate and lateral velocity track their respective desired value. The path following model has been shown in Fig. 2.1, and can be described by (2.2). The control objective is to globally and asymptotically stabilize e and ψ at zero, such that the vehicle will track the desired path asymptotically. The desired yaw rate r_d is generated according to the path following desire (thus r_d is time-varying), and the desired lateral velocity is chosen as zero in accordance with practice (Tchamna and Youn, 2013). The control objective is to design a controller to complete the vehicle yaw and lateral motion control considering the tire forces saturations, system uncertainties and time-varying reference.

4.3 Nominal Controller Design using CNF

The path following control law is designed through the proposed ISM-CNF technique to improve the transient tracking performance in the presence of the changing road-curvature and system uncertainties. In this section, we will design a nominal controller using a modified CNF technique for the system without disturbance to have a desired trajectory, reduce the transient overshoots and eliminate

the steady-state errors.

The reference yaw rate r_d is to realize the path following objective, i.e., asymptotically stabilize the path following errors e and ψ. r_d can be found in (2.14).

Motion control performance for FWIA vehicles heavily depends on the effective actuation. Tire forces saturation problem has a destructive impact on the path following effects, and even probably leads to vehicle uncontrollability in handling limit situations. The external yaw moment input results from the different longitudinal tire forces generated by independent in-wheel motors, and its saturation limit value is determined by the limit of the torque of the electric motor. In FWIA vehicles, since the yaw moment can also achieve yaw stabilization, the magnitude of the steering angle is generally away from its saturation limit. Therefore, to guarantee the path following performance, only the tire force saturation issues are considered in the ISM-CNF controller design, which retains the advantage of standard CNF in handling the input saturation.

Considering the tire force saturation, (4.6) can be rewritten into the following state-space form

$$\begin{cases} \dot{x} = Ax + B\left[\overline{\text{sat}}\,(u) + d\right], \\ y = C_1 x, \\ z = C_2 x, \end{cases} \tag{4.15}$$

where $x = [r \;\; v_y]^T$ is the vehicle states, $u = [u_1 \;\; u_2]^T = [\delta \;\; \Delta M_z]^T$ is the control input, the partial saturation function $\overline{\text{sat}}\,(u)$: $\mathbb{R} \to \mathbb{R}$ is defined as $\overline{\text{sat}}\,(u) = [u_1 \;\; \text{sat}\,(u_2)]^T$, where the saturation function $\text{sat}\,(u_2)$: $\mathbb{R} \to \mathbb{R}$ is defined as

$$\text{sat}\,(u_2) = \text{sign}\,(u_2) \cdot \min\left\{u_{2\,\max},\ |u_2|\right\}, \tag{4.16}$$

where sign is the sign function, $u_{2\,\max} = \Delta M_{z\,\max}$ is the saturation limit for the external yaw moment. $y = [r \;\; v_y]^T$ is the measured output. $z = [r \;\; v_y]^T$ is the

controlled output. $\gamma = [r_d \ \ 0]^T$ is the reference for the controlled output z. The expressions of $A,\ B,\ C_1$ and C_2 are given by

$$A = \begin{bmatrix} a_{110} & a_{120} \\ a_{210} & a_{220} \end{bmatrix}, \quad B = \begin{bmatrix} b_{110} & b_{120} \\ b_{210} & 0 \end{bmatrix}, \tag{4.17}$$
$$C_1 = \text{diag}\{1,\ 1\}, \quad C_2 = \text{diag}\{1,\ 1\}.$$

where the model parameters in (4.17) are the nominal parameters obtained by substituting $c_f = c_{f0}$ and $c_r = c_{r0}$ in (4.7).

The following assumptions (Chen et al., 2003) which are commonly required as the preconditions for CNF design are satisfied for the investigated system (4.15):

1. $(A,\ B)$ is stabilizable;

2. $(A,\ C_1)$ is detectable;

3. $(A,\ B,\ C_2)$ has no invariant zero at $s^\dagger = 0$ ($s^\dagger$ means the Laplace variable);

4. Control gain matrix B is row full rank.

In the work below we will present the design of the nominal controller using modified CNF control through three steps. In the first step, a modified linear state feedback part will be designed in the presence of the time-varying multiple references, such that the closed-loop system response would have a fast rise time; in the second step, a nonlinear feedback portion will be designed to reduce the transient overshoots and eliminate the steady-state errors for the controlled outputs; in the third step, the linear feedback part and nonlinear feedback part will be integrated to form the modified CNF controller.

Step 1: A modified linear feedback controller for the system (4.15) considering

the time-varying multiple references is proposed as follows,

$$u_l = Fx + G\gamma + G_\gamma \dot{\gamma}, \tag{4.18}$$

where F is chosen such that 1) $A + BF$ is an asymptotically stable matrix, and 2) the closed-loop poles of $C_2\big(s^\dagger I - A - BF\big)^{-1}B$ have a dominant pair with a small damping ratio, which would in turn yield a fast rise time in the closed loop system response. Such an F can be generated based on some well-studied control techniques, such as the LQR, H_∞ or H_2 optimization approaches (Chen et al., 2003). G is chosen as

$$G = -[C_2(A + BF)^{-1}B]^{-1}, \tag{4.19}$$

and G_γ is chosen as

$$G_\gamma = B^T\big(BB^T\big)^{-1}G_e, \tag{4.20}$$

where

$$G_e = -(A + BF)^{-1}BG, \tag{4.21}$$

where F is designed to realize the feedback control, G and G_γ are designed to realize feedforward control. The linear feedback controller is designed to make the controlled output z track the reference r in the closed-loop system. Note that F, G, and G_γ are well defined since $(A,\ B,\ C_2)$ is assumed to have no invariant zeros at $s^\dagger = 0$. However, the linear feedback control law in (4.18) is difficult to guarantee good transient performance and may result in some steady-state errors for the controlled system outputs. To alleviate that problem, a nonlinear feedback portion is designed in CNF controller, which is used to adaptively change the damping ratio of the closed-loop system such that the overshoots and steady-state errors for the closed-loop system can be restrained. The nonlinear feedback control

law is designed in the following step.

Step 2: Given a positive definite symmetric matrix $W \in \mathbb{R}^{2\times 2}$, a real positive definite symmetric matrix $P > 0$ ($P \in \mathbb{R}^{2\times 2}$) can be solved from the following Lyapunov equation

$$(A + BF)^T P + P(A + BF) = -W. \tag{4.22}$$

Note that such a P always exists since $(A + BF)$ is designed to be asymptotically stable. Next, we define x_e as the reference for the system state x, given that r is the reference of the controlled output z

$$x_e = G_e \gamma, \tag{4.23}$$

which means that x will track x_e as z tracks γ. The nonlinear feedback portion u_n is designed as

$$u_n = \kappa(\gamma, z) B^T P (x - x_e), \tag{4.24}$$

where

$$\kappa(\gamma,\ z) = \mathrm{diag}\{\kappa_1(\gamma,\ z),\ \ \kappa_2(\gamma,\ z)\}, \tag{4.25}$$

where $\kappa_j(\gamma,\ z)$ $(j = 1,\ \ 2)$ is a non-positive and smooth function of $\|z - \gamma\|$, which is used to gradually change the damping ratio of the closed-loop system to obtain a better transient tracking performance.

Different forms for nonlinear function $\kappa(\gamma,\ z)$ have been proposed in previous literatures. Especially, the one proposed in Lan et al. (2010)

$$\kappa_j(\gamma,\ z) = -\phi_j \exp(-\alpha_j \alpha_0 \|\varepsilon\|), \quad (j = 1,\ \ 2) \tag{4.26}$$

is a scaled nonlinear function with better robustness to the variation of the target

reference, where $\varepsilon = z - \gamma$, and

$$\alpha_0 = \begin{cases} \dfrac{1}{\|\varepsilon(0)\|}, & \varepsilon(0) \neq 0, \\ 1 \quad , & \varepsilon(0) = 0, \end{cases} \tag{4.27}$$

where ϕ_j and α_j are tunable positive scalars to improve the tracking performance.

Step 3: In this step, the linear and nonlinear feedback portions are integrated to form the final CNF controller, which is given by

$$u_0 = u_l + u_n = Fx + G\gamma + G_\gamma \dot{\gamma} + \kappa(\gamma, z) B^T P \cdot (x - x_e). \tag{4.28}$$

where x_e is defined in (4.23).

Remark 4.3.1: Though the assumption of a constant vehicle longitudinal velocity is used, the proposed nominal controller can also deal with the situation with time-varying vehicle speed. In that case, the system matrices A and B in (4.15) are time-varying, thus the F in the linear feedback control part (4.18) is time-varying, so are the control gains G and G_γ. Note that there are only two states in the investigated system (4.15), the appropriate F can still be algebraically solved online using some well-studied control techniques (e.g., pole assignment, LQR) as long as A and B are given, no matter how they change. they change. Algebraically solving the matrix F is important for practical driving in real vehicle systems, since it avoids the time-consuming numerical computation.

4.4 Multivariable Continuous ISM Controller Design

Note that the above nominal controller in (4.28) does not consider the rejection of the unknown system disturbances. It does not guarantee the robustness for the closed-loop system response performance. To this end, we propose an ISM controller u_s, which is added with the proposed CNF controller u_0 to make overall control system robust to the system uncertainties, i.e., the control input for the vehicle system (4.15) is designed as $u = u_0 + u_s$. The nominal control u_0 is proposed to achieve the desired performance when system is free from disturbance. Note that the nominal control u_0 can be designed using other multivariable linear control techniques (such as proportion integration differentiation (PID), linear quadratic regulator (LQR), state feedback, etc.). In this section, a continuous ISM controller is designed based on multivariable STA to eliminate the effects of the lumped disturbance d and thus to make the path following controller robust to the variations of the vehicle parameters.

The integral sliding surface is defined as

$$s(x,t) = G_2 \left\{ x(t) - x(0) - \int_0^t (Ax + B\Delta)\, d\tau \right\}, \tag{4.29}$$

with Δ denoting the nominal controller in the presence of actuator saturation as

$$\Delta = \overline{\text{sat}}(u) - u_s, \tag{4.30}$$

where $G_2 \in \mathbb{R}^{2\times 2}$ is a constant projection matrix such that $G_2 B$ is uniformly invertible. In the above sliding surface the nominal controller u_0 is used to realize

specified and nominal trajectory if substituted into the nominal plant (4.15) without disturbance term $d(x,t)$. In this study, the modified CNF controller aims at improving the transient performance of the path following control. In the above sliding surface, $x(t)$ represents the actual trajectory, $x(0)$ is the initial value of the system state. $\int_0^t (Ax + B\Delta)\, d\tau$ represents the desired trajectory for the closed-loop system, and as the additional integral term, it provides one more degree of freedom than the linear sliding surface in the control law design. In this sense, the proposed integral sliding surface can be seen as the difference between the desired and the actual trajectory projected on G_2. This difference results from system uncertainties, and can be eliminated by using appropriate controller, such that the actual system trajectory can track the desired one.

The control objective of the ISM control is to design a control law to force the closed-loop system trajectory to reach and stay on the sliding surface at $s(x,t) = 0$. Therefore the actual control law becomes

$$u = u_0 + u_s = u_l + u_n + u_s. \tag{4.31}$$

To design the ISM control law, we can construct a Lyapunov function as

$$V_1(x,t) = \frac{1}{2} s^T(x,t)\, s(x,t). \tag{4.32}$$

Considering the input saturation in the actual system, the time-derivative of $V_1(x,t)$ can be given as

$$\begin{aligned} \dot{V}_1(x,t) &= [G_2\dot{x} - G_2(Ax + B\Delta)]^T s(x,t) \\ &= \{G_2(Bu_s + Bd)\}^T s(x,t) \\ &= [u_s + d]^T (G_2 B)^T s(x,t), \end{aligned} \tag{4.33}$$

where the ISM controller added to the nominal controller is used to enforce the sliding motion in the presence of system uncertainties. The common choice for the ISM control u_s is discontinuous given by

$$u_s = -M(x,t)\,\text{sign}\left[(G_2B)^T s(x,t)\right], \tag{4.34}$$

where $M(x,t)$ is a positive function and should satisfy $M(x,t) \geq d_m$. With this discontinuous control law we have $\dot{V}_1(x,t) < 0$. Without loss of generality we can consider $G_2B = I_{2\times 2}$ (otherwise the controller u_s is scaled by $(G_2B)^{-1}$), the derivative of s is given from (4.29) as

$$\dot{s} = u_s + d. \tag{4.35}$$

The control law in (4.34) is discontinuous and the actual effect of such a controller on a given plant is equal to the average of the control action which called "equivalent control" (Utkin and Shi, 1996). When the closed-loop system reaches the sliding surface, the equivalent value of the discontinuous control can be calculated by making the time-derivative of the sliding surface (4.35) equal to zero. For the analysis purpose, u_s can be replaced with its equivalent controller (Utkin, 1977)

$$(u_s)_{eq} = u_{seq} = -d(x,t). \tag{4.36}$$

Since the ISM controller u_s is generally designed as a discontinuous feedback control (4.34) to reject the disturbance, the overall control performance for the closed-loop system will also be discontinuous. Due to the discontinuity in the control law, chattering phenomenon is likely to be generated in actuators, and the practical implementation for control actuation is difficult and undesirable. To this end, to avoid chattering phenomenon and make the ISM controller more suitable

for actual implementation, a continuous ISM control law u_s is adopted in this section using the multivariable STA as shown in the following theorem:

Theorem 4.4.1: For a MIMO system (4.35), where the unknown bounded disturbance d is assumed to satisfy $|\dot{d}| \leq \dot{d}_m$, with the controller u_s based on the multivariable STA

$$\begin{cases} u_s = -\ell_1 \dfrac{s}{\|s\|^{1/2}} + \varpi - \ell_2 s, \\ \dot{\varpi} = -\ell_3 \dfrac{s}{\|s\|} - \ell_4 s, \end{cases} \tag{4.37}$$

where the controller gains ℓ_i $(i = 1,\ 2,\ 3,\ 4)$ are properly chosen to satisfy that

$$\begin{aligned} &\ell_1 > \sqrt{2\dot{d}_m}, \\ &\ell_2 > 0, \\ &\ell_3 > \max\left\{3\dot{d}_m + 2\dot{d}_m^2/\ell_1^2,\ \dot{d}_m - 2\ell_1^2\right\}, \\ &\ell_4 > \max\left\{\varsigma_1/\varsigma_2 + 2\ell_2^2,\ 0\right\}, \end{aligned} \tag{4.38}$$

where $\varsigma_1 = \left(1.5\ell_1^2\ell_2 + 3\dot{d}_m\ell_2\right)^2$, and $\varsigma_2 = \ell_3\ell_1^2 - 2\dot{d}_m^2 - 3\dot{d}_m\ell_1^2$, the closed-loop system (4.35) can be stabilized, s and $\dot{s}$ can be converged to zero globally and asymptotically in finite time.

Proof: After substituting u_s given by (4.37) into (4.35), one get

$$\begin{cases} \dot{s} = -\ell_1 \dfrac{s}{\|s\|^{1/2}} + \varpi - \ell_2 s + d, \\ \dot{\varpi} = -\ell_3 \dfrac{s}{\|s\|} - \ell_4 s. \end{cases} \tag{4.39}$$

Defining $h = \varpi + d$, one can rewrite (4.39) as

$$\begin{cases} \dot{s} = -\ell_1 \dfrac{s}{\|s\|^{1/2}} + h - \ell_2 s, \\ \dot{h} = -\ell_3 \dfrac{s}{\|s\|} - \ell_4 s + \dot{d}. \end{cases} \tag{4.40}$$

The stability proof can be found in Nagesh and Edwards (2014).

Remark 4.4.1: For the implementation of controller (4.37) and the enablement of the sliding motion, the initial conditions for s and ϖ are required. Based on the design of the sliding surface, the initial condition of s is zero, and one can always choose $\varpi(0) = 0$ as an initial condition since ϖ is a fictitious variable. Defining $h = \varpi + d$, although the initial value for the disturbance d is unknown, the sliding mode can also start after some finite time $t > t_\tau$ since h can be designed as small as possible by choosing appropriate controller gains in *Theorem* 4.4.1.

Once the s converges to zero, $\dot{s}$ becomes zero and it remains zero forever in spite of the disturbance. So finally from the definition of h, one gets $\varpi = -d$. Furthermore, from (4.37), we have $u_s = \varpi = -d$ (Nagesh and Edwards, 2014). This means that, when system reaches the sliding mode, the disturbance is canceled out by the continuous ISM controller u_s, whose equivalent value satisfies (4.36). Since the nominal controller and ISM controller are all continuous, the integrated ISM-CNF controller is also continuous thus the chattering effects can be avoided. Given that the ISM controller u_s can be replaced with its equivalent value from (4.36) for the analysis purpose, the overall stability of closed-loop system (4.15) with the proposed controller (4.31) considering the input saturation will be shown in the following theorem and proved by the succedent proof:

Theorem 4.4.2: Considering the given system (4.15) with saturation limit in the second input signal (the external yaw moment), there exists two scalars $\kappa_j^* > 0 \quad (j = 1,\ 2)$ such that for any $|\kappa_j(\gamma, z)| \leq \kappa_j^*$, the proposed ISM-CNF control law (4.31) which combines (4.28) and (4.37) will render the controlled output z (i.e. the real yaw rate r and the lateral velocity v_y) to track the time-varying reference r asymptotically without steady-state errors, provided that the following requirements are satisfied:

1) There exists a positive scalar $\tau \in (0,\ 1)$ and $c_\tau > 0$ being be the largest positive scalar such that

$$\begin{aligned} \forall \xi \in \boldsymbol{X}(F,\ c_\tau) = \left\{ \xi \,\middle|\, \xi^T P \xi \leqslant c_\tau \right\} \\ \Rightarrow \left| \bar{F}_2 \xi \right| \leqslant (1-\tau)\, u_{2\max}, \end{aligned} \tag{4.41}$$

where F is partitioned in accord with x_1 and x_2 as $F = \begin{bmatrix} \bar{F}_1 & \bar{F}_2 \end{bmatrix}^T$, and $\boldsymbol{X}(F,\ c_\tau)$ is a set of x which satisfies (4.41);

2) The initial condition $x_0 = [x_1(0),\ \ x_2(0)]^T$ satisfies

$$(x_0 - x_{e0}) \in \boldsymbol{X}(F,\ c_\tau); \tag{4.42}$$

3) The target reference signal γ, its time-derivative and the bound of the disturbance d satisfy

$$\left| \bar{H}_2 \gamma \right| + \left| \bar{G}_{\gamma 2} \dot{\gamma} \right| + d_{2\max} \leq \tau u_{2\max}, \tag{4.43}$$

where $H = G + F\bar{G}$, and H and G_γ are respectively partitioned in accord with x_1 and x_2 as $H = \begin{bmatrix} \bar{H}_1 & \bar{H}_2 \end{bmatrix}^T$, $G_\gamma = \begin{bmatrix} \bar{G}_{\gamma 1} & \bar{G}_{\gamma 2} \end{bmatrix}^T$.

Proof: Define the error between x and x_e as

$$\tilde{x} = x - x_e. \tag{4.44}$$

Then, the control law in (4.28) can be rewritten as

$$u = F\tilde{x} + H\gamma + G_\gamma \dot{\gamma} + \kappa(\gamma, z)\, B^T P \tilde{x} + u_s, \tag{4.45}$$

According to (4.21) and (4.23), it can be derived that

$$(A + BF)\, x_e + BG\gamma = 0. \tag{4.46}$$

According to the above equation and the definition of the error variables $\tilde{x}$, we can transform the system (4.15) into the closed-loop form as

$$\dot{\tilde{x}} = (A + BF)\, \tilde{x} + B\eta, \tag{4.47}$$

where η stands for

$$\eta = \overline{\text{sat}}\,(u) - (F\tilde{x} + H\gamma + G_\gamma \dot{\gamma} - d)\,. \tag{4.48}$$

Given the requirements 2) and 3) in *Theorem* 4.4.2 are satisfied, we have

$$\begin{aligned} &\left|\bar{F}_2\tilde{x} + \bar{H}_2\gamma + \bar{G}_{\gamma 2}\dot{\gamma} - d_2\right| \\ &\qquad \le \left|\bar{F}_2\tilde{x}\right| + \left|\bar{H}_2\gamma\right| + \left|\bar{G}_{\gamma 2}\dot{\gamma}\right| + d_{2\,\max} \\ &\qquad \le u_{2\,\max}. \end{aligned} \tag{4.49}$$

Partition B, η and u_s respectively in accord with x_1 and x_2 as $B = [B_1 \;\; B_2]$, $\eta = [\eta_1 \;\; \eta_2]^T$, and $u_s = [u_{s1} \;\; u_{s2}]^T$. Since this chapter only considers the input saturations for the tire forces, we have

$$\begin{aligned} \eta_1 &= u_1 - \left(\bar{F}_1\tilde{x} + \bar{H}_1\gamma + \bar{G}_{\gamma 1}\dot{\gamma} - d_1\right) \\ &= \kappa_1\,(\gamma,\; z)\, B_1^T P\tilde{x} + u_{s1} + d_1 \\ &= \kappa_1\,(\gamma,\; z)\, B_1^T P\tilde{x}. \end{aligned} \tag{4.50}$$

According to the magnitude of u_2 (where $u = [u_1 \;\; u_2]^T$), the value of η_2 can be

calculated from (4.45) and (4.48) in the following three cases:

1) If $|u_2| \leq u_{2\max}$, thus based on $u_s + d(x,t) = 0$, we have

$$\begin{aligned} \eta_2 &= u_2 - \left(\bar{F}_2\tilde{x} + \bar{H}_2\gamma + \bar{G}_{\gamma 2}\dot{\gamma} - d_2\right), \\ &= \kappa_2(\gamma, z) B_2^T P\tilde{x} + u_{s2} + d_2, \\ &= \kappa_2(\gamma, z) B_2^T P\tilde{x}; \end{aligned} \tag{4.51}$$

2) If $u_2 < -u_{2\max}$, therefore,

$$\begin{aligned} \eta_2 &= -u_{2\max} - \left(\bar{F}_2\tilde{x} + \bar{H}_2\gamma + \bar{G}_{\gamma 2}\dot{\gamma} - d_2\right), \\ &= -u_{2\max} - \left(\bar{F}_2\tilde{x} + \bar{H}_2\gamma + \bar{G}_{\gamma 2}\dot{\gamma} + u_{s2}\right), \\ &= -u_{2\max} - u_2 + \kappa_2(\gamma,\ z) B_2^T P\tilde{x}, \end{aligned} \tag{4.52}$$

From (4.49) it is deduced that

$$\kappa_2(\gamma,\ z) B_2^T P\tilde{x} < \eta_2 < 0; \tag{4.53}$$

3) If $u_2 > u_{2\max}$, therefore,

$$\begin{aligned} \eta_2 &= u_{2\max} - \left(\bar{F}_2\tilde{x} + \bar{H}_2\gamma + \bar{G}_{\gamma 2}\dot{\gamma} - d_2\right), \\ &= u_{2\max} - \left(\bar{F}_2\tilde{x} + \bar{H}_2\gamma + \bar{G}_{\gamma 2}\dot{\gamma} + u_{s2}\right), \\ &= u_{2\max} - u_2 + \kappa_2(\gamma,\ z) B_2^T P\tilde{x}. \end{aligned} \tag{4.54}$$

From (4.49) it is deduced that

$$0 < \eta_2 < \kappa_2(\gamma,\ z) B_2^T P\tilde{x}. \tag{4.55}$$

Based on (4.50) and all possible situations from (4.51)-(4.54), we can always

write η as

$$\eta = q\kappa B^T P\tilde{x}, \tag{4.56}$$

where $q = \text{diag}\{q_1,\ q_2\}$ $(q_1 = 1)$, and q_2 is a nonnegative variable and $q_2 \in [0, 1]$. Given the three requirements in *Theorem* 4.4.2 are satisfied, the system (4.15) controlled by control law (4.31) can be written as

$$\dot{\tilde{x}} = \left(A + BF + q\kappa BB^T P\right)\tilde{x}. \tag{4.57}$$

In the following work, we will prove the asymptotical stability of the closed-loop system (4.57) provided that the initial conditions x_0, the target reference γ and the bound for the disturbance satisfy those requirements listed in the *Theorem* 4.4.2. A Lyapunov function can be constructed as

$$V_2 = \tilde{x}^T P\tilde{x}, \tag{4.58}$$

whose time derivative can be expressed as

$$\begin{aligned}\dot{V_2} &= -\tilde{x}^T W\tilde{x} + 2\tilde{x}^T PB\eta \\ &= \tilde{x}^T\left[-W + 2q\kappa\left(B^T P\right)^T B^T P\right]\tilde{x} \\ &\leq -\tilde{x}^T W\tilde{x},\end{aligned} \tag{4.59}$$

For any nonpositive matrix function $\kappa(\gamma,\ z)$ satisfying $|\kappa_j(\gamma, z)| \leq \kappa_j^*$, we have $\dot{V_2} < 0$. Since the closed-loop system (4.57) is asymptotically stable, we have

$$\lim_{t\to\infty}\tilde{x} = 0 \Rightarrow \lim_{t\to\infty} x(t) = x_e, \tag{4.60}$$

eventually we have

$$\lim_{t\to\infty} z\left(t\right) = \lim_{t\to\infty} C_2 x\left(t\right) = C_2 x_e = \gamma. \tag{4.61}$$

This completes the proof.

4.5 Simulation Results

In this section, we implement two simulation cases, a J-turn maneuver and an S-turn maneuver, based on a high-fidelity and full-car model via CarSim-Simulink platform. In the two maneuvers, different tire-road friction coefficients and different vehicle longitudinal velocities are adopted to verify the robustness of the proposed controller, thus the system uncertainties and disturbances are already included in the simulations. The control objective is to make the vehicle follow the desired path with guaranteed stability. The vehicle parameters used in the simulation is presented in Table 4.1. In the simulation, the saturation limit for the external yaw moment is assumed as 4.0 kNm (Du et al., 2010). To verify the advantage of the proposed ISM-CNF technique, we have compared it with the standard CNF proposed in Chen et al. (2003), which does not consider the rejection of the system disturbance or the variation of the target reference.

Table 4.1: Vehicle parameter used in the simulation.

Symbol	Description	Values and Units
m	Vehicle total mass	1500 kg
l_s	Half of the wheel-base	0.75 m
l_f	Distance of front wheel axle from CG	1 m
l_r	Distance of rear wheel axle from CG	1.6 m
I_z	Vehicle moment of inertia about yaw axis	3240 kg·m^2
c_{f0}	Cornering stiffness of the front tires	160000 N/rad
c_{r0}	Cornering stiffness of the rear tires	160000 N/rad

Fig. 4.1 and Fig. 4.6 provide the curvatures of the desired path, which are designed to approximate a J-turn and an S-turn paths, respectively. This chapter investigates the path following control, whose control objective is to make the vehicle track a predefined desired path in real geometric environment. In real driving situations, the desired path has a fixed curvature, which is geographically defined and time-invariant. Thus the curvature of the desired path at a given point (e. g., point T in Fig. 2.1) is fixed, and changes only with the geographic position of this point, but not with the time. In the simulation studies, we make the vehicle track two clothoid curves, which are designed to approximate a J-turn and an S-turn paths. The clothoid curve designed here includes three path primitives: straights, clothoids and arcs. The curvature of each path segment is defined as the different functions of the distance along the path, as shown in Fig. 4.1 and Fig. 4.6. A straight path is a path segment with zero curvature, i.e., $\kappa(\sigma) = 0$; A clothoid curve is a path defined by a linearly varying curvature related with its distance, i.e., $\kappa(\sigma) = c\sigma$, where c is the rate of the curvature changing rate, or sharpness (Funke and Gerdes, 2013); An arc has a nonzero constant curvature, i.e., $\kappa(\sigma) = 1/R_a$, where R_a is the radius of the arc. For all of the three primitives, the tangent direction (or the heading $\psi_d(\sigma)$) and the coordinate $[x(\sigma), y(\sigma)]$

along the path along the path can be given by

$$\begin{cases} \psi_d(\sigma) = \int_0^\sigma \kappa(\zeta) d\zeta + \psi_0, \\ x(\sigma) = \int_0^\sigma \cos[\psi_d(\zeta)] d\zeta + x_0, \\ y(\sigma) = \int_0^\sigma \sin[\psi_d(\zeta)] d\zeta + y_0, \end{cases} \tag{4.62}$$

where ψ_0 and $[x_0,\ y_0]$ are the initial heading and position, respectively.

In this study we aim to make the simulations cover more different driving scenarios so as to verify the robustness of the proposed ISM-CNF controller. In a slippy road (e.g., μ=0.4), the vehicle usually needs to slow down and run at a low speed (e.g., v_x=10 m/s), while in a dry road (e.g., μ=0.8), the vehicle can speed up and run at a high speed (e.g., v_x=30 m/s). Note that the curvature magnitude in J-turn is much larger than that in S-turn, that is because it is dangerous to make a sharp turning in high-speed driving (e.g., in highway), and vehicle usually needs to slow down to pass through a sharp corner. Therefore, in the simulations we test different driving cases with different tire-road friction coefficients and different vehicle speeds with the same controller, to verify the effectiveness of the proposed strategy and adapt the vehicle to more different driving conditions.

4.5.1 J-Turn Simulation

In the first simulation, the vehicle runs at a low speed (v_x = 10 m/s) on a road with low tire-road friction coefficient (μ = 0.4, where μ is the tire-road friction coefficient), and is supposed to make a J-turn path, which is approximated by a clothoid curve. The curvature κ is designed as the a function of the traveled distance σ (Funke and Gerdes, 2013) as shown in Fig. 4.1.

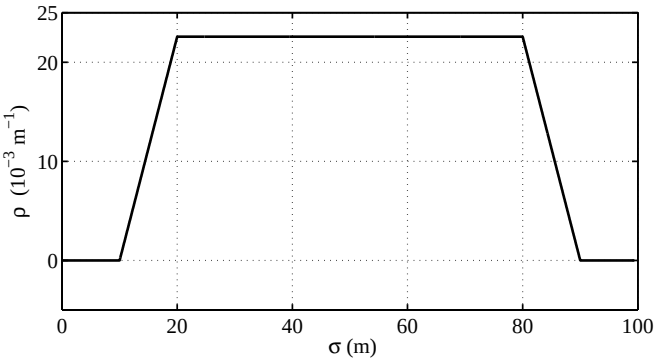

Figure 4.1: The curvature of the clothoid curve in J-Turn Simulation.

The lateral offset and heading error results are shown in Fig. 4.2. From this figure, one can observe that both methods can stabilize the path following errors, but for the ISM-CNF case, the transient performances of the path following errors responses are apparently improved. Path following errors obtain faster responses with lower overshoots and lower steady-state errors using ISM-CNF method than using the standard CNF method. Note that in both ISM-CNF and CNF control frameworks, the heading errors can not be converged to zero, that is caused by the nonzero sideslip angle which is useful for a smooth turning when the vehicle is following a curve path. Due to the same reason, the changing trend of the heading error in steady state is consistent with that of the path curvature. One can refer to our previous work Hu et al. (2015) for the detailed analysis on that phenomenon. Given that the transient response of lateral-offset is of great significance for vehicles in critical manoeuvres (such as lane changing or collision avoidance), the proposed method is able to considerably enhance the vehicle security.

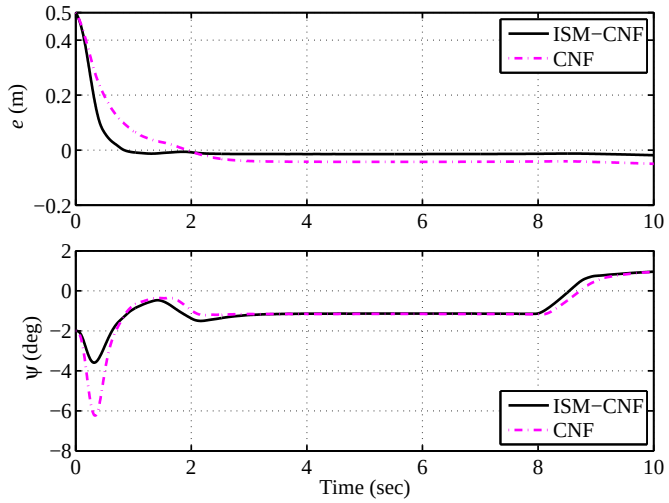

Figure 4.2: The lateral offset and heading error results in the J-turn simulation.

The results of the investigated vehicle states, yaw rate and lateral velocity, are shown in Fig. 4.3. It is shown that both of the ISM-CNF and CNF can maintain the yaw rate and lateral velocity in reasonable regions, but the ISM-CNF can clearly improve their transient performance through reducing the overshoots. The steady-state values of the vehicle states using both method are equal. The changing trends of the vehicle states coincide with that of the path curvature. The lateral velocity is maintained at a relatively small magnitude, that is because a small sideslip angle helps reduce the steady-state errors for the path following errors, and realize a smooth steering. There are some fluctuations in the vehicle states, which are caused by the system disturbances.

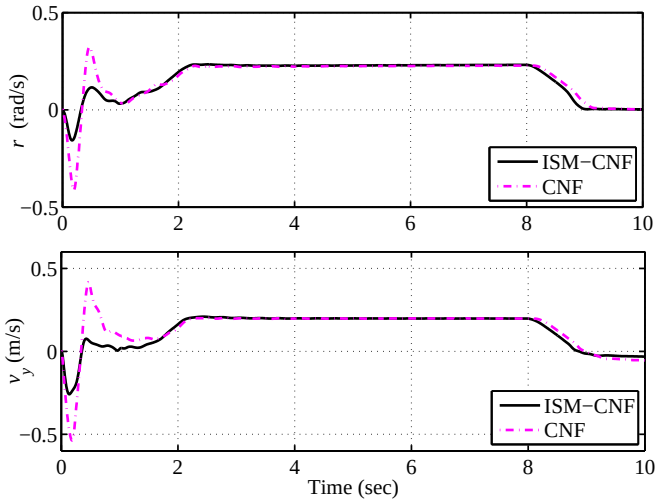

Figure 4.3: The yaw rate and lateral velocity results in the J-turn simulation.

The control inputs, including the steering angle of the front wheel and the external yaw moment are shown in Fig. 4.4. One can see that the control inputs using both methods are maintained at reasonable magnitude, and the external yaw moment is maintained within the saturation limit. Similarly, the ISM-CNF can reduce the overshoots in the control inputs, which show similar varying trends as the path curvature. One can observe that the steering angle is relatively small for both of the control techniques, that is because the yaw moment can also achieve yaw stabilization. Precisely for that reason, the magnitude of the steering angle control input in FWIA is generally away from its saturation limit, thus in this chapter only the saturation issue for the tire forces is considered.

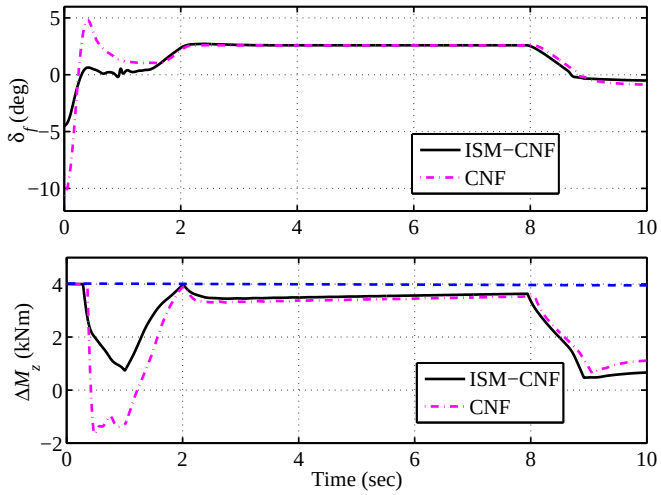

Figure 4.4: The steering angle and yaw moment results in the J-turn simulation.

The path following trajectory results are shown in Fig. 4.5. It is found that the ISM-CNF method can effectively reduce the overshoots in path following errors, and considerably increase the accuracy of path tracking. Thus one can conclude that the path following controller using ISM-CNF has retained advantages of CNF and SMC, and is much faster and more accurate than using standard CNF.

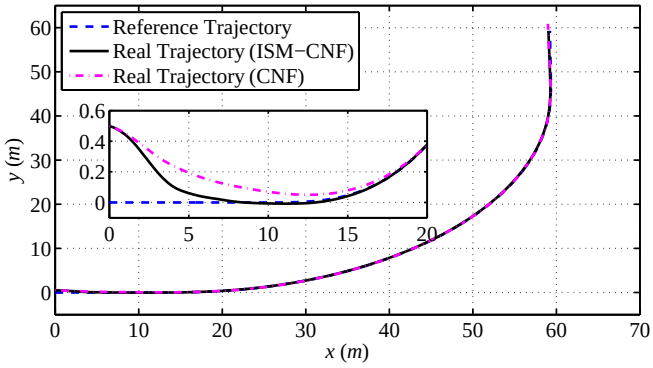

Figure 4.5: The path following trajectory results in J-turn simulation.

4.5.2 S-turn Simulation

In the second simulation, the vehicle runs at a high speed ($v_x = 30$ m/s) on a road with high tire-road friction coefficient ($\mu = 0.8$). Similarly, the vehicle is

controlled to track a clothoid curve, which is designed to approximate an S path. The corresponding road curvature κ_1 is defined as a function of the distance σ (Funke and Gerdes, 2013) shown in Fig. 4.6.

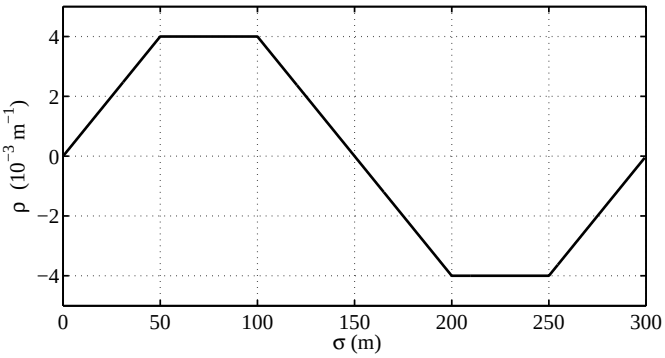

Figure 4.6: The curvature of the clothoid curve in S-turn simulation.

The simulation results for lateral offset and heading error are shown in Fig. 4.7. It can be observed that the path following errors are stabilized by both methods. The lateral offset converges to zero quickly based on ISM-CNF, which can be very critical for AGVs in emergence situations. Similarly, for both methods, the heading error is not converged to zero, and its changing trend is consistent with the road curvature, even though the lateral velocity is already small (shown in Fig. 4.8). Compared with the CNF technique, ISM-CNF can effective reduce the magnitude of the transient overshoot, quicken the system response, and eliminate the steady-state error for the path following errors. For autonomous driving, the magnitude of the lateral offset is very crucial for vehicle safety, since the width of the driving lane for AGVs should be limited. Note that the steady-state error for the heading error in S-turn simulation is relatively smaller than that in J-turn simulation (shown in Fig. 4.2). That is because the path curvature used in the S-turn is much smaller that that in J-turn simulation. It is found that in both cases the steady-state errors of the lateral offset can be eliminated by ISM-CNF technique.

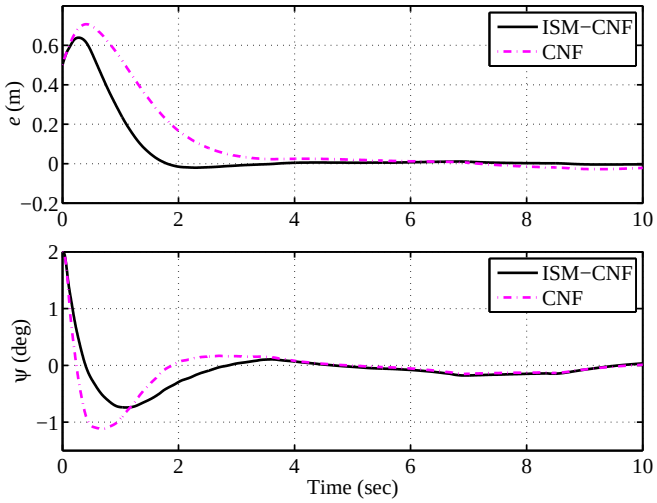

Figure 4.7: The lateral offset and heading error results in the S-turn simulation.

The simulation results for the yaw rate and the lateral velocity are shown in Fig. 4.8. It can be observed that the vehicle states are maintained in reasonable region for both of the control techniques, but the ISM-CNF can relatively alleviate the fluctuations. Since the road curvature continuously changes in the S-turn simulation, it is clearly found that the changing trends of the vehicle states are same as the path curvature. It can be inferred that the road curvature heavily impacts on the vehicle states, thus it is reasonable that the variation of the path curvature should be taken into consideration in the controller design. In both of the two control frameworks, the lateral velocities are stabilized and converged to nonzero values, since certain degree of the lateral velocity contributes to a more smooth turning. Note that the lateral velocity has an important impact on the responses for the path following errors, the lateral velocities for both of the methods are maintained at a equal magnitude.

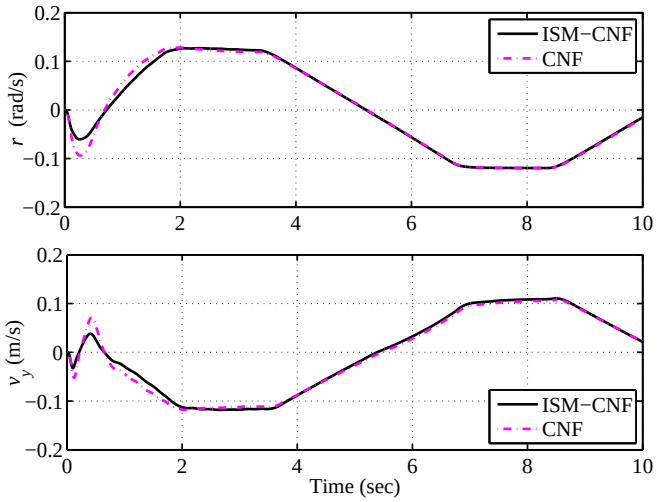

Figure 4.8: The yaw rate and lateral velocity results in the S-turn simulation.

Fig. 4.9 shows the steering angle and the external yaw moment in the S-turn simulation. Both the two control inputs are maintained in reasonable regions. For the control inputs, it is found that the steering angle is maintained at a relatively small value for both control techniques, that is because the yaw moment also contributes to yaw rate stabilization. For the yaw moment, both methods can handle the tire forces saturation issues. Similarly, one can find that ISM-CNF can relatively reduce the overshoots in control inputs. Note that the steady-state values for the steering angle and yaw moment for S-turn simulation is smaller than that of J-turn case, which is because the road curvature is much small in S-turn case.

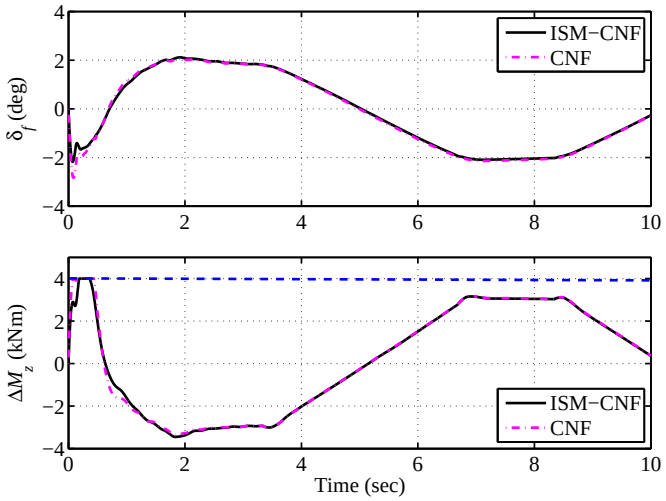

Figure 4.9: The steering angle and yaw moment results in the S-turn simulation.

The trajectory of the path following is shown in Fig. 4.10. One can clearly see that the overshoot phenomenon for the global trajectory for path following is considerably alleviated by using ISM-CNF. The path following objective is completed more satisfactorily using the proposed method, which indicates the possibility of vehicle surpassing the safe driving zone is considerably reduced.

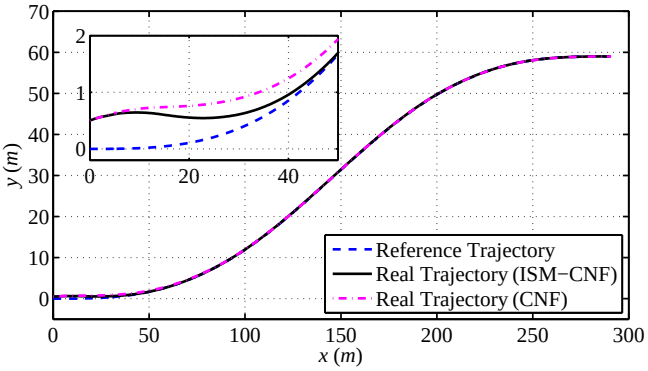

Figure 4.10: The path following trajectory results in S-turn simulation.

Remark 4.5.1: Although the performance improvement of the proposed ISM-CNF compared with CNF is not very significant, the advantage of the ISM-CNF approach about having better transient performance and robustness is still apparent. Note that in extreme conditions even a very small enhancement may make a

difference, e.g., it may prevent the vehicle from surpassing the safe driving lane, or stabilize the vehicle yaw rate after the first collision to avoid a second collision. Also, since the comparing controller in this work is designed by CNF, whose control effect is already good, the overshoots for the system responses are not very large, so the ISM-CNF's improvement effect is not that significant. The computation complexity seems to be increased by using ISM-CNF, yet actually not distinctly. According to the authors' literature review, the indexes for evaluating the computation cost in the control area generally include running time, storage, software and computer used (Bellenger and Coorevits, 2007; Jiao et al., 2014). We use the same computer with the same storage, and the same software (CarSim-Simulink platform) to conduct the verifying simulations, where it is found that the running times for the two methods are basically the same. Considering that the computation cost is not increased distinctly by using ISM-CNF method, which has better transient performance and disturbance rejection property, it is valuable to use ISM-CNF method in real situations, since in extreme conditions, a small improvement on the vehicle transient performance may avoid a crash, or reduce the crash damage or casualties.

4.6 Conclusion

This chapter deals with the path following control issue for FWIA AGVs with considerations of the tire forces saturations, system uncertainties, and the variation of the desired-path curvature. A novel ISM-CNF method which retains the respective advantages of the CNF and SMC algorithms is proposed to improve the transient performance, eliminate the steady-state errors in path following, and reject the impacts caused by the system uncertainties and time-varying reference. The path following is accomplished through converging the yaw rate and lateral velocity to

their respective desired values, where the desired yaw rate is generated based on the path following errors and thus is time-varying. To avoid the chattering effects, a multivariable STA is proposed to design the continuous ISM controller. The results of CarSim-Simulink joint simulations for two curve-following manoeuvres based on a high-fidelity and full-car model verify that, compared with standard CNF, the proposed ISM-CNF can further reduce the overshoots, eliminate the steady-state errors for the controlled outputs, and achieve faster and more accurate robust path following control in the presence of the tire force saturations. In our future work, the constraints on the vehicle states need to be taken into consideration, e. g., when the vehicle makes a sharp turning, the vehicle yaw rate and sideslip angle should be controlled under their limits.

References

Chen, Ben M., T. H. Lee, Kemao Peng, et al. "Composite nonlinear feedback control for linear systems with input saturation: theory and an application." *IEEE Transactions on Automatic Control* 48.3 (2003): 427-439.

Cheng, Guoyang, and Kemao Peng. "Robust composite nonlinear feedback control with application to a servo positioning system." *IEEE Transactions on Industrial Electronics* 54.2 (2007): 1132-1140.

Wang, Chongwen, Xiao Yu, and Weiyao Lan. "Semi-global output regulation for linear systems with input saturation by composite nonlinear feedback control." *International Journal of Control* 87.10 (2014): 1985-1997.

Yang, Qingyun, and Mou Chen. "Robust control for uncertain linear system subject to input saturation." *Journal of Applied Mathematics* 2014 (2014).

Majd, Vahid Johari, and Saleh Mobayen. "An ISM-based CNF tracking controller design for uncertain MIMO linear systems with multiple time-delays and external disturbances." *Nonlinear Dynamics* 80.1-2 (2015): 591-613.

Zhang, Bo, and Weiyao Lan. "Improving transient performance for output regulation problem of linear systems with input saturation." *International Journal of Robust and Nonlinear Control* 23.10 (2013): 1087-1098.

Mobayen, Saleh. "Design of CNF-based nonlinear integral sliding surface for matched uncertain linear systems with multiple state-delays." *Nonlinear Dynamics* 77.3 (2014): 1047-1054.

Abe, Masato. *Vehicle handling dynamics: theory and application*. Butterworth-Heinemann, 2015.

Hsu, Yung-Hsiang Judy. *Estimation and control of lateral tire forces using steering torque*. Ph.D. thesis, Stanford Univ., Stanford, CA, Mar. 2009.

C. Hu, Hui Jing, Hui Jing, F. Yan, et al. "Robust H_∞ output-feedback control for path following of autonomous ground vehicles." *Mechanical Systems and Signal Processing* 70 (2016): 414-427.

Canale, Massimo, Lorenzo Fagiano, Antonella Ferrara, et al. "Comparing internal model control and sliding-mode approaches for vehicle yaw control." *IEEE Transactions on Intelligent Transportation Systems* 10.1 (2009): 31-41.

Zhang, Hui, Xinjie Zhang, and Junmin Wang. "Robust gain-scheduling energy-to-peak control of vehicle lateral dynamics stabilisation." *Vehicle System Dynamics* 52.3 (2014): 309-340.

Du, Haiping, Nong Zhang, and Weihua Li. "Robust tracking control of vehicle lateral dynamics." *International Journal of Vehicle Design* 65.4 (2014): 314-335.

Tchamna, R., and I. Youn. "Yaw rate and side-slip control considering vehicle longitudinal dynamics." *International Journal of Automotive Technology* 14.1 (2013): 53-60.

Lan, Weiyao, Chin Kwan Thum, and Ben M. Chen. "A hard-disk-drive servo system design using composite nonlinear-feedback control with optimal nonlinear

gain tuning methods." *IEEE Transactions on Industrial Electronics* 57.5 (2010): 1735-1745.

Utkin, Vadim, and Jingxin Shi. "Integral sliding mode in systems operating under uncertainty conditions." *Decision and Control, 1996., Proceedings of the 35th IEEE Conference on*. Vol. 4. IEEE, 1996.

Utkin, Vadim. "Survey paper variable structure systems with sliding modes." *IEEE Transactions on Automatic control* 22.2 (1977): 212-222.

Nagesh, Indira, and Christopher Edwards. "A multivariable super-twisting sliding mode approach." *Automatica* 50.3 (2014): 984-988.

Du, Haiping, Nong Zhang, Guangming Dong. "Stabilizing vehicle lateral dynamics with considerations of parameter uncertainties and control saturation through robust yaw control," *IEEE Transactions on Vehicular Technology* 59.5 (2010): 2593-2597.

Funke, Joseph, and J. Christian Gerdes. "Simple clothoid paths for autonomous vehicle lane changes at the limits of handling." *ASME 2013 Dynamic Systems and Control Conference*. American Society of Mechanical Engineers, 2013.

Hu, Chuan, Rongrong Wang, Fengjun Yan, et al. "Should the desired heading in path following of autonomous vehicles be the tangent direction of the desired path?" *IEEE Transactions on Intelligent Transportation Systems* 16.6 (2015): 3084-3094.

Bellenger, Emmanuel, and Patrice Coorevits. "Controlled cost of adaptive mesh refinement in practical 3D finite element analysis." *Advances in Engineering Software* 38.11 (2007): 846-859.

Jiao, Zaibin, Xiaobing Wang, and Heteng Gong. "Wide area measurement/wide area information-based control strategy to fast relieve overloads in a self-healing power grid." *IET Generation, Transmission & Distribution* 8.6 (2014): 1168-1176.

Chapter 5

Robust CNF Path Following Control for IA AGVs with DDAS

This chapter includes the following **published IEEE Transactions journal paper**:

Chuan Hu, Rongrong Wang, Fengjun Yan, and Hamid Reza Karimi, "Robust Composite Nonlinear Feedback Path-Following Control for Independently Actuated Autonomous Vehicles with Differential Steering," ***IEEE Transactions on Transportation Electrification***, vol. 2, no. 3, pp. 312-321, Sep. 2016.

C. Hu is with the Department of Mechanical Engineering, McMaster University, Hamilton, ON L8S4L8, Canada, and also with the School of Mechanical Engineering, Southeast University, Nanjing 211189, China.

R. Wang is with the School of Mechanical Engineering, Southeast University, Nanjing 211189, China.

F. Yan is with the Department of Mechanical Engineering, McMaster University, Hamilton, ON L8S4L8, Canada.

H. R. Karimi is with the Department of Engineering, Faculty of Engineering and Science, University of Agder, N-4898 Grimstad, Norway.

Co-authorship Declaration: The control issue of the vehicle motion control using differential steering was proposed by Prof. Wang. In this control scenario, I proposed the ideas of using CNF to improve the transient performance in the path following control with DDAS, and making the traditional CNF robust to the external disturbances with unknown bounds. Prof. Wang suggested me adopt a nonlinear disturbance observer, which then was proved to be effective to estimate multiple disturbances, and suitable to be integrated in the CNF framework. I completed the controller design and stability analysis, and Prof. Wang checked the overall proof of the stability and robustness of the control system. Before the simulations, I had discussed with Prof. Yan about the contributions of this paper. I also discussed with Prof. Karimi, and got some useful suggestions about the integrated control strategy from him by Email. Then I completed the major work of the paper writing, revisions and replies according to the review comments.

Abstract

This paper investigates utilizing the front-wheel differential drive assisted steering (DDAS) to achieve the path following control for independently actuated (IA) electric autonomous ground vehicles (AGVs), in the case of the complete failure of

the active front-wheel steering system. DDAS, which is generated by the differential torque between the left and right wheels of IA electric vehicles, can be utilized to actuate the front wheels as the sole steering power when the regular steering system fails, and thus avoid dangerous consequences for AGVs. As an inherent emergency measure and an active safety control method for the steering system of electric vehicles, DDAS strategy is a valuable fault-tolerant control approach against active steering system failure. To improve the transient performance of the fault-tolerant control with the DDAS, a novel multiple-disturbances observer-based composite nonlinear feedback (CNF) approach is proposed to realize the path following control for IA AGVs considering the tire force saturations. The disturbance observer is designed to estimate the external multiple disturbances with unknown bounds. CarSim-Simulink joint simulation results indicate that the proposed controller can effectively achieve the fault-tolerant control and improve the transient performance for path following in the faulted-steering situation.

Index Terms

Autonomous ground vehicles, path following, differential drive assisted steering, disturbance observer, composite nonlinear feedback.

5.1 Introduction

Path following control for ground vehicles requires that control strategies are able to handle the inevitable tire sliding effects, model uncertainties, and disturbances. There are plentiful path following control strategies proposed for AGVs, however, few literatures dealt with the transient performance improvement issue which impacts the maneuverability and the riding comfort in vehicle motion control,

especially in faulted-actuator driving conditions. Even though modern commercial cars are usually equipped with some fault-tolerant control mechanisms for actuator failures, the fault diagnosis and control strategy switching require a certain amount of time, deteriorating the transient control performance and vehicle handling. In this sense, transient performance improvement has practical value for fault-tolerant control to yield fast and better response performance in faulted situations.

There actually have been several control strategies proposed to improve the transient performance of the real engineering control systems, nevertheless, the related application in path following control of autonomous vehicles is rather limited. One of the control algorithms that may give an inspiration in AGVs control field is the composite nonlinear feedback (CNF) (Chen et al., 2003; He et al., 2005). By adaptively changing the damping ratio of the closed-loop system and thus improving the transient performance, CNF can be adopted to enhance the vehicle maneuverability and the ride comfort for motion control of AGVs. Note that the model uncertainties and external disturbances commonly exist in real engineering control system. However, based on our literature review, the current CNF technique is hard to deal with systems with single disturbance, or disturbance with strict conditions. Existing literatures with CNF-based robust control techniques (Zhang and Lan, 2013; Majd and Mobayen, 2015) usually need some strict assumptions for the disturbances. In Zhang and Lan (2013); Wang et al. (2014), different disturbance observer-based CNF control strategies were presented for disturbance compensation, and the disturbance was assumed to be generated by a linear exogenous system. Mobayen (2014) and Majd and Mobayen (2015) investigated CNF-based tracking control for uncertain MIMO linear systems with multiple external disturbances, where the bound of the disturbance was assumed

to be known. Actually, the bound of the external disturbance, which is usually arbitrary in engineering application, is usually unknown. A previously proposed multiple-disturbances observer (Yang et al., 2011; Do et al., 2008), which does not require any strict assumptions for the disturbance, is one of the feasible solutions to enhance the robustness for the traditional CNF algorithm. Yang et al. (2011) properly designed a novel disturbance observer-based composite controller to counteract the "mismatched" lumped disturbances from the output channels, where the disturbances were assumed to converge to constant values in steady state. In Do et al. (2008), a multiple-disturbances observer was designed for a nonlinear system, with only one requirement for the disturbances that the changing rates of the disturbances were bounded, but the bounds were not necessarily to be known. However, these disturbance observer-based control strategies did not consider the transient performance improvement.

To this end, this chapter proposes a novel multiple-disturbances observer-based CNF control strategy for the path following of IA AGVs. In this work, DDAS is employed as a sole steering power in the presence of the complete failure of the regular steering system. The main contributions of the chapter lie on: 1) The path following control issue for IA AGVs based on the DDAS is presented in case of the complete failure of the active front-wheel steering, and thus dangerous consequences for vehicles can be avoided; 2) A novel multiple-disturbances observer-based CNF control is proposed to deal with multiple unknown disturbances in the DDAS system and improve the transient performance of path following control of IA AGVs in the faulted-steering situation, where the strict assumptions on the disturbances are relaxed, only requiring that the disturbances and their changing rates are bounded. Note that when the regular active steering system completely breaks, DDAS will be activated and generated by the differential torque to steer

the front wheels. Therefore, the front steering angle is not a control input any more, but a vehicle state controlled by the longitudinal tire force difference of the front wheels. The path following is then achieved by the tracking control of the yaw rate towards its desired value, which is generated according to the path following errors.

The advantages of the proposed controller can be summarized in several aspects. First of all, CNF approach can effectively improve the transient performance of the closed-loop system, including reducing the overshoots and eliminating the steady-state errors, by adaptively changing the damping ratio considering the input saturation. Note that transient performance improvement is a specific property involving the sophisticated control that many popular and well-studied control techniques (e.g., SMC, MPC, H_∞ control, optimal control, etc.) may not own. Currently CNF has seldom been used in vehicle control field, where the manoeuvre smoothness and ride comfort are very critical for vehicle operations. Yet based on the authors' observation, traditional CNF lacks the ability to handle multiple disturbances or bound-unknown disturbance. To this end, a novel robust CNF algorithm based on disturbance observer is proposed in this chapter, which can deal with multiple disturbances whose bounds are unknown, and a strict stability-proof of the closed-loop system is given using Lyapunov method. Admittedly, the concept of the CNF algorithm is not originally proposed by the authors, but to the authors' best knowledge, at present hardly any literature investigated how to deal with multiple bound-unknown disturbances with CNF algorithm to improve the transient performance in the vehicle path following control circumstance.

In terms of specifics, the novelties of the proposed methodology of this study lie on two respects: 1) The DDAS is used for path following control with the differential torque between the left and right wheels of IA electric vehicles being

the sole steering power when the regular steering system fails; 2) A novel robust CNF algorithm based on disturbance observer is proposed to deal with multiple disturbances whose bounds are unknown, and a stability proof of the closed-loop system is given using Lyapunov method. Admittedly, the concept of DDAS mechanism or the CNF algorithm is not new, but to the authors' best knowledge, yet hardly any literature investigated any of the above two issues in the vehicle path following control framework. For a typical steer-by-wire (SbW) system, there is no mechanical connection between the steering wheel for the driver and the steering motor. In order to improve the reliability of the SbW steering system, hardware redundancies (such as dual-motor, dual-microcontroller control system architectures) are usually adopted for SbW systems (Zheng and Anwar, 2008; Wada et al., 2013) in modern vehicle design, which inevitably increase the steering system cost. The proposed DDAS strategy, which is an active safety control method, can potentially replace the redundant components in a regular SbW steering system, since the steering torque generated from the front-wheel differential drive can accomplish the normal steering function. As an inherent emergency measure and mechanical redundancy in front-wheel IA vehicle steering system, DDAS can be a spare and complementary steering actuation system for coordinated control of active front steering (AFS) and direct yaw moment control DYC (or only DYC) without any additional mechanical components, and thus can exempt or reduce the cost spent on other redundant steering mechanism or related hardware. In this chapter, the DDAS is used for automatic steering in the path following control in active steering failure circumstance. A novel robust CNF method is proposed to deal with disturbances with unknown bounds caused by the unmeasured vehicle states and the friction torque in the steering system. The research objective is to

improve the smooth and speediness of the path following manoeuvre with transient performance improvement in the emergent circumstance. Thus the proposed robust CNF, which can enhance the robustness property of CNF and retain its advantage on transient performance improvement, is applicable and novel for path following control for IA vehicles based on DDAS.

The rest of this chapter is organized as following. The modelings of path following, vehicle lateral dynamics and steering system are described in Section 5.2. The multiple-disturbances observer-based CNF controller design with the DDAS is presented in Section 5.3. Simulations based on CarSim-Simulink platform using a high-fidelity and full-vehicle model are conducted in Section 5.4. Followed is the conclusion in Section 5.5.

5.2 Modelings of Vehicle Lateral Dynamics

Vehicle dynamics modelling, the pitch, roll and vertical motions are neglected. A 2-DoF bicycle model of vehicles is presented for controller design as shown in Fig. 5.1. The vehicle has the mass m, the moment of inertia I_z through the the CG about the yaw axis. The front and rear wheel axles are located at distances l_f and l_r from CG, respectively. F_{yf} and F_{yr} are the lateral tire forces of the front and rear wheel, respectively. Note that in this work the driving forces are provided by the front wheels, where are equipped with two independently-actuated motors. α_f and α_r are the tire slip angles of the front and rear wheel, respectively. δ_f is the steering angle of the front wheel.

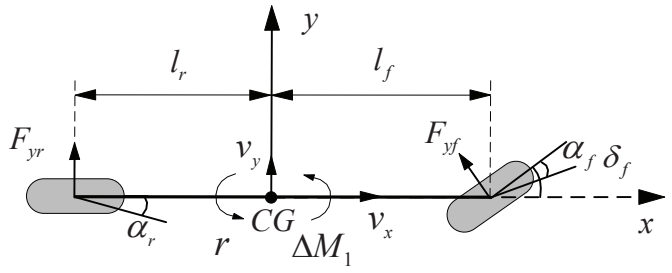

Figure 5.1: Schematic of the vehicle bicycle model.

The vehicle yaw motion can be modeled as (Wang et al., 2011)

$$I_z\dot{r} = F_{yf}l_f - F_{yr}l_r + \Delta M_1, \tag{5.1}$$

where the lateral tire force can be expressed in the linear form provided a small tire slip angle

$$F_{yi} = c_i\alpha_i, \quad (i = f,\ r), \tag{5.2}$$

where c_i is the tire corning stiffness, α_i is the tire slip angle expressed as

$$\alpha_f = -(\frac{v_y + l_f r}{v_x} - \delta_f), \quad \alpha_r = -\frac{v_y - l_r r}{v_x}. \tag{5.3}$$

ΔM_1 is the front external yaw moment generated by the longitudinal tire force difference between the front wheels. Assuming the front wheel steering angle is small, ΔM_1 can be given by

$$\Delta M_1 = (F_{xfr} - F_{xfl})l_s, \tag{5.4}$$

where $F_{xfj} \quad (j = l,\ r)$ is the longitudinal tire force of front-left and front-right wheels, respectively, and l_s is the half of wheel track. Utilizing (5.2) and (5.3), the

vehicle yaw dynamics (5.1) can be rewritten as

$$\dot{r} = \frac{c_f l_f \delta_f}{I_z} - \frac{c_f l_f^2 + c_r l_r^2}{v_x I_z} r + \frac{\Delta M_1}{I_z} - \frac{(c_f l_f - c_r c_r l_r) v_y}{I_z v_x}. \tag{5.5}$$

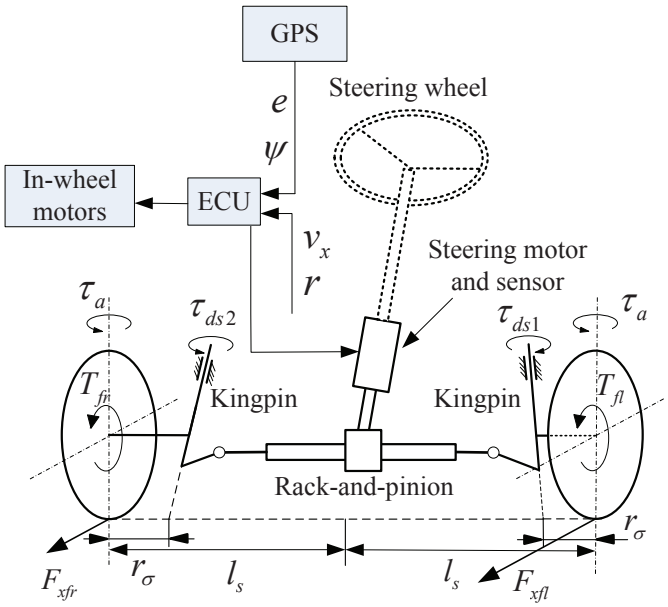

Figure 5.2: Steering system model with the DDAS system for AGVs.

The configuration of a SbW system of the AGV with in-wheel motors is presented in Fig. 5.2, where T_{fl} and T_{fr} are the left and right wheel torque generated by the in-wheel motor, respectively. Note that there is no mechanical connection between steering wheel and steering actuator. This chapter deals with the occasion when the steering motor completely fails, and then the vehicle is steered by the differential torque of in-wheel motors. In this situation, the control input signal will be transmitted to the in-wheel motors to actuate and steer the front wheels. As can be clearly seen from Fig. 5.2, the different longitudinal tire forces F_{xfr} and F_{xfl} will respectively generate a torque as

$$\tau_{ds1} = F_{xfr} \cdot r_\sigma, \quad \tau_{ds2} = F_{xfl} \cdot r_\sigma, \tag{5.6}$$

where r_σ is the scrub radius. When the regular steering system is in complete failure, the resulting differential torque

$$\tau_{ds1} - \tau_{ds2} = (F_{xfr} - F_{xfl}) \cdot r_\sigma \tag{5.7}$$

between the front wheels produced by the different longitudinal tire forces will generate a steering angle, which is the differential steering angle studied in this work. The actuator switching can be conducted according to vehicle fault diagnosis, which has been extensively investigated by the previous literatures (Wang and Wang, 2011). Once the fault of the steering motor is detected, the DDAS mechanism will be activated to actuate the steering wheels.

Remark 5.2.1: Many researches have been carried on the motion control of IA electric ground vehicles with differential driving which is used to provide certain degree of steering power to relieve the driver's turning effort on the steering wheel (Wu et al., 2008; Wang et al., 2011; Nozaki, 2005). However, few previous literatures investigated the case that the differential drive acts as the only power source for the steering, which can be a potential emergency control approach against active steering system failure. When the steering motor breaks down, the front wheels in vehicle with regular steering system will be liberated from the manipulation of the driver, the vehicle will consequently be out of control and vulnerable. In that case, if the DDAS, which is generated by the differential drive torque of the front axle through the steering system mechanism, is used to regulate the front wheel steering, the front wheel can still steer even though there is no steering power from the steering motor. This principle can be utilized for automatic steering without external steering power in faulted-steering condition, but few researchers investigated that benefit. In this chapter, we use the differential torque of the front wheels as the only power source for steering, and adopt DDAS

as the only control input for path following control of autonomous vehicles, which is different from previous literatures.

The dynamic equation of the steering system can be given as

$$J_{\text{eff}}\ddot{\delta}_f + b_{\text{eff}}\dot{\delta}_f = \tau_a + \Delta M_1' - \tau_f, \tag{5.8}$$

where J_{eff} and b_{eff} are the effective moment of inertia and effective damping of the steering system, respectively. τ_f and τ_a are the friction torque and the tire self-aligning moment, respectively. Employing the brush model (Ahn et al., 2013) and the small tire slip angle assumption, τ_a can be expressed as $\tau_a = \lambda_1 c_f \alpha_f$, where α_f is the front tire slip angle, and $\lambda_1 = l^2/3$ is a constant with l being the half of the tire contact length. The steering assisted torque $\Delta M_1'$ in equation (5.8) is generated by the difference between the right and left wheel driving forces, and can be given by

$$\Delta M_1' = \tau_{ds1} - \tau_{ds2} = (F_{xfr} - F_{xfl}) r_\sigma, \tag{5.9}$$

where r_σ is the scrub radius, τ_{ds1} and τ_{ds2} are the right and left differential moment on steering system, respectively. Since $\Delta M_1'$ is the moment on steering system produces by ΔM_1, we can denote $\Delta M_1{}' = \lambda_2 \Delta M_1$, where it can be deduced that $\lambda_2 = \Delta M_{1'}/\Delta M_1 = r_\sigma / l_s$. Based on the above analysis, system (5.8) can be arranged as

$$\dot{\delta}_f = \frac{\lambda_1 c_f \delta_f}{b_{\text{eff}}} - \frac{\lambda_1 c_f l_f r}{v_x b_{\text{eff}}} + \frac{\lambda_2 \Delta M_1}{b_{\text{eff}}} - \frac{\tau_f + J_{\text{eff}}\ddot{\delta}_f}{b_{\text{eff}}}. \tag{5.10}$$

Denote the control input as $u = \Delta M_1$, and rewrite the vehicle model as

$$\begin{cases} \dot{r} = -\dfrac{c_f l_f^2 + c_r l_r^2}{v_x I_z} r + \dfrac{c_f l_f}{I_z}\delta_f + \dfrac{1}{I_z}u + d_1, \\ \dot{\delta}_f = -\dfrac{\lambda_1 c_f l_f}{v_x b_{\text{eff}}} r + \dfrac{\lambda_1 c_f}{b_{\text{eff}}}\delta_f + \dfrac{\lambda_2}{b_{\text{eff}}}u + d_2, \end{cases} \tag{5.11}$$

where

$$d_1 = -\frac{(c_f l_f - c_r l_r)v_y}{I_z v_x},\ d_2 = \frac{1}{b_{\text{eff}}}(\lambda_1 c_f \frac{v_y}{v_x} - \tau_f - J_{\text{eff}}\ddot{\delta}_f). \tag{5.12}$$

The second derivative of front-wheel steering angle $\ddot{\delta}_f$ and the friction torque of steering system τ_f are usually sufficiently small, and thus can be assumed bounded due to their physical limits. τ_f is defined as $\tau_f = F_s \text{sign}(\dot{\delta}_f)$, where F_s is the Coulomb friction constant which can be assumed bounded (Wang et al., 2014), and $\text{sign}(\dot{\delta}_f)$ is the sign function of the time-derivative of the steering angle δ_f. The vehicle lateral velocity v_y is difficult to measure with low cost sensors, and is usually small in normal driving conditions. Therefore, to facilitate the controller design, v_y is regarded as a bounded disturbance. Based on the above analysis, d_1 and d_2 are regarded as two bounded lumped disturbances. Meanwhile, it is reasonable to assume that the disturbances d_1 and d_2 have bounded changing rates, respectively, i.e., $|d_i| \leq \vartheta_{di}$, $\left|\dot{d}_i\right| \leq \zeta_{di}$, $(i = 1, 2)$, but the values of the bounds ϑ_{di} and ζ_{di} are not necessarily to be known.

Note that the front wheel steering angle in (5.11) is not a control input any more, but a vehicle state. The reason is that this chapter investigates the situation of the complete failure of the active steering system, i.e., the steering motor shown in Fig. 5.2 breaks down, so there is no steering wheel torque transferred to the front wheels. Once this failure occurs, DDAS will be activated and produced by the yaw moment of the front wheels to perform the normal front-wheel steering function. Consequentially, the only input in system (5.11) is the yaw moment of

the front axle.

Define the following state variables: $x_1 = r$, $x_2 = \delta_f$ and $x = [x_1 \quad x_2]^T$. Considering the saturation issue for the front external yaw moment, the state-space form of the dynamic model (5.11) can be given as

$$\begin{cases} \dot{x} = Ax + B\text{sat}\,(u) + Ed, \\ y = C_1 x, \\ z = C_2 x, \end{cases} \tag{5.13}$$

where

$$\begin{aligned} A &= \begin{bmatrix} -\dfrac{c_f l_f^2 + c_r l_r^2}{v_x I_z} & \dfrac{c_f l_f}{I_z} \\ -\dfrac{\lambda_1 c_f l_f}{v_x b_{\text{eff}}} & \dfrac{\lambda_1 c_f}{b_{\text{eff}}} \end{bmatrix}, \; B = \begin{bmatrix} \dfrac{1}{I_z} \\ \dfrac{\lambda_2}{b_{\text{eff}}} \end{bmatrix}, \\ E &= \begin{bmatrix} 1 & 0 \\ 0 & 1 \end{bmatrix}, C_1 = \begin{bmatrix} 1 & 0 \\ 0 & 1 \end{bmatrix}, C_2 = \begin{bmatrix} 1 & 0 \end{bmatrix}, \end{aligned} \tag{5.14}$$

and the vector d is denoted as $d = [d_1 \quad d_2]^T$, $u = \Delta M_1$ is the control input. The saturation function $\text{sat}\,(u)$ $\mathbb{R} \to \mathbb{R}$ represents the actuator saturation, which can be defined as

$$\text{sat}\,(u) = \text{sgn}\,(u) \cdot \min\left\{u_{\max}, \; |u|\right\}, \tag{5.15}$$

where $u_{\max} = \Delta M_{1\max}$ is the saturation limit of the front yaw moment, respectively. $y = [r, \quad \delta_f]^T$ is the measured output, where all the system states are assumed to be measurable for the state feedback. $z = r$ is the controlled output. r is the reference yaw rate for the controlled output z, which will be given later. The disturbance matrix E is retained in the following derivations though E is the identity matrix here, since remaining E in the control law design can potentially contribute to extend the application scope of the proposed robust CNF controller, as sometimes E is not the identity matrix in vehicle motion control field. The

proposed robust CNF can provide some inspiration for other related engineering control problems, thus we retain E in the whole deduction. The following assumptions is commonly required in the CNF control framework (Chen et al., 2003), and can be satisfied for the system (5.13):

1. $(A,\ B)$ is stabilizable;

2. $(A,\ C_1)$ is detectable;

3. $(A,\ B,\ C_2)$ has no invariant zero at $s^\dagger = 0$;

4. z is a subset of y, i.e., z is also measurable;

Remark 5.2.2: DDAS strategy proposed in this work is an active safety control method, and can be a valuable fault-tolerant control approach against active steering system failure. As an inherent emergency measure in the steering system of IA electric vehicles, DDAS can be a complementary and spare steering actuation system for the path following control. Without any additional mechanical connection, DDAS mechanism offers a considerable superiority in reducing the cost spent on other related hardware or redundant steering mechanism in AGVs.

In this work the path following problem is translated into the vehicle yaw control, i.e., making the vehicle yaw rate track its desired value. The path following model has been shown in Fig. 2.1, and can be described by (2.2). The control objective is to globally and asymptotically stabilize e and ψ at zero, such that the vehicle will track the desired path asymptotically. The desired yaw rate r_d is generated according to the path following desire. The control objective is to design a controller to complete the vehicle path following control with DDAS considering the tire forces saturations and system uncertainties when the AFS system is in complete failure.

5.3 Disturbance Observer-based CNF Path Following Control Design

In this section, we turn the path following control issue into the yaw control issue, i.e., rendering the real yaw rate to track its reference value to achieve the path following purpose, where the lateral velocity of the vehicle is assumed sufficiently small. The path following control law is designed through the CNF technology to improve the transient tracking performance.

The desired yaw rate r_d is generated to realize the path following objective, i.e., globally and asymptotically stabilizing the system states e and ψ at zero, can be found in (2.14).

In the following work we will present the design of CNF control law through four steps. In the first step, a linear state-feedback portion will be designed; in the second step, a nonlinear feedback portion will be proposed to reduce the overshoot caused by the linear part and eliminate the steady-states errors; in the third step, a disturbance observer (Yang et al., 2011; Do, 2010) is designed to estimate the multiple disturbances; in the final step, the linear feedback portion, nonlinear feedback portion, and the disturbance observer will be integrated to form the CNF controller.

The following assumptions are usually required in the CNF control frame (Chen et al., 2003), and are satisfied for the system (5.13) in this work: 1) $(A,\ B)$ is stabilizable; 2) $(A,\ C_1)$ is detectable; 3) $(A,\ B,\ C_2)$ has no invariant zero at $s^\dagger = 0$; 4) d is a bounded disturbance vector with a bounded changing rate; 5) z is a subset of y, i.e., z is also measurable. Note that in this study we investigate the case that the bounds of the multiple disturbances and their changing rates are both unknown. These assumptions are standard requirements in CNF control framework

to guarantee that the CNF control design is feasible for the given system. They are preconditions in terms of different aspects for CNF control design, thus they are independent of each other. The first assumption is to guarantee that the system can be controlled, and a controller design is feasible; the second assumption is to guarantee that the output y can be measured. There is no requirement that C_1 is the identity matrix in the assumptions, because these assumptions are for general control systems. In our case, (A, C_1) is detectable. The third assumption that (A, B, C_2) has no invariant zero at $s = 0$ is used to avoid singularity for the matrix $G = -\left[C_2(A + BF)^{-1}B\right]^{-1}$. The symbol "$s^{\dagger}$" here means the Laplace variable. The fourth assumption is a prerequisite for adopting the multiple-disturbances observer. The fifth assumption requires that z is a subset of y (y means the measurable states), i.e., z is also measurable, because CNF controller will increase the damping ratio of the closed-loop system as the system output approaches the target reference to reduce the overshoot, and in the nonlinear part of the CNF controller, the tracking error $(z - r_d)$ will be used, i.e., the real value of the controlled output z will be used. More detailed descriptions can be found in Chen et al. (2003), He et al. (2005). Since these assumptions are just theoretical assumptions that guarantee the feasibility of the design of CNF controller, thus they do not have any physical meanings. The proposed robust CNF controller is designed through the following steps:

Step 1: The linear state feedback portion for the system (5.13) is designed as

$$u_L = Fx + F_d d + Gr_d, \tag{5.16}$$

where F is chosen such that 1) $A + BF$ is an asymptotically stable matrix, and 2) the closed-loop poles of $C_2\left(s^{\dagger}I - A - BF\right)^{-1}B$ have a dominant pair with a small damping ratio, which would yield a fast rise time for the closed-loop system.

It should be noted that such an F can be generated using some well-studied approaches such as the LQR, H_∞ or H_2 optimization approaches (He et al., 2005). G is chosen as

$$G = -[C_2(A + BF)^{-1}B]^{-1}, \tag{5.17}$$

and F_d is chosen as

$$F_d = -[C_2(A + BF)^{-1}B]^{-1}[C_2(A + BF)^{-1}E], \tag{5.18}$$

where G is designed to realize the feedback control, and F_d is designed to compensate the disturbances in the control law. F_d and G are designed to make the controlled output z track the reference r_d in the closed-loop system. Note that $F,\ G,$ and F_d are well defined as since $(A,\ B,\ C_2)$ is assumed to have no invariant zeros at $s^\dagger = 0$. The unknown lumped disturbance term d in the control law will be replaced with its estimated value, which will be presented in *Step 3*.

Step 2: Given a positive definite symmetric matrix $W \in \mathbb{R}^{2\times2}$, $P > 0$ ($P \in \mathbb{R}^{2\times2}$) can be calculated by solving the following Lyapunov equation:

$$(A + BF)^T P + P\,(A + BF) = -W, \tag{5.19}$$

such a solution always exists since $(A + BF)$ is asymptotically stable. The matrix P is designed to be used in the nonlinear portion of the CNF controller to guarantee the closed-loop stability of the nonlinear controller. Then we denote

$$x_e = G_e r_d, \tag{5.20}$$

where x_e is designed as the reference for the system state x. G_e is defined as

$$G_e = -(A + BF)^{-1}BG, \tag{5.21}$$

such that the controlled output z will track the reference value r_d if x tracks x_e.

Then the nonlinear feedback portion u_{N} is designed as

$$u_{\mathrm{N}} = \kappa\left(r_d,\ z\right) B^T P \left(x - x_e\right), \tag{5.22}$$

where $\kappa\left(r_d,\ z\right)$ is a smooth and non-positive function of $\|z - r_d\|$, which is used to gradually change the damping ratio of the closed-loop system to achieve a better transient tracking performance. The selection of the design parameters $\kappa\left(r_d, z\right)$ and W will be presented later.

Step 3: The multiple disturbances in (5.13) can be estimated by adopting:

Remark 5.3.1: (Yang et al., 2011; Do, 2010) Consider a multi-input multi-output (MIMO) linear system with multiple disturbances and input saturation issue depicted by

$$\begin{cases} \dot{x} = Ax + B\mathrm{sat}\left(u\right) + Ed, \\ y = Cx, \end{cases} \tag{5.23}$$

where $x \in R^n$, $u \in R^m$, $d \in R^h$, and $y \in R^l$ are state, control input, unknown lumped disturbance, and output vector, respectively. The system matrices A, B, E, and C are with dimensions of $n \times n$, $n \times m$, $n \times h$, and $l \times n$, respectively. It is assumed that there exists a nonnegative constant C_d such that $||\dot{d}\left(x,\ t\right)|| \leq C_d$. The disturbance estimation value $\hat{d}$ obtained by the following state-space

disturbance observer

$$\begin{cases} \hat{d} = p + Lx, \\ \dot{p} = -LE\left(p + Lx\right) - L[Ax + B\mathrm{sat}\left(u\right)], \end{cases} \tag{5.24}$$

can asymptotically track the real lumped disturbance d, with the disturbance observer error $\tilde{d} = \hat{d} - d$ exponentially converging to a ball centered at the origin if the observer gain matrix L is chosen such that matrix $-LE$ is Hurwitz, where p is an auxiliary vector.

Step 4: The linear feedback portion, the nonlinear feedback portion and the disturbance observer obtained in the previous steps are integrated to form the final CNF controller, which is given by

$$u = Fx + F_d\hat{d} + Gr_d + \kappa\left(r_d,\ z\right)B^T P(x - x_e), \tag{5.25}$$

where the estimated values $\hat{d}$ is given in (5.24).

To facilitate the deduction, the following denotation is employed as $A_v = BF_d$. Then we can choose a positive definite matrix $W_Q \in \mathbb{R}^{2\times 2}$ such that $W_Q > A_v^T P W^{-1} P A_v$, and solve the following Lyapunov equation for a positive-definite matrix Q

$$\bar{A}_v^T Q + Q\bar{A}_v = -W_Q. \tag{5.26}$$

Note that such a matrix Q always exists since $\bar{A}_v = -LE$ is asymptotically stable. The matrix A_v and Q will be used in the Lyapunov function based stability proof process for the closed-loop system later. Based on the above controller design, a conclusive theorem is given as:

Theorem 5.3.1: Considering the system (5.13) with input saturation and the multiple disturbances which satisfy $|d_i| \leq \vartheta_{di},\ \left|\dot{d}_i\right| \leq \zeta_{di},\ (i = 1, 2)$, there

exists a scalar $\kappa^* > 0$ such that for any $|\kappa(r_d, z)| \leq \kappa^*$, the CNF control law (5.25) will render the controlled output z (i.e. the real yaw rate r) to track its reference r_d asymptotically without steady-state error, provided that the following requirements are satisfied:

1) There exists a positive scalar $\tau \in (0,\ 1)$ and $c_\tau > 0$ being the largest positive scalar such that

$$\begin{aligned} \forall \xi \in \boldsymbol{X}(F,\ F_d,\ c_\tau) = \left\{ \xi \left| \xi^T \begin{bmatrix} P & 0 \\ 0 & Q \end{bmatrix} \xi \leqslant c_\tau \right. \right\} \\ \Rightarrow |[F \ \ F_d]\,\xi| \leqslant (1-\tau)\,u_{\max}, \end{aligned} \tag{5.27}$$

where $\boldsymbol{X}(F,\ F_d,\ c_\tau)$ is a set of x which satisfies (5.27);

2) The initial conditions $x_0 = [x_{10},\ \ x_{20}]^T = [x_1(0),\ \ x_2(0)]^T$ for system (5.13) and $p_0 = p(0)$ satisfy

$$\begin{bmatrix} x_0 - x_{e0} \\ p_0 - (-Lx_0 + \varpi) \end{bmatrix} \in \boldsymbol{X}(F,\ F_d,\ c_\tau), \tag{5.28}$$

for $\varpi = [\varpi_1 \ \ \varpi_2]^T$, with $\varpi_i = -\vartheta_{di}$, 0, and ϑ_{di}, $(i = 1, 2)$, where $x_{e0} = x_e(0) = G_e r_d(0)$.

3) The target reference signal r_d and disturbance bound ϑ_d satisfy

$$|Hr_d| + |F_d\vartheta_d| \leqslant \tau u_{\max}, \tag{5.29}$$

where $H = G + FG_e$ and $\vartheta_d = [\vartheta_{d1} \ \ \vartheta_{d2}]^T$.

Remark 5.3.2: The design of the CNF and disturbance observer in this chapter actually follows standard procedures (Chen et al., 2003; He et al., 2005; Yang et al., 2011; Do et al., 2008; Do, 2010; Yang and Chen, 2014; Cheng and Peng,

2007), thus the correctness of the mathematical deduction can be guaranteed. Admittedly the novelty of this work lies on the integration of the traditional CNF and the multiple-disturbances observer to form a novel robust CNF technique. Since the existing algorithms are adopted, we just extract the crucial deduction steps to form the robust CNF controller in order to avoid duplication. CNF is a special sophisticated control strategy that specializes in transient performance improvement, and has been not only strictly proved from the theoretical side, but also soundly verified from the experiment side by abundant previous literatures. Therefore in this chapter the motivations for the derivations of the CNF controller are neglected for the sake of brevity.

Remark 5.3.3: Note that the disturbance bound ϑ_d is actually not needed for the disturbance observation design or the robust CNF controller design. That is only mentioned here as a theoretical prerequisite to deal with the input saturation constraint. Otherwise, if the magnitude of disturbance is very large, the input saturation constraint will be hard to satisfy. The assumption of a known disturbance bound is only used to achieve the integrality of the control law presentation. In fact the requirement 3) can generally be satisfied in real vehicle manoeuvre circumstances, that is because the magnitudes of the disturbance and the yaw rate reference in vehicle path following manoeuvre are usually sufficiently small.

Remark 5.3.4: Note that the control action would limit the damping ratio, depending on the input saturation. Simultaneously, the controller is limited by the disturbance and input saturation, which has been shown in the three requirements in *Theorem* 5.3.1, since the choosing of the controller gains should satisfy these requirements to address the input saturation and disturbance. The concept of this work is to choose as suitable a controller gain as possible. Indeed there is a

trade-off between the input saturation and the damping ration. However, based on the authors' experiences and the later simulation results in this work, it can be guaranteed that the input saturation limit for a common ground vehicle is large enough to ensure a small enough damping ratio, if the appropriate in-wheel electric motors are chosen. A large $|F|$ ($A + BF$ is an asymptotically stable matrix) can generate a small damping ratio, which would yield a fast rise time for the closed-loop system. At the same time, F should satisfy the requirements in *Theorem* 5.3.1. Therefore, appropriately choosing a controller gain can make the transient performance much better. As long as the appropriate in-wheel motors are chosen, the input saturation limit can be large enough to ensure that a large enough $|F|$ can be chosen in the presence of disturbances (actually the investigated disturbances in this study are sufficiently small).

Proof: Define the estimation error for d as $\tilde{d} = \hat{d} - d$. Combining system (5.13), disturbance observer (5.24), the estimation error can be expressed as $\dot{\tilde{d}} = -LE\tilde{d} - \dot{d}$ (Yang et al., 2011; Do, 2010). Define the error between x and x_e as $\tilde{x} = x - x_e$. Then the control law in (5.25) can be rewritten as

$$u = [F \quad F_d] \begin{bmatrix} \tilde{x} \\ \tilde{d} \end{bmatrix} + [H \quad F_d] \begin{bmatrix} r_d \\ d \end{bmatrix} + \kappa B^T P \tilde{x}, \tag{5.30}$$

where note that for simplicity of presentation, we will drop the variables (r_d, z) of the nonlinear function $\kappa(r_d, z)$ throughout this proof. According to (5.20) and (5.21), it can be derived that

$$(A + BF) x_e + BGr + (BF_d + E) d = 0. \tag{5.31}$$

According to the above equation, and the definitions of the error variables $\tilde{x}$ and

$\tilde{d}$, we can transform the system (5.13) into the closed-loop form as

$$\dot{\tilde{x}} = (A + BF)\,\tilde{x} + A_v\tilde{d} + B\eta, \tag{5.32}$$

where η stands for

$$\eta = \mathrm{sat}\,(u) - [F \quad F_d]\begin{bmatrix} \tilde{x} \\ \tilde{d} \end{bmatrix} - [H \quad F_d]\begin{bmatrix} r_d \\ d \end{bmatrix}. \tag{5.33}$$

Given the requirements 2) and 3) in *Theorem* 5.3.1 are satisfied, we have

$$\begin{aligned} &\left| [F \quad F_d]\begin{bmatrix} \tilde{x} \\ \tilde{d} \end{bmatrix} + [H \quad F_d]\begin{bmatrix} r_d \\ d \end{bmatrix} \right| \\ &\qquad \le \left| [F \quad F_d]\begin{bmatrix} \tilde{x} \\ \tilde{d} \end{bmatrix} \right| + |Hr| + |F_d d| \le u_{\max}. \end{aligned} \tag{5.34}$$

According to the magnitude of u, the value of η can be calculated from (5.30) and (5.33) in the following three cases:

$$\begin{cases} \kappa B^T P\tilde{x} < \eta < 0, & u < -u_{\max}, \\ \eta = \kappa B^T P\tilde{x}, & |u| \le u_{\max}, \\ 0 < \eta < \kappa B^T P\tilde{x}, & u > u_{\max}. \end{cases} \tag{5.35}$$

For all possible situations, we can always write η as

$$\eta = q\kappa B^T P\tilde{x}, \tag{5.36}$$

where q is a nonnegative variable and $q \in [0, 1]$. Hence for $\begin{bmatrix} \tilde{x} & \tilde{d} \end{bmatrix}^T \in \boldsymbol{X}(F,\ F_d,\ c_\tau)$ and $|Hr| + |F_d\vartheta_d| \le \tau u_{\max}$, the system (5.13) controlled by control law (5.25) based

on the disturbance observer (5.24) can be given by

$$\begin{bmatrix} \dot{\tilde{x}} \\ \dot{\tilde{d}} \end{bmatrix} = \begin{bmatrix} A + BF + \bar{P} & A_v \\ 0 & \bar{A}_v \end{bmatrix} \begin{bmatrix} \tilde{x} \\ \tilde{d} \end{bmatrix} + \begin{bmatrix} 0 \\ -\dot{d} \end{bmatrix}, \tag{5.37}$$

where $\bar{P} = q\kappa BB^T P$ and $\bar{A}_v = -LE$.

In the following analysis, we will prove the asymptotically stability of the closed-loop system (5.37) provided that the initial conditions x_0 and p_0, and the target reference r_d satisfy those requirements listed in *Theorem* 5.3.1. For system (5.37), firstly, we assume that $\dot{d} = 0$, a Lyapunov function can be constructed as

$$V = \begin{bmatrix} \tilde{x} \\ \tilde{d} \end{bmatrix}^T \begin{bmatrix} P & 0 \\ 0 & Q \end{bmatrix} \begin{bmatrix} \tilde{x} \\ \tilde{d} \end{bmatrix}, \tag{5.38}$$

whose time derivative can be expressed as

$$\begin{aligned} \dot{V} &= \begin{bmatrix} \tilde{x} \\ \tilde{d} \end{bmatrix}^T \begin{bmatrix} -W + 2P\bar{P} & PA_v \\ {A_v}^T P & -W_Q \end{bmatrix} \begin{bmatrix} \tilde{x} \\ \tilde{d} \end{bmatrix} \\ &\leqslant \begin{bmatrix} \tilde{x} \\ \tilde{d} \end{bmatrix}^T \begin{bmatrix} -W & PA_v \\ {A_v}^T P & -W_Q \end{bmatrix} \begin{bmatrix} \tilde{x} \\ \tilde{d} \end{bmatrix} \\ &= \begin{bmatrix} \tilde{x}_\perp \\ \tilde{d} \end{bmatrix}^T \begin{bmatrix} -W & 0 \\ 0 & -\bar{W}_Q \end{bmatrix} \begin{bmatrix} \tilde{x}_\perp \\ \tilde{d} \end{bmatrix}, \end{aligned} \tag{5.39}$$

where

$$\tilde{x}_\perp = \tilde{x} - W^{-1} P A_v \tilde{d}, \tag{5.40}$$

and

$$\bar{W}_Q = W_Q - {A_v}^T P W^{-1} P A_v. \tag{5.41}$$

According to the definition of W_Q, there exists two scalars $\kappa^* > 0$ such that for any $|\kappa(r_d, z)| \leq \kappa^*$, so we have $\bar{W}_Q \geqslant 0$. Hence, for any nonpositive matrix function $\kappa(r_d,\ z)$ satisfying $|\kappa(r_d, z)| \leq \kappa^*$, we have $\dot{V} < 0$. From the above derivation, it is identified that the matrix

$$N = \begin{bmatrix} A + BF + \bar{P} & A_v \\ 0 & \bar{A}_v \end{bmatrix} \tag{5.42}$$

is Hurwitz.

As for the case that the changing rate of the disturbance is with an unknown bound, i.e., $||\dot{d}(x,\ t)|| \leq C_d$, it can be proved that the system state $[\tilde{x}\ \ \tilde{d}]^T$ exponentially converges to a ball centered at the origin. The radius of this ball can be made arbitrarily small by adjusting the Hurwitz matrix N (Do et al., 2008). Since the closed-loop system (5.37) is asymptotically stable, we have the following conclusion by choosing appropriate controller gains $\lim_{t\to\infty} [\tilde{x}(t) \quad \tilde{d}(t)]^T = 0 \Rightarrow \lim_{t\to\infty} x(t) = x_e$, eventually we have $\lim_{t\to\infty} z(t) = \lim_{t\to\infty} C_2 x(t) = C_2 x_e = r_d$. This completes the proof.

The previous literatures (Chen et al., 2003; He et al., 2005) had proposed several forms of nonlinear function $\kappa(r_d,\ z)$. Especially, the one proposed in Lan et al. (2010) is a scaled nonlinear function with a better robustness performance to the variation of tracking references. Since the desired references in this work are time-varying, the nonlinear function just mentioned is adopted here as

$$\kappa(r_d,\ z) = -\phi e^{-\alpha\alpha_0\|\varepsilon\|}, \tag{5.43}$$

where $\varepsilon = z - r_d$, ϕ and α are tunable positive scalars for improving tracking performances, and α_0 is defined by (4.27).

In order to quantificationally justify the advantage of the proposed method in

transient performance improvement, three performance indexes (Li and Huang, 2010; Mobayen and Majd, 2012) are used to make the comparisons for the controlled outputs (path following errors) and control input;

1) A direct and simple performance index, the integral of absolute-value of error (IAE) can be used to evaluate the performances of the controlled outputs with the following formula

$$\text{IAE} = \int_0^{t_f} |error|\, dt, \tag{5.44}$$

where $error$ means the corresponding controlled output, and t_f represents the total running time, similarly hereinafter;

2) To include the settling time and the transient overshoot simultaneously, the integral of time-multiplied absolute-value of error (ITAE) is used as

$$\text{ITAE} = \int_0^{t_f} t\,|error|\, dt. \tag{5.45}$$

3) To show the energy consumption, the integral of the square value (ISV) of the control input is represented by the following formula

$$\text{ISV} = \int_0^{t_f} |input|^2 dt, \tag{5.46}$$

where $input$ means the real control input for the controlled system. Note that the $input$ in RCNF control framework has already taken into consideration of the input saturation.

5.4 Simulation Results

In this section, simulations for two driving manoeuvres, J-turn and singe-lane change, are conducted to validate the effectiveness of the proposed control method. As the dynamics response of the in-wheel motor is much faster that of the vehicle, the dynamics characteristic of the in-wheel motor is not considered in this work. Actually, the motor torque can be controlled by regulating the current that flows through the motor. Since this chapter focuses on the control algorithm improvement and its application, the confirmatory simulation is conducted based on the assumption that the motors are appropriately chosen to satisfy the actuation demands. Some detailed descriptions and parameters choosing about the motors for real experiments of IA vehicles can be found in Wang et al. (2011). The steering motor is assumed to completely fail in the simulations. The control objective is to make the vehicle follow the reference path with only the DDAS. The simulations are based on a high-fidelity and full-vehicle model via CarSim-Simulink platform. The comparison scenarios in this work include the J-turn and lane change manoeuvres, where we present the path curvatures, vehicle longitudinal velocities, vehicle parameters and have set the tire-road friction conditions, which have included the main necessary descriptions about CarSim simulations. To validate the robustness of the proposed controller, both the high μ and low μ roads (μ is the tire-road adhesion coefficient) are tested on. We also choose large initial values of the path following errors to verify the saturation-handling feature of the CNF algorithm. The vehicle parameters are listed in Table 5.1. In the simulation, we assume the saturation limit in the front external yaw moment is 2.0 kNm (Du et al., 2010). , the upper bound of the Coulomb friction constant F_s can be assumed as 3.2 Nm (Wang et al., 2014). The controller gains in the reference yaw rate generation for both of the two cases are: $k_1 = 3/v_x,\ k_2 = 30k_1$. For the

linear part of the CNF controller, F is chosen such that $(A + BF)$ has poles at $[-0.01 - 0.01]$, and W is chosen as $\mathrm{W} = \mathrm{diag}\{0.01,\ \ 0.01\}$. The observer gain is chosen as $L = \mathrm{diag}\{0.01,\ 0.01\}$. For the nonlinear part of the CNF controller, the gains are chosen as $\phi = 25$, and $\alpha = 1$. A comparative simulation case using LQR method is presented to highlight the advantages of the proposed robust CNF approach. Some related explanations are given as: Firstly the merit of the CNF algorithm about transient performance improvement has been sufficiently verified by plentiful comparative simulations or experiments with other several basic methods (e.g., conventional proportional-integral-derivative (PID) control, linear control) in the previous literatures (Chen et al., 2003; Peng et al., 2005). The existing extended CNF methods lack the ability to deal with multiple random bound-unknown disturbances (or even multiple disturbances with known bounds). In addition, based on the authors' literature review, it is difficult to design controller which can simultaneously improve the transient performance and deal with bound-unknown multiple disturbances. Hence, it is hard to find an existing control method appropriate for comparing with CNF in our case. Based on the above considerations, we only add one existing method, LQR, which was seldom used previously for comparison with CNF in peers' work. The reason for choosing LQR is that LQR technique is a commonly-used optimal control strategy thanks to its superiority in yielding low steady state error with fast response (Khatoon et al., 2014). To enhance the robust property of LQR to cope with external disturbances, here a robust LQR (RLQR) approach proposed in Yang et al. (2011) is adopted for simulation comparison in this work. Note that the RLQR controller is based on the same disturbance observer proposed in the CNF control design. In the figures of the simulation results, "RCNF" and "RLQR" stand for the proposed robust CNF approach and the adopted robust LQR approach, respectively.

Table 5.1: Vehicle parameters used in the simulation

Definition and Symbol	Value
Vehicle mass m	1500 kg
Vehicle moment of inertia about yaw axis I_z	2000 kg $\cdot$ m^2
Effective steering damping b_{eff}	100 N $\cdot$ s/(m $\cdot$ rad)
Half of the tire contact length l	0.05 m
Half of wheel track l_s	0.75 m
Distance of CG from front axle l_f	1.0 m
Distance of CG from rear axle l_r	1.6 m
Scrub radius r_σ	0.08 m
Cornering stiffness of front tires c_f	80000 N/rad
Cornering stiffness of rear tires c_r	80000 N/rad

5.4.1 J-turn Simulation

In this case, the vehicle runs at a low speed ($v_x = 10\ m/s$) on a slippery road with a low road friction ($\mu = 0.4$, μ is the tire-road adhesion coefficient), and is supposed to make a J-turn. We make the vehicle track a clothoid curve, which is designed to approximate a J-turn path. The clothoid curve is designed here consisting of three path primitives: straights, clothoids and arcs. The curvature ρ of each path segment is defined as the different functions of the distance s along the path (Funke and Gerdes, 2013), as shown in Fig. 5.3. From 1 second to 9 seconds, the vehicle will make a J-turn maneuver. The longitudinal speed of the vehicle is maintained at 10 m/s by controlling the accelerator pedal. We aim at controlling the vehicle such that the actual vehicle can follow the reference path and can be stabilized.

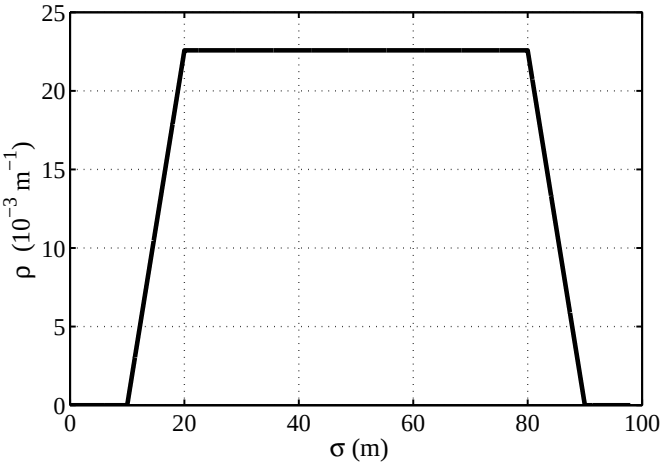

Figure 5.3: The curvature of the desired path in the J-turn simulation case.

The lateral offset and heading error result is shown in Fig. 5.4. One can see that for RCNF, the path following errors can be stabilized quickly, while RLQR obtains large overshoots. At the moments of 1 second and 9 second, the road curvature begins to change respectively, so there are some fluctuations in the path following errors. Note that the lateral offset can converge to zero in steady state, but the heading error can not. This is because the existence of the nonzero sideslip angle in curve-path following, which is needed for a smooth turning. One can refer to our recent work (Hu et al., 2015) for the detailed elaboration on this issue. It is found that compared to RLQR, RCNF can effectively yield small tracking errors for path following control and eliminate the steady-state error for the lateral offset. The yaw rate and lateral velocity results are shown in Fig. 5.5. It is shown that for both methods they can be stabilized and converged in reasonable regions, which indicates that the vehicle is stable through the path following process. The some fluctuations in them are caused by the large initial values of path following errors we choose. It can be deduced that RCNF control based on differential steering can effectively achieve fault-tolerant yaw control in case of the steering-system failure, and improve the transient performance for the path following of AGVs,

while RLQR generates large overshoots in the responses.

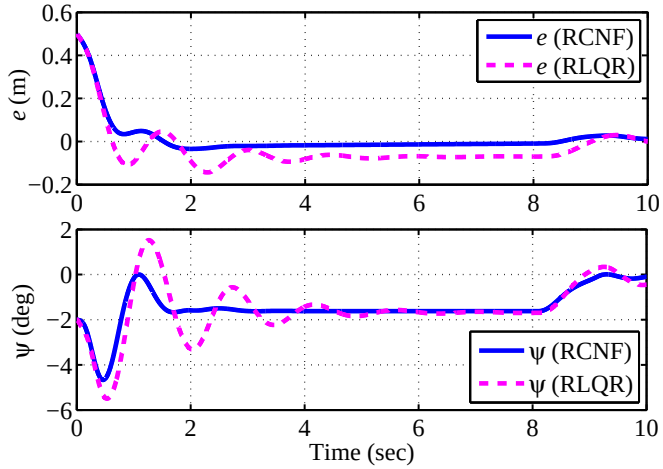

Figure 5.4: The path following error results in the J-turn simulation case.

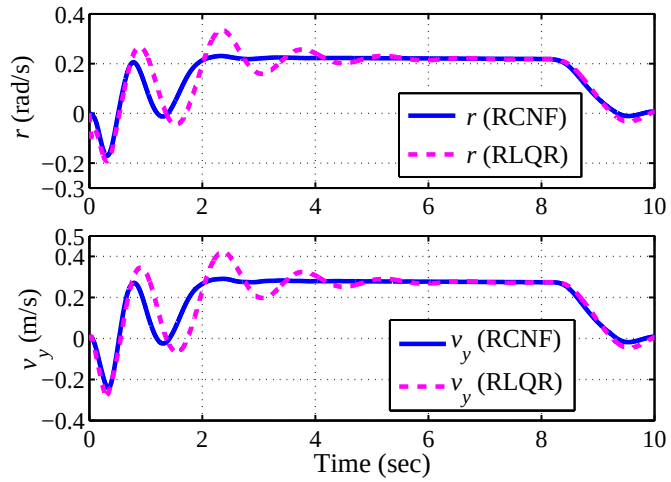

Figure 5.5: The vehicle states results in the J-turn simulation case.

The actual steering angle of the front wheels and the lateral acceleration are presented in Fig. 5.6. We can see for both methods the differential steering angle is maintained in reasonable region, and has a highly similar varying trend compared with the curvature of the desired path defined in this simulation. Thus it is identified that the proposed DDAS mechanism is effective to perform normal steering function in case of the active steering system failure. The lateral acceleration is maintained in reasonable region, showing the lateral stability of the vehicle

in the simulation. Similarly, RCNF can obtain better transient performance in the responses. The front external yaw moment and the longitudinal forces of the front tire are plotted in Fig. 5.7. One can see for RCNF the control inputs are maintained in saturation limits, which has proved the saturation-handling feature of the RCNF controller compared with RLQR controller, which makes the control input surpass the saturation limit. The fluctuations in the figure are caused by the large initial values. The disturbance estimation results are shown in Fig. 5.8, it can be seen that the disturbance is small and can be estimated well by the proposed observer. The path following trajectory is shown in Fig. 5.9, we can see that the J-turn manoeuvre is completed for both methods, but the RCNF can achieve better trajectory tracking performance than RLQR. The performance comparison for J-turn simulation is shown in Table 5.2. We can see that the system response has smaller IAE, ITAE and ISV by using the proposed RCNF than using RLQR, which means the system has smaller overshoots and requires smaller control energy. This quantificationally demonstrates the superior transient performance improvement of the proposed method over the RLQR.

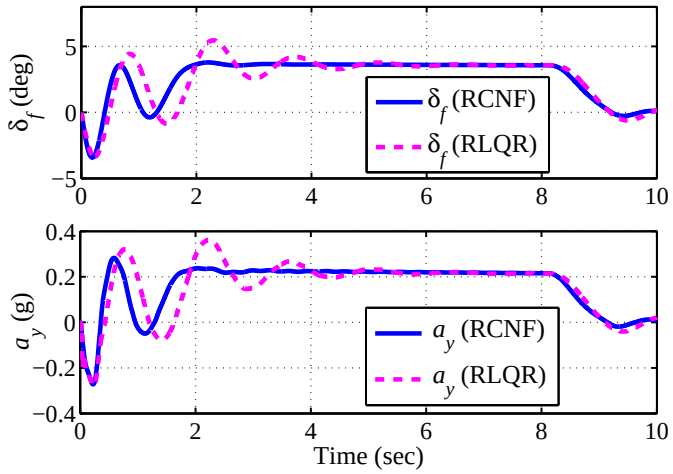

Figure 5.6: The steering angle and the lateral acceleration results in the J-turn simulation case.

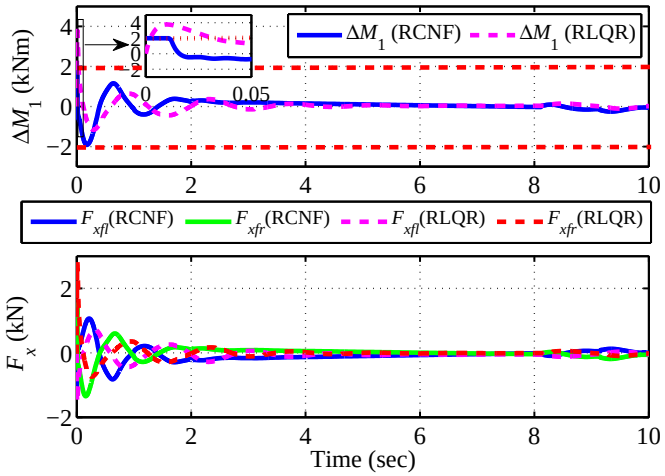

Figure 5.7: The front external yaw moment and the longitudinal forces of the front tires results in the J-turn simulation case.

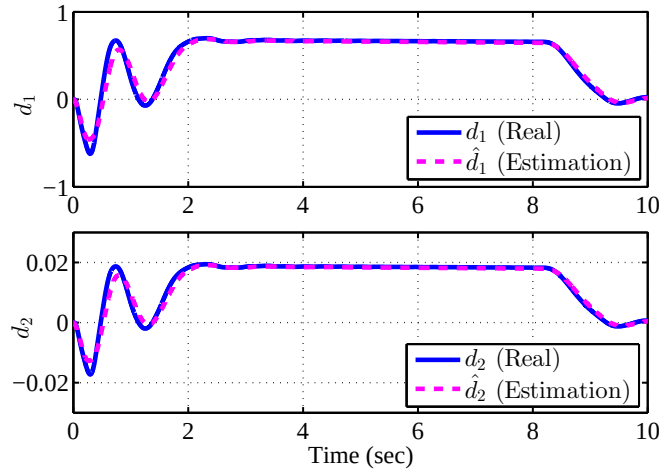

Figure 5.8: The real and estimation values of the disturbance using the proposed observer in the J-turn simulation case.

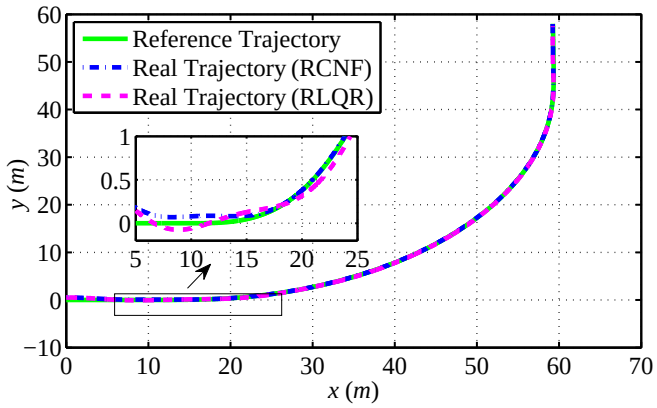

Figure 5.9: The path following trajectory in the J-turn simulation case.

Table 5.2: Performance comparison for J-turn simulation.

Method	IAE (e)	IAE (ψ)	ITAE (e)	ITAE (ψ)	ISV
RCNF	0.665	0.557	0.831	1.068	1.045×10^6
RLQR	1.069	1.587	2.891	2.142	7.813×10^6

5.4.2 Lane Change Simulation

In the second case, the vehicle is made to complete a singe-lane change with a high speed ($v_x = 30\ m/s$) on a dry road with a high tire-road friction ($\mu = 0.8$). We also make the vehicle track a clothoid curve, which is designed to approximate a single-lane change path. The curvature ρ of each path segment is defined as the different functions of the distance s along the path, as shown in Fig. 5.10. From 4 seconds to 6 seconds, the vehicle will make a lane change maneuver. The longitudinal speed of the vehicle is maintained at 30 m/s by controlling the accelerator pedal.

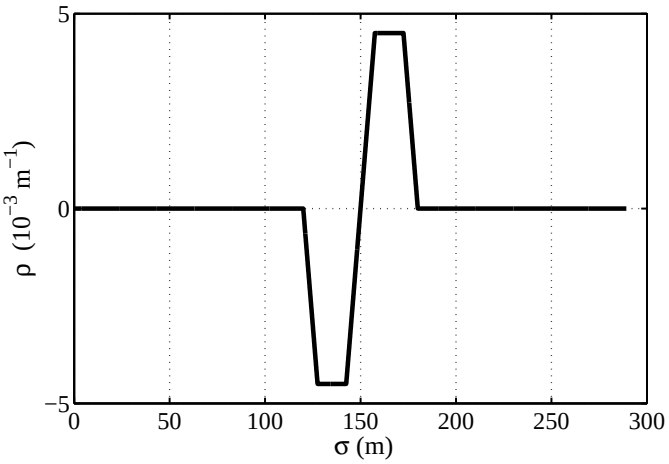

Figure 5.10: The curvature of the desired path in the single-lane change simulation case.

The lateral offset and heading error result is shown in Fig. 5.11. One can see that for RCNF the path following errors can be converged to zero fast in the line part of the desired path, with small overshoots. Since the vehicle begins to change the lane from 4 seconds, the lateral offset begins to shake until the lane change manoeuvre is completed. The vehicle finishes the lane change in 2 seconds, thus the lateral offset does not have enough time to be converged. However, by using the RCNF method, it can be observed that the overshoots of the path following errors in lane change are minor and acceptable, while system has larger overshoots using RLQR. The yaw rate and lateral velocity results are plotted in Fig. 5.12. We can see for both methods the real yaw rate and lateral speed are maintained in reasonable region, with several fluctuations, which is caused by the large initial values of the path following errors. However, RCNF yields much smaller fluctuations in the responses than RLQR. The magnitude of the lateral velocity reveals the lateral vehicle stability in the simulation. By Fig. 5.11 and Fig. 5.12, it is observed that the path following control is well achieved using only the DDAS strategy, and the differential steering based RCNF method can

effectively improve the transient performance and maintain low steady-state errors. Therefore the effectiveness of the differential steering mechanism of performing normal steering function and maintaining good path following performance in the emergency situation is demonstrated.

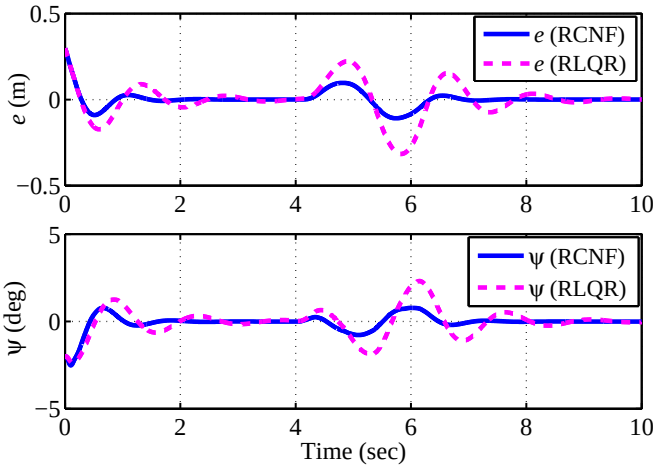

Figure 5.11: The lateral offset and heading error results in the single-lane change simulation case.

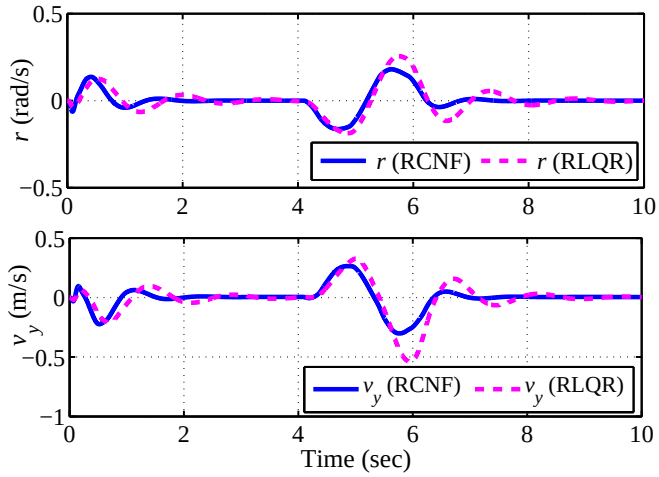

Figure 5.12: The yaw rate and lateral velocity results in the single-lane change simulation case.

The steering angle and the lateral acceleration are shown in Fig. 5.13. One can see that for both methods the real steering angle is controlled in reasonable level,

and has an analogous variation trend compared to the curvature of the desired path. This verifies the rationality of the proposed controller on the steering angle control in high speed driving. The lateral acceleration shows that the vehicle runs within the tire-road friction limit. The front external yaw moment and the longitudinal tire forces are plotted in Fig. 5.14, from which we can see that the RCNF can effectively handle the input saturation issue. It is proved that as an inherent steering actuation redundance, the differential steering can lend a strong support for the driving safety in emergency conditions. The disturbance estimation results in Fig. 5.15 prove the effectiveness of the proposed observer. The path following trajectory is presented in Fig. 5.16. It is observed that the lane change manoeuvre is completed well with smaller overshoots and fluctuations using RCNF than using RLQR.

The performance comparison for lane change simulation is shown in Table 5.3. One can see that compared with RLQR, the proposed RCNF has considerably reduced the overshoots of the controlled outputs, and saved the control energy. It can also be found that the control energy required in lane change manoeuvre is smaller than in J-turn manoeuvre, that is because the path curvature in the former manoeuvre is much smaller than in the latter one.

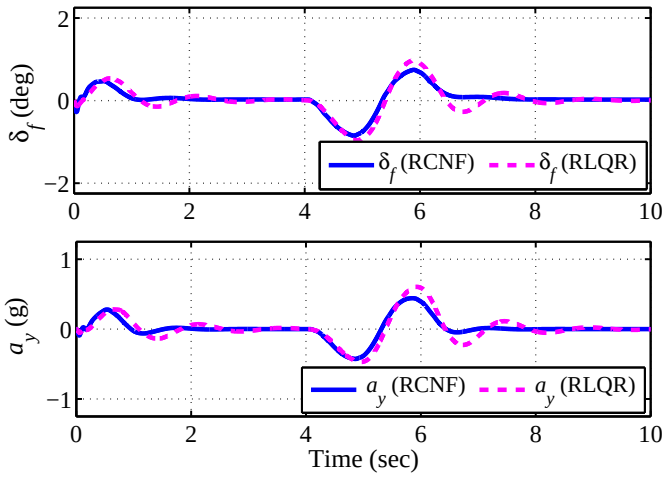

Figure 5.13: The steering angle and the lateral acceleration results in the single-lane change simulation case.

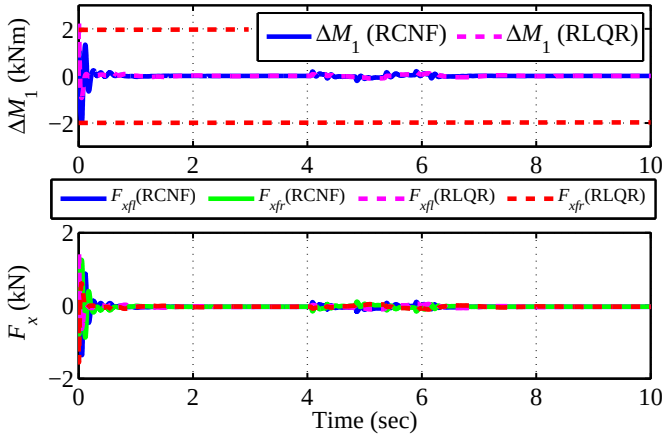

Figure 5.14: The front external yaw moment and the longitudinal forces of the front tires results in the single-lane change simulation case.

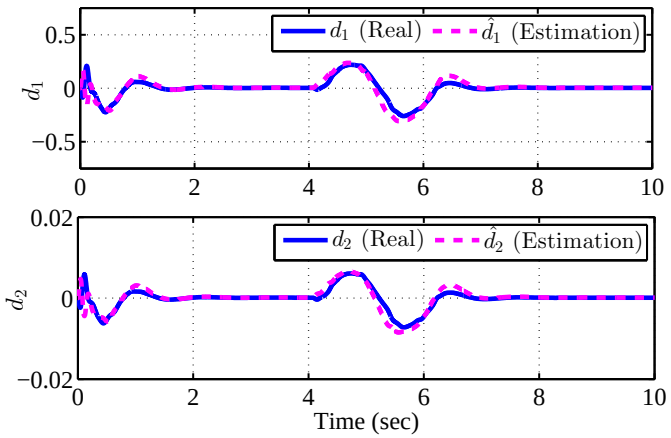

Figure 5.15: The real and estimation values of the disturbance using the proposed observer in the single-lane change simulation case.

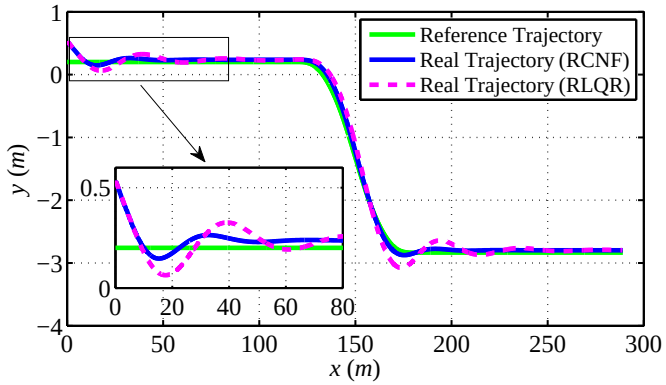

Figure 5.16: The path following trajectory in the single-lane change simulation case.

Table 5.3: Performance comparison for lane change simulation.

Method	IAE (e)	IAE (ψ)	ITAE (e)	ITAE (ψ)	ISV
RCNF	0.535	0.0745	0.85	0.125	2.83×10^5
RLQR	0.979	0.132	3.041	0.411	5.36×10^5

5.5 Conclusion

In this study, the path following control issue for IA AGVs is investigated in the presence of the complete failure of the active steering system, with only the differential steering generated by the independently actuated front in-wheel motors. Since the steering motor is assumed to completely fail, the steering angle is not a control input, but a vehicle state produced by the differential torque between the left and right wheels. A novel disturbance observer-based CNF controller is proposed to achieve the path following control and improve the transient performance. The disturbance observer is designed to estimate the unknown multiple external disturbances, whose bounds are unknown. Simulation results based on a high-fidelity CarSim model validate the effectiveness of the proposed controller. Note that during the RCNF controller design, the parametric uncertainties in the system modeling are not considered, which is left for our future study.

References

Chen, Ben M., T. H. Lee, Kemao Peng, et al. "Composite nonlinear feedback control for linear systems with input saturation: theory and an application." *IEEE Transactions on Automatic Control* 48.3 (2003): 427-439.

He, Yingjie, Ben M. Chen, and Chao Wu. "Composite nonlinear control with state and measurement feedback for general multivariable systems with input saturation." *Systems & Control Letters* 54.5 (2005): 455-469.

Zhang, Bo, and Weiyao Lan. "Improving transient performance for output regulation problem of linear systems with input saturation." *International Journal of Robust and Nonlinear Control* 23.10 (2013): 1087-1098.

Majd, Vahid Johari, and Saleh Mobayen. "An ISM-based CNF tracking controller design for uncertain MIMO linear systems with multiple time-delays and external disturbances." *Nonlinear Dynamics* 80.1-2 (2015): 591-613.

Wang, Chongwen, Xiao Yu, and Weiyao Lan. "Semi-global output regulation for linear systems with input saturation by composite nonlinear feedback control." *International Journal of Control* 87.10 (2014): 1985-1997.

Mobayen, Saleh. "Design of CNF-based nonlinear integral sliding surface for matched uncertain linear systems with multiple state-delays." *Nonlinear Dynamics* 77.3 (2014): 1047-1054.

Yang, Jun, Argyrios Zolotas, Wen-Hua Chen, et al. "Robust control of nonlinear MAGLEV suspension system with mismatched uncertainties via DOBC approach." *ISA transactions* 50.3 (2011): 389-396.

Do, K. D., and J. Pan. "Nonlinear control of an active heave compensation system." *Ocean Engineering* 35.5 (2008): 558-571.

Zheng, Bing, and Sohel Anwar. "Fault-tolerant control of the road wheel subsystem in a steer-by-wire system." *International Journal of Vehicular Technology* 2008 (2008).

Wada, Nobutaka, Kosuke Fujii, and Masami Saeki. "Reconfigurable fault-tolerant controller synthesis for a steer-by-wire vehicle using independently driven wheels." *Vehicle System Dynamics* 51.9 (2013): 1438-1465.

Wang, Jun-nian, Q. Wang, L. Jin, et al. "Independent wheel torque control of 4WD electric vehicle for differential drive assisted steering." *Mechatronics* 21.1 (2011): 63-76.

Wang, Rongrong, and Junmin Wang. "Fault-tolerant control with active fault diagnosis for four-wheel independently driven electric ground vehicles." *IEEE Transactions on vehicular technology* 60.9 (2011): 4276-4287.

Wu, F., and T. J. Yeh. "A control strategy for an electrical vehicle using two in-wheel motors and steering mechanism." *Proceedings of AVEC*. Vol. 8. 2008.

Nozaki, Hiromichi. *Effect of differential steering assist on drift running performance*. No. 2005-01-3472. SAE Technical Paper, 2005.

Ahn, Changsun, Huei Peng, and Hongtei Eric Tseng. "Robust estimation of road frictional coefficient." *IEEE Transactions on Control Systems Technology* 21.1 (2013): 1-13.

Wang, Hai, Zhihong Man, Weixiang Shen, et al. "Robust control for steer-by-wire systems with partially known dynamics." *IEEE Transactions on Industrial Informatics* 10.4 (2014): 2003-2015.

Du, Haiping, Nong Zhang, Guangming Dong. "Stabilizing vehicle lateral dynamics with considerations of parameter uncertainties and control saturation through robust yaw control," *IEEE Transactions on Vehicular Technology* 59.5 (2010): 2593-2597.

Do, Khac Duc. "Control of nonlinear systems with output tracking error constraints and its application to magnetic bearings." *International Journal of Control* 83.6 (2010): 1199-1216.

Yang, Qingyun, and Mou Chen. "Robust control for uncertain linear system subject to input saturation." *Journal of Applied Mathematics* 2014 (2014).

Cheng, Guoyang, and Kemao Peng. "Robust composite nonlinear feedback control with application to a servo positioning system." *IEEE Transactions on Industrial Electronics* 54.2 (2007): 1132-1140.

Do, K. D., and J. Pan. "Nonlinear control of an active heave compensation system." *Ocean Engineering* 35.5 (2008): 558-571.

Lan, Weiyao, Chin Kwan Thum, and Ben M. Chen. "A hard-disk-drive servo system design using composite nonlinear-feedback control with optimal nonlinear gain tuning methods." *IEEE Transactions on Industrial Electronics* 57.5 (2010): 1735-1745.

Li, Tzuu-Hseng S., and Yun-Cheng Huang. "MIMO adaptive fuzzy terminal sliding-mode controller for robotic manipulators." *Information Sciences* 180.23 (2010): 4641-4660.

Mobayen, Saleh, and Vahid Johari Majd. "Robust tracking control method based on composite nonlinear feedback technique for linear systems with time-varying uncertain parameters and disturbances." *Nonlinear Dynamics* 70.1 (2012): 171-180.

Wang, Rongrong, Yan Chen, Daiwei Feng, et al. "Development and performance characterization of an electric ground vehicle with independently actuated in-wheel motors." *Journal of Power Sources* 196.8 (2011): 3962-3971.

Peng, Kemao, B. M. Chen, Guoyang Cheng, et al. "Modeling and compensation of nonlinearities and friction in a micro hard disk drive servo system with nonlinear feedback control." *IEEE Transactions on Control Systems Technology* 13.5 (2005): 708-721.

Khatoon, Shahida, Dhiraj Gupta, and L. K. Das. "PID & LQR control for a quadrotor: Modeling and simulation." *Advances in Computing, Communications and Informatics (ICACCI, 2014 International Conference on.* IEEE, 2014.

Funke, Joseph, and J. Christian Gerdes. "Simple clothoid paths for autonomous vehicle lane changes at the limits of handling." *ASME 2013 Dynamic Systems and Control Conference.* American Society of Mechanical Engineers, 2013.

Hu, Chuan, Rongrong Wang, Fengjun Yan, et al. "Should the desired heading in path following of autonomous vehicles be the tangent direction of the desired path?" *IEEE Transactions on Intelligent Transportation Systems* 16.6 (2015): 3084-3094.

Chapter 6

Experiment Study of DDAS

This chapter includes the experiment study results of path following control using DDAS, including the model verification and lane change control experiments using DDAS. The contents of this chapter had not had time to be published at the time when this thesis was completed. The used FWIA vehicle test platform was constructed by Prof. Rongrong Wang and his research group at Southeast University, China. The experiment schemes were jointly developed by Prof. Wang and me. The experiments were conducted by me and Prof. Wang's master student, Mr. Yunke Shi. The control strategy in the experiments, data processing and analysis were completed by me. The experiment study of DDAS in the sixth chapter was written by me.

6.1 Experimental Vehicle Setup

In order to validate the DDAS mechanism, we have conducted the modeling and mechanism verification experiments with an FWIA vehicle. The used vehicle in the experiment is shown in Fig. 6.1. The vehicle states, such as the velocities, yaw rate and accelerations are accurately measured by an GPS-RT navigation system.

Due to the requirements on the power compactness, density, lightweight, and cost, the permanent-magnet brushless direct-current electric motors were chosen to make the in-wheel motors (Chau et al., 2008). The used electric motor has the rated power 10 kw, the peak power 20 kw, and the maximum current 300A. The sampling time/step size in the experiment is 0.01 sec, thus the control frequency is 100Hz. The nominal voltage of the batteries for generating the driving force is 72V, and the nominal voltage of the batteries for powering the MircroAutobox and GPS-RT is 12V. The parameters of the vehicle used in the experiment are shown in Table 6.1. The main sensors include the bus current sensor, inertial GPS-RT which can measure all the dynamics signals of the vehicle motion including the vehicle orientation and angle, velocity and angular velocity, acceleration and angular acceleration in three directions x, y, z in 3-D space, wheel speed sensor, and steering-wheel sensor which can measure the steering wheel velocity, angle and torque. The structure of the test vehicle is consistent with the prototype FWIA electric ground vehicle developed in Prof. Junmin Wang's group at The Ohio State University. Please refer to the previous published papers Wang et al. (2011); Chen and Wang (2012); Huang and Wang (2013) for the details of the experimental FWIA vehicle.

The experiments include two parts: the first one is the open-loop model validation experiment, which is used to validate the feasibility of DDAS mechanism, that is, to prove that the differential torque between the front left and right wheel can generate a steering angle when the active steering system completely fails, and identify the parameters of an FWIA vehicle. The second one is the closed-loop lane change control experiment, which is used to verify the accuracy of the estimation of the lateral velocity using a sliding mode observer, and verify the capability of DDAS to perform normal steering function. Note that in the lane

change control experiment with DDAS, we only used the feedback control of the yaw rate and used the measured value of the yaw rate, that is, we did not use the information of the lateral velocity. The lateral velocity is estimated by using the measured yaw rate based on a sliding mode observer.

Figure 6.1: The used vehicle in the experiment.

Table 6.1: Parameters of the Vehicle Model in the Experiment

Definition and Symbol	Value
Vehicle mass m	745 kg
Vehicle moment of inertia about yaw axis I_z	447.6 kg $\cdot$ m^2
Effective steering damping b_{eff}	100 N $\cdot$ s/(m $\cdot$ rad)
Half of the tire contact length l	0.05 m
Half of wheel track l_s	0.635 m
Distance of CG from front axle l_f	1.1 m
Distance of CG from rear axle l_r	1.3 m
Scrub radius r_σ	0.08 m
Cornering stiffness of front tires c_f	80000 N/rad
Cornering stiffness of rear tires c_r	80000 N/rad

6.2 Open-loop Model Validation Experiment

The open-loop model validation experiment is used to verify that the DDAS can generate a differential steering angle. We have conducted two experiment cases

using different control inputs for the front external yaw moment: sine input and step input. The experiment results using a sine input are shown in Fig. 6.2-6.7, including, in order, the longitudinal velocity, lateral velocity, lateral acceleration, yaw rate, front steering angle and front external yaw moment. The vehicle longitudinal speed is controlled by the accelerator pedal. From these figures, one can find that when a sine input is imported into the vehicle system for the front external yaw moment, a sine steering angle is outputted. The yaw rate also changes with the control input. The rest of the vehicle states are maintained in reasonable regions. The results of the experiments using a step input are shown in Fig. 6.8-6.13. Similarly, when there is a step input for the external yaw moment, the steering angle also displays a clear step tendency, and the other vehicle states are maintained in safe regions. From these two open-loop experiments, we can conclude that the differential torque between the front wheels does generate a front steering angle.

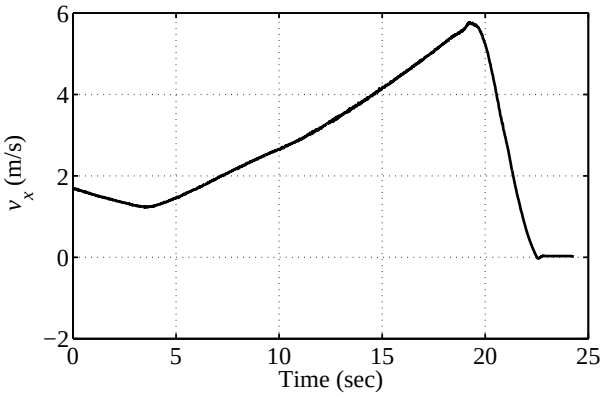

Figure 6.2: The longitudinal velocity in the open-loop experiment with a sine input.

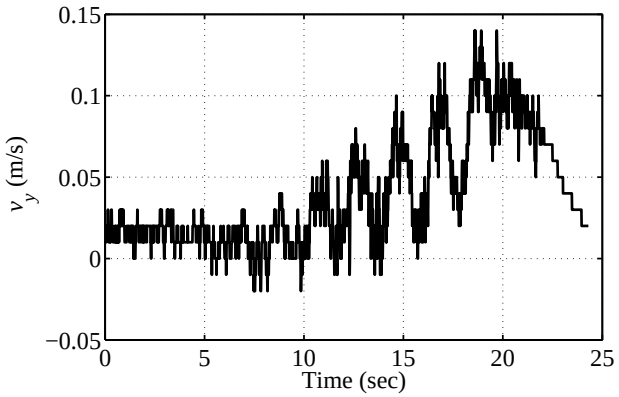

Figure 6.3: The lateral velocity in the open-loop experiment with a sine input.

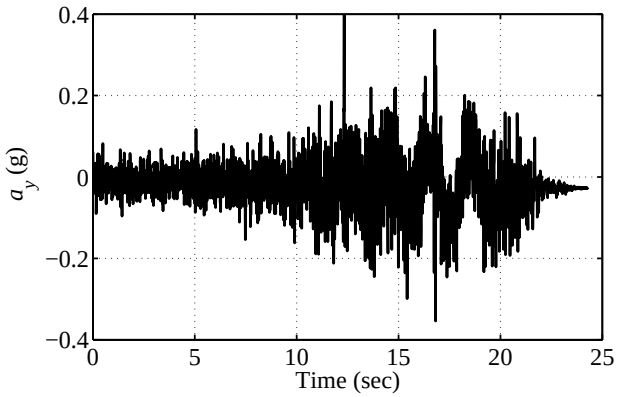

Figure 6.4: The lateral acceleration in the open-loop experiment with a sine input.

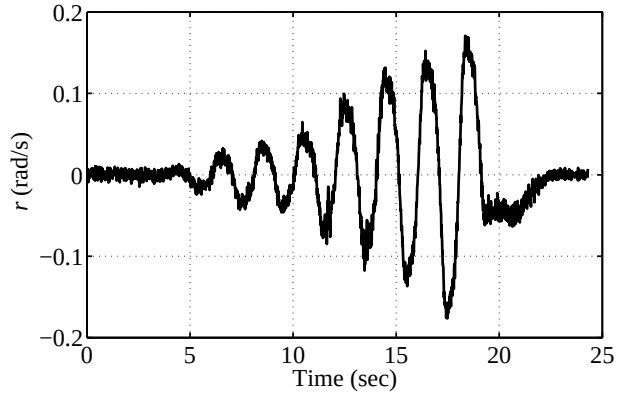

Figure 6.5: The yaw rate in the open-loop experiment with a sine input.

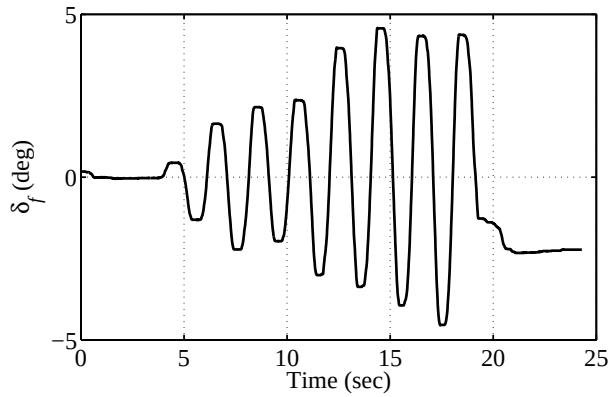

Figure 6.6: The front steering angle in the open-loop experiment with a sine input.

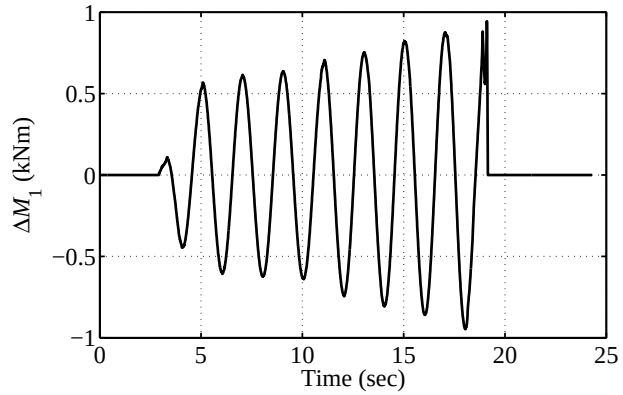

Figure 6.7: The front external yaw moment in the open-loop experiment with a sine input.

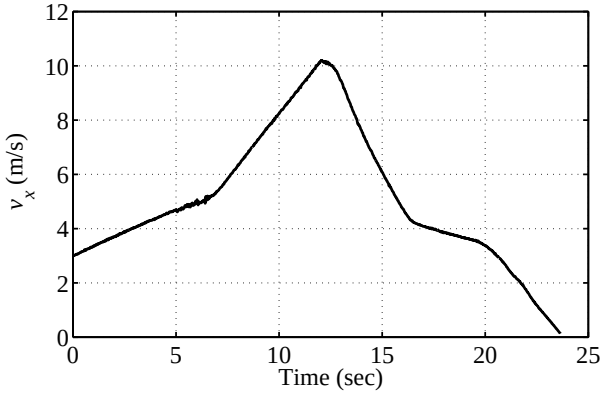

Figure 6.8: The longitudinal velocity in the open-loop experiment with a step input.

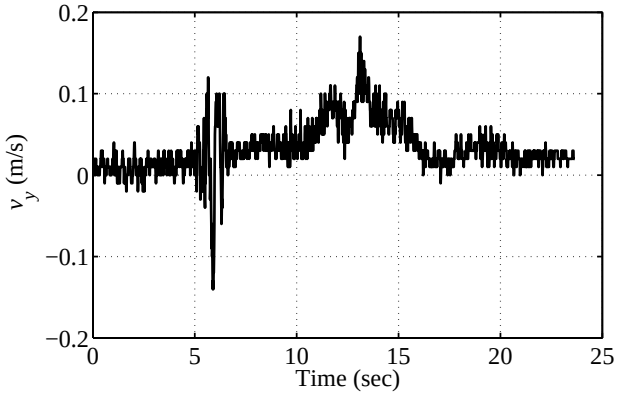

Figure 6.9: The lateral velocity in the open-loop experiment with a step input.

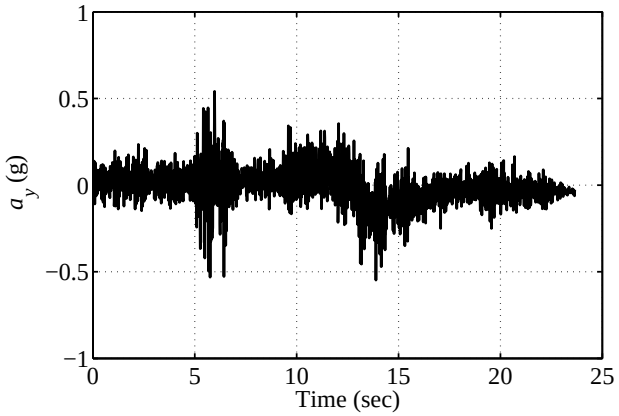

Figure 6.10: The lateral acceleration in the open-loop experiment with a sine input.

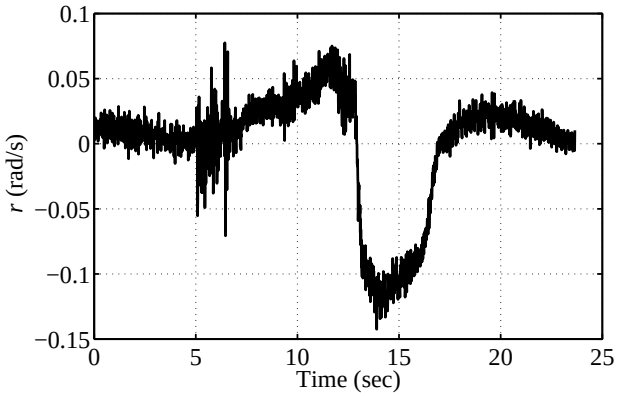

Figure 6.11: The yaw rate in the open-loop experiment with a sine input.

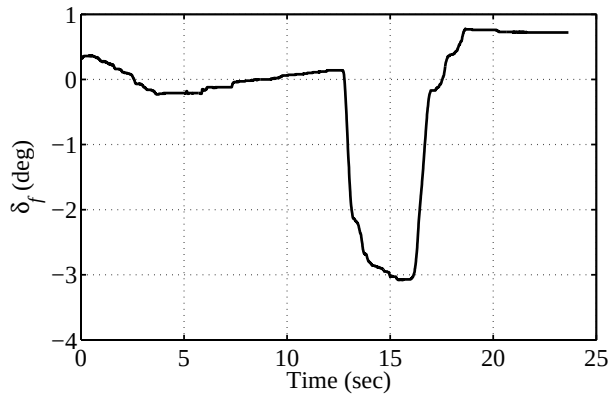

Figure 6.12: The front steering angle in the open-loop experiment with a sine input.

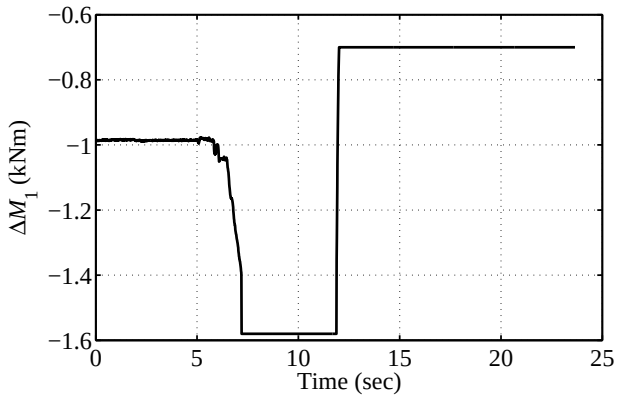

Figure 6.13: The front external yaw moment in the open-loop experiment with a sine input.

6.3 Closed-loop Lane Change Experiment with Lateral Velocity Estimation

A. Lateral Velocity Observer Design

Vehicle lateral velocity is usually hard to measure with low-cost sensor. In this subsection, a second-order sliding mode observer is proposed to estimate the sideslip angle using the measured yaw rate.

Recall the 2-DoF bicycle model (4.6)

$$\begin{cases} \dot{r} = a_{11}r + a_{12}v_y + b_{11}\delta_f + b_{12}\Delta M_z, \\ \dot{v}_y = a_{21}r + a_{22}v_y + b_{21}\delta_f, \end{cases} \tag{6.1}$$

where the model parameters in (4.6) are given as

$$\begin{aligned} a_{11} &= -\frac{\left({l_f}^2 c_f + {l_r}^2 c_r\right)}{v_x I_z}, \quad a_{12} = \frac{(l_r c_r - l_f c_f)}{I_z v_x}, \\ a_{21} &= -v_x - \frac{(l_f c_f - l_r c_r)}{m v_x}, \quad a_{22} = -\frac{(c_f + c_r)}{m v_x}, \\ b_{11} &= \frac{l_f c_f}{I_z}, \quad b_{12} = \frac{1}{I_z}, \quad b_{21} = \frac{c_f}{m}. \end{aligned} \tag{6.2}$$

System (4.6) can be transformed into the following state-space form as

$$\begin{cases} \dot{x} = Ax + Bu, \\ y = C_1 x, \end{cases} \tag{6.3}$$

where $x = [r \;\; v_y]^T$ is the system state, $u = [\delta_f \;\; \Delta M_z]^T$ is the control input, y is the measured output, and the system matrices are given by

$$A = \begin{bmatrix} a_{11} & a_{12} \\ a_{21} & a_{22} \end{bmatrix}, \; B = \begin{bmatrix} b_{11} & b_{12} \\ b_{21} & 0 \end{bmatrix}, \; C_1 = \begin{bmatrix} 1 & 0 \end{bmatrix}. \tag{6.4}$$

Denote

$$B = \begin{bmatrix} B_1 \\ B_2 \end{bmatrix} = \begin{bmatrix} b_{11} & b_{12} \\ b_{21} & 0 \end{bmatrix}, \tag{6.5}$$

where $B_1 = [b_{11} \;\; b_{12}]$, and $B_2 = [b_{21} \;\; 0]$.

The second-order sliding mode observer for the system (6.3) can be designed

using the super-twisting algorithm (Shtessel et al., 2014) as

$$\begin{cases} \dot{\hat{x}}_1 = a_{11}x_1 + a_{12}\hat{x}_2 + B_1u + c_1|x_1 - \hat{x}_1|^{1/2}\text{sign}\,(x_1 - \hat{x}_1)\,, \\ \dot{\hat{x}}_2 = a_{12}x_1 + a_{22}\hat{x}_2 + B_2u + c_2\text{sign}\,(x_1 - \hat{x}_1)\,, \end{cases} \tag{6.6}$$

where $\hat{x}_1$ and $\hat{x}_2$ are the estimated value of r and v_y, respectively, and c_1 and c_2 are two appropriately chosen constants. Then we have the following theorem about the estimation:

Theorem 6.3.1: For system (6.3), if the sliding mode observer is chosen as (6.6), then the estimation values $\hat{x}_1$ and $\hat{x}_2$ will converge to x_1 and x_2 respectively after a finite time.

Proof: Denote $\tilde{x}_1 = x_1 - \hat{x}_1$ and $\tilde{x}_2 = x_2 - \hat{x}_2$ as the estimation errors. The system (4.6) can be rewritten as

$$\begin{cases} \dot{x}_1 = a_{11}x_1 + a_{12}x_2 + B_1u, \\ \dot{x}_2 = a_{21}x_1 + a_{22}x_2 + B_2u. \end{cases} \tag{6.7}$$

Thus by integrating the observer (6.6), the dynamics of the observer errors can be modeled as

$$\begin{cases} \dot{\tilde{x}}_1 = a_{12}\tilde{x}_2 - c_1|\tilde{x}_1|^{1/2}sign\,(\tilde{x}_1)\,, \\ \dot{\tilde{x}}_2 = F\,(\tilde{x}_2) - c_2\text{sign}\,(\tilde{x}_1)\,, \end{cases} \tag{6.8}$$

where

$$F\,(\tilde{x}_2) = a_{22}x_2. \tag{6.9}$$

Note that in actual driving conditions, the vehicle lateral velocity is usually sufficiently small, so it can be assumed that there is a constant L_o, such that $|F\,(\tilde{x}_2)| < L_0$. Next, we will prove the finite-time convergence of the closed-loop system (6.8). Denote $e_1 = \tilde{x}_1/(a_{12}L_0)$ and $e_2 = \tilde{x}_2/L_0$. Combining (6.8) with

(6.9), we obtain the following differential inclusion:

$$\begin{cases} \dot{e}_1 = e_2 - \dfrac{c_1}{(a_{12}L_0)^{1/2}}|e_1|^{1/2}\text{sign}\,(e_1)\,, \\ \dot{e}_2 = \dfrac{F\,(\tilde{x}_2)}{L_0} - \dfrac{c_2}{L_0}\text{sign}\,(e_1)\,, \end{cases} \tag{6.10}$$

where we have

$$\frac{F\,(\tilde{x}_2)}{L_0} \in [-1,\ 1]. \tag{6.11}$$

Also, since $\text{sign}\,(e_1) = \text{sign}\,(e_2 - \dot{e}_1)$, (6.10) can be written as

$$\begin{cases} \dot{e}_1 = e_2 - \dfrac{c_1}{(a_{12}L_0)^{1/2}}|e_1|^{1/2}\text{sign}\,(e_1)\,, \\ \dot{e}_2 = \dfrac{F\,(\tilde{x}_2)}{L_0} - \dfrac{c_2}{L_0}\text{sign}\,(e_2 - \dot{e}_1)\,. \end{cases} \tag{6.12}$$

The rest of the proof can be found in Shtessel et al. (2014), and thus is omitted for brevity. The sign function in the observer (6.8) is a critical item to provide the strong robustness and the finite-time convergence of the closed-loop estimation system. From Theorem 6.3.1 it can be found that if such a sign function is replaced with a saturation function or a linear function, the finite-time stability is hard to guarantee.

B. Closed-loop Lane Change Control Experiment

In this experiment, we use the PI control to make the vehicle complete a lane-change manoeuvre using DDAS mechanism, when the steering motor fully fails. The control objective can be translated into the yaw rate control, which aims at making the real yaw rate track the desired value. The desired yaw rate can be found in Du et al. (2010).

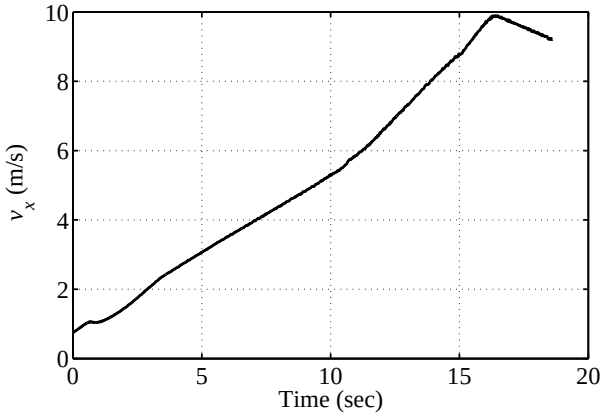

Figure 6.14: The longitudinal velocity in the closed-loop lane change experiment.

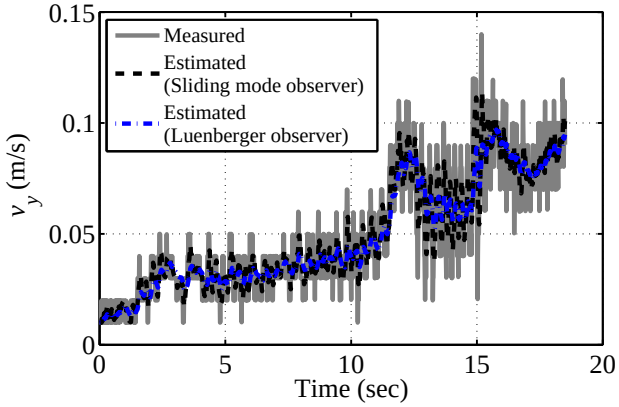

Figure 6.15: The measured and estimated lateral velocities in the closed-loop lane change experiment.

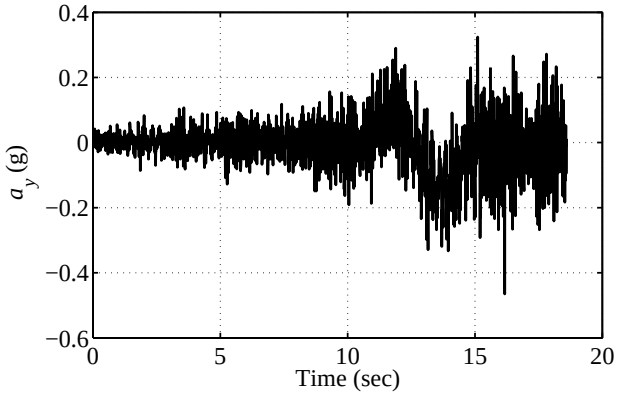

Figure 6.16: The lateral acceleration in the closed-loop lane change experiment.

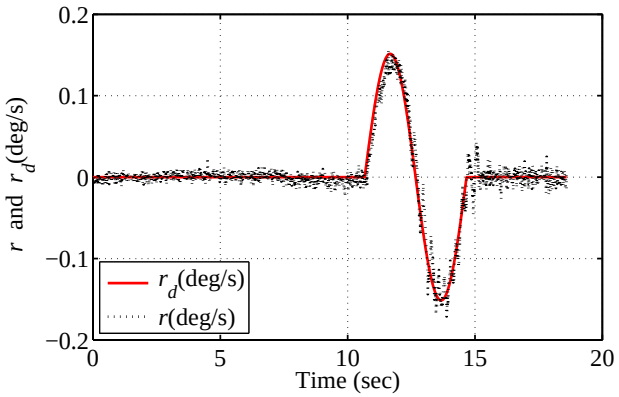

Figure 6.17: The yaw rate in the closed-loop lane change experiment.

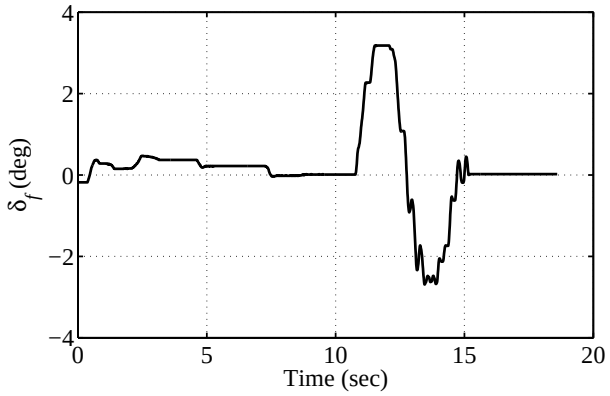

Figure 6.18: The front steering angle in the closed-loop lane change experiment.

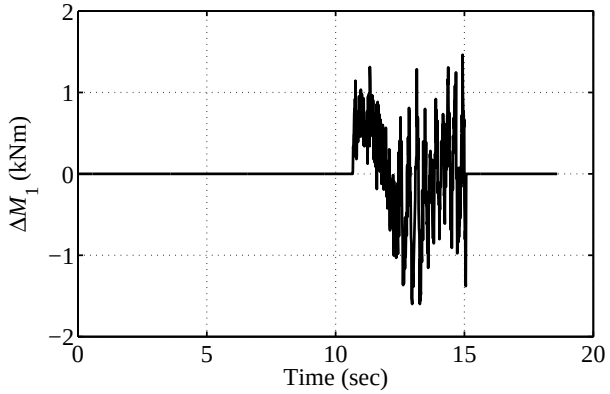

Figure 6.19: The front external yaw moment in the closed-loop lane change experiment.

The results of the closed-loop lane change experiment are shown in Fig. 6.14-6.19, including, in order, the longitudinal velocity, measured and estimated lateral velocities, lateral acceleration, yaw rate, front steering angle and front external yaw moment. The proposed sliding mode observer can effectively estimate the lateral velocity, and the estimation error is much smaller than that of a Luenberger observer, which is adopted here for comparison using the proposed method in Fang et al. (2011). The advantage of such a sliding mode observer lies in that it can estimate the variable in a finite time, and has strong robustness for the closed-loop system. The result of the lateral acceleration shows that the vehicle is driving within the handling limit in the lane change. The real yaw rate can track the desired yaw rate well by using the PI control strategy. The steering angle and control input are maintained in reasonable regions. Through the closed-loop lane-change experiment, we can find that by using appropriate controller, DDAS can complete normal driving function, thus can be employed as a fault-tolerant control strategy to increase the reliability of the electric vehicles.

6.4 Conclusion

In this chapter, I had conducted some experiments to verify the effectiveness of the DDAS mechanism. The open-loop test was used to prove that the differential torque can generate a differential steering angle. The closed-loop experiment is used to verify that the differential torque can be used to complete the normal steering manoeuvre if the active steering system completely fails. From the experiment results, it is found that DDAS mechanism is an effective fault-tolerant control strategy to generate steering angle and guarantee normal steering performance when the steering motor completely fails.

Acknowledgement about the Experiment Study

I would like to acknowledge that the design and construction of the FWIA test vehicle in this experiment were previously completed by Prof. Rongrong Wang and his research group in southeast University, China. The experiment schemes were jointly developed by Prof. Wang and me. The experiments were conducted by me and Prof. Wang's master student Mr. Yunke Shi. The control strategy in the experiments, data processing and analysis were completed by me. The experiment study of DDAS in the sixth chapter was written by me. Here I would like to thank Prof. Wang in lending the experimental vehicle and test equipments/field to me, and thank the time and effort that he and Mr. Yunke Shi spent on me. The conduction of the experiment would be not possible without their kind help and guidance.

References

Chau, K. T., Ching Chuen Chan, and Chunhua Liu. "Overview of permanent-magnet brushless drives for electric and hybrid electric vehicles." *IEEE Transactions on industrial electronics* 55.6 (2008): 2246-2257.

Wang, Rongrong, Yan Chen, Daiwei Feng, et al. "Development and performance characterization of an electric ground vehicle with independently actuated in-wheel motors." *Journal of Power Sources* 196.8 (2011): 3962-3971.

Chen, Yan, and Junmin Wang. "Design and evaluation on electric differentials for overactuated electric ground vehicles with four independent in-wheel motors." *IEEE Transactions on Vehicular Technology* 61.4 (2012): 1534-1542.

Huang, Xiaoyu, and Junmin Wang. "Longitudinal motion based lightweight vehicle payload parameter real-time estimations." *Journal of Dynamic Systems, Measurement, and Control* 135.1 (2013): 011013.

Shtessel, Yuri, Christopher Edwards, Leonid Fridman, et al. *Sliding Mode Control and Observation*. Springer, New York (2014).

Du, Haiping, Nong Zhang, Guangming Dong. "Stabilizing vehicle lateral dynamics with considerations of parameter uncertainties and control saturation through robust yaw control," *IEEE Transactions on Vehicular Technology* 59.5 (2010): 2593-2597.

Fang, Hao, Lihua Dou, Jie Chen, et al. "Robust anti-sliding control of autonomous vehicles in presence of lateral disturbances." *Control Engineering Practice* 19.5 (2011): 468-478.

Chapter 7

Conclusions and Future Work

7.1 Conclusions

Security is one of the most important objectives for the research and development of AGVs, and the active safety control strategies are increasingly crucial for security control of AGVs. Preventing the vehicle from surpassing the safe boundaries is highly conducive to reducing the vehicle's possibility of impacting other vehicles. In this context, this thesis studies the motion control of IA AGVs, and concentrates on constraint control and transient performance improvement for the path following errors from a safety perspective. The controller design in this work has considered practical interference factors in path following, including the vehicle/road parametric uncertainties, system disturbances, and input saturations of tire force. The ultimate research aim is to make the AGV more secure, intelligent and efficient.

To fulfill the research aim on the path following control, this thesis has proposed a novel nonlinear control technique to constrain the lateral offset in the reasonable scope, and a novel path following modeling approach and two novel nonlinear control techniques to reduce the overshoots and steady-state errors in the path

following control of AGVs, respectively. The contributions of this thesis can be summarized into four achievements: Firstly, this thesis points out the selection of traditional desired heading may deteriorate the path-following performance. Then a novel definition of the desired heading is proposed, which can considerably reduce the steady-state errors for path following caused by the non-zero sideslip-angle and large or changing road curvature. Secondly, to compactly constrain the lateral offset, a novel nonlinear control approach is proposed, which can effectively reduce the overshoots of the lateral offset. By the proposed method, the vehicle can be effectively restricted in safe lanes. Thirdly, to improve the transient performance of all the path following errors, an ISM-CNF approach is proposed to reduce the overshoots and steady-state errors in vehicle path following, considering the system uncertainties/disturbances and input saturations. Fourthly, to increase the redundancy and then the reliability of the AFS system in IA AGVs, the DDAS angle is utilized to achieve the path following in the case of the complete failure of the AFS system. A novel multiple-disturbances observer-based CNF approach is proposed to realize the path following control considering the tire force saturation. Experiments have been conducted to verify the existence and effectiveness of the DDAS mechanism. In sum, the ultimate control objective is to increase the path following accuracy and speed, and reduce the AGV's possibility of surpassing the safety lanes, thus to improve the vehicle maneuverability and stability as well as the vehicle ride comfort.

Here we would like to declare that in the controller design of this thesis, we have not explicitly considered the sensor noise, but we have considered the sensor noise in the lumped disturbances. In the simulations, we have directly used the measurement values of the vehicle states from CarSim. It should be pointed out that the CarSim software may not have real sensor noise in the measurement of

the vehicle states compared with experiments. However, the experiments we have conducted do have sensor noise in the GPS and other common sensors, which can be observed from the experiment results. Although the sensor noise is critical in the controller design, it is not the research focus in this thesis.

7.2 Future Work

7.2.1 Path-Following Topic

For the path-following research topic investigated in this thesis, my work uses the linear vehicle model and tire model, and does not include some other critical control issues in AGVs. In my future study about path following control, several more practical factors will be taken into consideration:

1. The nonlinearities of the vehicle dynamics and tire model will be considered. The tire force is a highly nonlinear function of the tire slip angle, and has a saturation characteristic, which makes the tire modelling very complex and difficult. Using a nonlinear model will make the control strategy more practical;

2. State constraints will be considered. Especially, the sideslip angle, yaw rate, lateral acceleration need to be constrained in reasonable regions to guarantee the vehicle safety; roller prevention needs to be considered, as the AGVs will be in danger of rollover when passing corners with high speeds;

3. In my current work, the path following is converted to the yaw stabilization control, with the reference yaw rate predefined according to the path following errors. However, a problem worth studying is how to find the most appropriate reference yaw rate, which simultaneously considers the vehicle

safety and mobility efficiency. This issue is related with the optimal trajectory planning.

7.2.2 Next Research Topic

My next research direction will focus on the trajectory planning, obstacle avoidance, and post-impact motion control for AGVs. Collisions of electric vehicles will cause large hurts to the passengers due to their small qualities, and simultaneously, easily bring about the displacement or damage and thus combustion to the batteries due to small crumple zones. Statistics data shows that after a first collision, a vehicle has high probability for a secondary collision, which will cause much larger harm to the passengers. In order to effectively reduce the probability of the secondary collision for electric vehicles after losing stability caused by the rear-end collisions or side-impacts, my future research will focus on the dynamics control issues for vehicle losing stability after collision. The planned schemes are divided into three parts:

1. Dynamics modeling and analysis for vehicle after losing stability; systematically analyze the dynamic characteristics of the wheel, wheel-axle and whole car after stability losing, and design the criterion for the loss of stability;

2. Design estimation methods for the collision characteristics based on the changes of the vehicle body states; study the states prediction and the optimal-trajectory planning issues after vehicle stability loss, and select the optimal, achievable vehicle state and driving trajectory considering the tire forces limits;

3. Explore the vehicle control strategies after vehicle stability loss through combining AFS and DYC; study the control allocation methods for vehicle chassis in extreme conditions. The proposed research program is expected to reduce the second-collision probability for electric vehicles after losing stability, and minimize the harm to passengers caused by unavoidable crashes.

Main References

Anderson, James M., Nidhi Kalra, Karlyn D. Stanley, et al. *Autonomous vehicle technology: A guide for policymakers*. Rand Corporation, 2014.

Litman, Todd. "Autonomous Vehicle Implementation Predictions." *Victoria Transport Policy Institute* 28 (2014).

Bizon, Nicu, Lucian Dascalescu, and Naser Mahdavi Tabatabaei. *Autonomous Vehicles: Intelligent Transport Systems and Smart Technologies*. Nova Science Publishers, 2014.

Snider, Jarrod M. "Automatic steering methods for autonomous automobile path tracking." *Robotics Institute, Pittsburgh, PA, Tech. Rep. CMU-RITR-09-08* (2009).

Girbés, Vicent, Leopoldo Armesto, and Josep Tornero. "Path following hybrid control for vehicle stability applied to industrial forklifts." *Robotics and Autonomous Systems* 62.6 (2014): 910-922.

Khodayari, Alireza, Ali Ghaffari, Sina Ameli, et al. "A historical review on lateral and longitudinal control of autonomous vehicle motions." *2010 International Conference on Mechanical and Electrical Technology*. 2010.

Bishop, Richard. "Intelligent vehicle applications worldwide." *IEEE Intelligent Systems and Their Applications* 15.1 (2000): 78-81.

Zhao, Pan, Jiajia Chen, Tao Mei, et al. "Dynamic motion planning for autonomous vehicle in unknown environments." *Intelligent Vehicles Symposium (IV), 2011 IEEE*. IEEE, 2011.

Marino, Riccardo, Stefano Scalzi, and Mariana Netto. "Nested PID steering control for lane keeping in autonomous vehicles." *Control Engineering Practice* 19.12 (2011): 1459-1467.

Fang, Hao, Lihua Dou, Jie Chen, et al. "Robust anti-sliding control of autonomous vehicles in presence of lateral disturbances." *Control Engineering Practice* 19.5 (2011): 468-478.

Matveev, Alexey S., Michael Hoy, Jayantha Katupitiya, et al. "Nonlinear sliding mode control of an unmanned agricultural tractor in the presence of sliding and control saturation." *Robotics and Autonomous Systems* 61.9 (2013): 973-987.

Lenain, Roland, Benoit Thuilot, Christophe Cariou, et al. "High accuracy path tracking for vehicles in presence of sliding: Application to farm vehicle automatic guidance for agricultural tasks." *Autonomous robots* 21.1 (2006): 79-97.

Raffo, Guilherme V., Guilherme K. Gomes, Julio E. Normey-Rico, et al. "A predictive controller for autonomous vehicle path tracking." *IEEE transactions on intelligent transportation systems* 10.1 (2009): 92-102.

Tsui, Willie, Mohamed Slim Masmoudi, Fakhreddine Karray, et al. "Soft-computing-based embedded design of an intelligent wall/lane-following vehicle." *IEEE/ASME Transactions on Mechatronics* 13.1 (2008): 125-135.

Silva, Marco, Luís Garrote, Fernando Moita, et al. "Autonomous electric vehicle: Steering and path-following control systems." *MELECON, IEEE* (2012): 442-445.

Nunes, Urbano, and L. Conde Bento. "Data fusion and path-following controllers comparison for autonomous vehicles." *Nonlinear Dynamics* 49.4 (2007): 445-462.

Arogeti, Shai A., and Nadav Berman. "Path following of autonomous vehicles in the presence of sliding effects." *IEEE Transactions on Vehicular Technology* 61.4 (2012): 1481-1492.

Goodarzi, A., A. Sabooteh, and E. Esmailzadeh. "Automatic path control based on integrated steering and external yaw-moment control." *Proceedings of the Institution of Mechanical Engineers, Part K: Journal of Multi-body Dynamics* 222.2 (2008): 189-200.

Yang, Derong, Timothy J. Gordon, Bengt Jacobson, et al. "Quasi-linear optimal path controller applied to post impact vehicle dynamics." *IEEE transactions on intelligent transportation systems* 13.4 (2012): 1586-1598.

Enache, N. Minoiu, M. Netto, S. Mammar, et al. "Driver steering assistance for lane departure avoidance." *Control engineering practice* 17.6 (2009): 642-651.

Wu, Jianyong, Qingping Wang, Xue Wei, et al. "Studies on improving vehicle handling and lane keeping performance of closed-loop driver Cvehicle system with integrated chassis control." *Mathematics and Computers in Simulation* 80.12 (2010): 2297-2308.

Enache, Nicoleta Minoiu, Saïd Mammar, Mariana Netto, et al. "Driver steering assistance for lane-departure avoidance based on hybrid automata and composite Lyapunov function." *IEEE Transactions on Intelligent Transportation Systems* 11.1 (2010): 28-39.

Enache, Nicoleta Minoiu, Saïd Mammar, Benoit Lusetti, et al. "Active steering assistance for lane keeping and lane departure prevention." *Journal of Dynamic Systems, Measurement, and Control* 133.6 (2011): 061003.

Pérez, Joshué, Vicente Milanés, and Enrique Onieva. "Cascade architecture for lateral control in autonomous vehicles." *IEEE Transactions on Intelligent Transportation Systems* 12.1 (2011): 73-82.

Hu, Xiaosong, Jiuchun Jiang, Bo Egardt, et al. "Advanced power-source integration in hybrid electric vehicles: Multicriteria optimization approach." *IEEE Transactions on Industrial Electronics* 62.12 (2015): 7847-7858.

Zou, Yuan, Fengchun Sun, Xiaosong Hu, et al. "Combined optimal sizing and control for a hybrid tracked vehicle." *Energies* 5.11 (2012): 4697-4710.

Li, Shengbo Eben, Shaobing Xu, Xiaoyu Huang, et al. "Eco-Departure of Connected Vehicles With V2X Communication at Signalized Intersections." *IEEE Transactions on Vehicular Technology* 64.12 (2015): 5439-5449.

Wang, Rongrong, Yan Chen, Daiwei Feng, et al. "Development and performance characterization of an electric ground vehicle with independently actuated in-wheel motors." *Journal of Power Sources* 196.8 (2011): 3962-3971.

Wang, Rongrong, and Junmin Wang. "Fault-tolerant control with active fault diagnosis for four-wheel independently driven electric ground vehicles." *IEEE Transactions on vehicular technology* 60.9 (2011): 4276-4287.

Wang, Rongrong, Hui Jing, Fengjun Yan, et al. "Optimization and finite-frequency H_∞ control of active suspensions in in-wheel motor driven electric ground vehicles." *Journal of the Franklin Institute* 352.2 (2015): 468-484.

Naranjo, Jose E., Carlos Gonzalez, Ricardo Garcia, et al. "Lane-change fuzzy control in autonomous vehicles for the overtaking maneuver." *IEEE Transactions on Intelligent Transportation Systems* 9.3 (2008): 438-450.

Shim, Taehyun, Sehyun Chang, and Seok Lee. "Investigation of sliding-surface design on the performance of sliding mode controller in antilock braking systems." *IEEE Transactions on Vehicular Technology* 57.2 (2008): 747-759.

Hu, Jia-Sheng, Dejun Yin, and Yoichi Hori. "Fault-tolerant traction control of electric vehicles." *Control Engineering Practice* 19.2 (2011): 204-213.

Doumiati, Moustapha, Olivier Sename, Luc Dugard, et al. "Integrated vehicle dynamics control via coordination of active front steering and rear braking." *European Journal of Control* 19.2 (2013): 121-143.

Wang, Junmin. *Coordinated and reconfigurable vehicle dynamics control*. Ph.D. dissertation, Dept. Mech. Eng., Univ. Texas, Austin, TX, USA, 2007.

Geng, Cong, Lotfi Mostefai, Mouloud Denai, et al. "Direct yaw-moment control of an in-wheel-motored electric vehicle based on body slip angle fuzzy observer." *IEEE Transactions on Industrial Electronics* 56.5 (2009): 1411-1419.

Mashadi, Behrooz, and Majid Majidi. "Integrated AFS/DYC sliding mode controller for a hybrid electric vehicle." *International Journal of Vehicle Design* 56.1-4 (2011): 246-269.

Nam, Kanghyun, Hiroshi Fujimoto, and Yoichi Hori. "Lateral stability control of in-wheel-motor-driven electric vehicles based on sideslip angle estimation using lateral tire force sensors." *IEEE Transactions on Vehicular Technology* 61.5 (2012): 1972-1985.

Shuai, Zhibin, Hui Zhang, Junmin Wang, et al. "Combined AFS and DYC control of four-wheel-independent-drive electric vehicles over CAN network with time-varying delays." IEEE Transactions on Vehicular Technology 63.2 (2014): 591-602.

C. Hu, Hui Jing, Hui Jing, F. Yan, et al. "Robust H_∞ output-feedback control for path following of autonomous ground vehicles." *Mechanical Systems and Signal Processing* 70 (2016): 414-427.

Li, W., T. E. C. Potter, and R. P. Jones. "Steering of 4WD vehicles with independent wheel torque control." *Vehicle System Dynamics* 29.S1 (1998): 205-218.

Hoogterp, Francis B., and William R. Meldrum. *Differential torque steering for future combat vehicles*. No. 1999-01-3740. SAE Technical Paper, 1999.

Besselink, B. C. "Computer controlled steering system for vehicles having two independently driven wheels." *Computers and electronics in agriculture* 39.3 (2003): 209-226.

Jang, Bong-Choon, Yeo-Heung Yun, and Seong-Cheol Lee. "Simulation of vehicle steering control through differential braking." International Journal of Precision Engineering and Manufacturing 5.3 (2004): 26-34.

Nozaki, Hiromichi. *Effect of differential steering assist on drift running performance*. No. 2005-01-3472. SAE Technical Paper, 2005.

Shuang, Gao, Norbert C. Cheung, K. W. Eric Cheng, et al. "Skid steering in 4-wheel-drive electric vehicle." *2007 7th International Conference on Power Electronics and Drive Systems*. IEEE, 2007.

Wu, F., and T. J. Yeh. "A control strategy for an electrical vehicle using two in-wheel motors and steering mechanism." *Proceedings of AVEC*. Vol. 8. 2008.

Thacher, Russell James. "Differential steering assist system for utility vehicle." U.S. Patent No. 7,578,361. 25 Aug. 2009.

Wang, Jun-nian, Q. Wang, L. Jin, et al. "Independent wheel torque control of 4WD electric vehicle for differential drive assisted steering." *Mechatronics* 21.1 (2011): 63-76.